UNIVERSITÀ DEGLI STUDI DI TRIESTE

XXX CICLO DEL DOTTORATO DI RICERCA IN INGEGNERIA E ARCHITTETTURA
CURRICULUM INGEGNERIA MECCANICA, NAVALE, DELL'ENERGIA E DELLA
PRODUZIONE

EXPERIMENTAL TEST AND MODELLING OF PERFORMANCE DEGRADATION OF HT-PEM FUEL CELLS FOR USE IN MICRO-CHP SYSTEMS

Settore scientifico-disciplinare: ING-IND/09

DOTTORANDO
TANCREDI CHINESE

COORDINATORE
PROF. DIEGO MICHELI

SUPERVISORI DELLA TESI
PROF. RODOLFO TACCANI
PROF. DIEGO MICHELI

ANNO ACCADEMICO 2016/2017

Sintesi

I sistemi micro-cogenerativi (micro-CHP) a celle a combustibile mantengono un buon rendimento per impianti di piccola taglia e a carico parziale rendendoli adatti alle applicazioni domestiche.

Le celle a combustibile polimeriche ad alta temperatura (HT-PEM) sono una tecnologia promettente per i sistemi micro-CHP, soprattutto grazie alla loro elevata tolleranza alla presenza di CO nel combustibile che le rendono adatte ad operare anche con combustibili diversi dall'idrogeno. Ciononostante, il costo, le prestazioni e il degrado restano le problematiche da superare per raggiungerne la piena commercializzazione. Riguardo al degrado prestazionale, le condizioni operative incidono molto sulla durata di vita delle membrane.

Lo scopo di questa ricerca è di determinare in che modo il problema del degrado prestazionale delle celle HT-PEM, installate in sistemi micro-CHP, può essere gestito in modo da rendere il sistema adatto al funzionamento su lunghi periodi.

A questo scopo, si è sviluppata una specifica metodologia sperimentale e di modellizzazione del degrado prestazionale delle celle HT-PEM in sistemi micro-CHP.

Sono stati raccolti dati sperimentali su 8 membrane fatte funzionare con diversi test di degrado accelerato. Per valutare le prestazioni delle celle, Curve di Polarizzazione (PC), Elettroscopie ad Impedenza (EIS) e Ciclovoltametrie (CV) sono state registrate durante i test di invecchiamento. Come previsto, il degrado del voltaggio è fortemente influenzato dalle condizioni operative. Il tasso di degrado registrato a 200 mA/cm^2 è stato di circa 30 μV/h per il funzionamento a carico costante, 34 μV/h per i cicli triangolari ([0.01 – 0.5]V), 45 μV/h per i cicli triangolari con permanenza all'OCV ([0 – 0.5]V - 2s OCV), 81 μV/h per i cicli di Start/Stop, mentre per la permanenza costante all'OCV si è riscontrata un'ampia variabilità del valore di degrado.

Per analizzare l'evoluzione nano-morfologica dello strato di catalizzatore su porzioni ampie della membrana, si è usata la tecnica della Small Angle X-Ray Scattering (SAXS). I risultati della SAXS hanno mostrato un aumento della dimensione media delle particelle di platino fino al 130%, per membrane sottoposte a cicli di carico. I dati della SAXS sono stati confrontati con i dati ottenuti con la tecnica della Transmission Electron Microscopy (TEM) che ha confermato l'andamento di crescita delle particelle.

I dati sperimentali, raccolti durante questa ricerca, hanno permesso di determinare il degrado prestazionale in varie condizioni di carico e hanno permesso di definire un modello che è poi stato implementato in un macro-modello di simulazione di un sistema CHP.

Si è dimostrato che il degrado dello stack di celle a combustibile continua ad essere un problema per il completo sfruttamento di questa tecnologia, ma nella configurazione CHP,

la produzione di calore può parzialmente compensare la perdita di energia elettrica dovuta al degrado e l'effetto del degrado può essere mitigato tramite alcune strategie operative e aumentando la taglia dell'impianto, anche se questo influisce sul costo del sistema.

Infine, il modello può essere un valido strumento per condurre analisi di sensibilità e per trovare la taglia ottimale dei componenti del sistema tenendo conto del degrado prestazionale nel tempo. In futuro, questo modello potrà essere migliorato introducendo diversi tipi di degrado per ogni condizione operativa riscontrabile durante la vita utile del sistema CHP.

Abstract

Fuel cells based Micro Combined Heat and Power (micro-CHP) systems maintain good efficiencies for small size plants and at partial load making them suitable for domestic applications.

High Temperature Polymer Electrolyte Membrane (HT-PEM) fuel cells are a promising technology for micro-CHP system, especially thanks to their high CO tolerance that allows the use of fuels other than hydrogen. Nevertheless, cost, performance and degradation issues are still to be overcome to fully achieve commercialization. Regarding performance degradation, operating conditions strongly affect their durability.

The purpose of this research is to determine how the degradation issues for HT-PEM fuel cells, installed in micro-CHP systems, can be handled to make the system become suitable for long term operation, in terms of performance.

To do so, a specific methodology has been developed for experimental testing and modelling of performance degradation of HT-PEM fuel cells for use on micro-CHP systems.

Data of 8 Membrane Electrode Assemblies (MEAs) operated with different accelerated ageing tests have been collected and compared with literature. In order to assess the cell performance, Polarization Curves (PC), Electro Impedance Spectroscopy (EIS) and Cyclic Voltammetry (CV) have been recorded during the ageing tests. As expected, voltage degradation was strongly influenced by operating conditions. The voltage decay rate at 200 mA/cm^2 was found to be about 30 µV/h for constant load operation, 34 µV/h for triangular load cycle ([0.01 − 0.5]V), 45 µV/h for triangular load cycle with permanence at OCV ([0 − 0.5]V - 2s OCV), 81 µV/h for Start/Stop cycles, while for constant permanence at OCV a wide variability of the degradation rate has been encountered.

In order to analyse the nano-morphological evolution of the catalyst layer on large portions of the MEA, Small Angle X-Ray Scattering (SAXS) has been carried out. The

SAXS results showed a mean size increase of the platinum nanoparticles up to 130% when the MEA is subjected to load cycles. SAXS data has then been compared with data obtained by Transmission Electron Microscopy (TEM) analysis confirming the catalyst particles growing trend.

The experimental data collected during this research activity allowed to identify the performance degradation of the fuel cell over different load conditions and allowed to infer a performance degradation model that has then been implemented in a CHP system process simulation model.

Stack degradation has been shown to be still an issue that hampers the full exploitation of the technology, but, in CHP configuration, heat production can partially compensate electrical energy loss due to degradation and its detrimental effect can be mitigated choosing some operational control strategies and increasing the size of the stack, even if this affects system cost.

Finally, the model can be a valuable tool for conducting sensitivity analysis and find optimal size of system components taking into account the system performance degradation over time. In the future this model could be upgraded introducing different degradation behaviour for each operational condition encountered during the lifetime of the CHP-system.

Acknowledgments

Index

INDEX

8

Index of figures

INDEX OF FIGURES

Index of Tables

List of acronyms

AFC	Alkaline Fuel Cells
AFM	Atomic Force Microscopy
ASAXS	Anomalous Small Angle X-Ray Scattering
AST	Accelerated Stress Test
BOP	Balance of Plant
CHP	Combined Heat and Power
CL	Catalyst Layer
CV	Cyclic Voltammetry
DMFC	Direct Methanol Fuel Cells
DOE	US Department of Energy
ECSA	Electro Chemical Surface Area
EIS	Electro Impedance Spectroscopy
FC	Fuel Cell
FCHEA	Fuel Cell Hydrogen Energy Association
GDL	Gas Diffusion Layer
HT-PEM	High Temperature PEM
HT-PEM FC	High Temperature PEM Fuel Cells
HOR	Hydrogen Oxidation Reaction
ICE	Internal Combustion Engine
IEC	International Electrotechnical Commission
JCGM	Joint Committee for Guides in Metrology
JRC	European Joint Research Centre
kW_e	Kilowatt of electricity
kW_{th}	Kilowatt of thermal energy
LHV	Lower Heating Value
LT-PEM	High Temperature PEM
LT-PEM FC	Low Temperature PEM Fuel Cells
MCFC	Molten Carbonate Fuel Cells
MEA	Membrane Electrode Assembly
MGT	Micro Gas Turbines
Micro-CHP	Micro Combined Heat and Power
MPL	Micro Porous Layer
MRC	Micro Ranking Cycles
MRI	Magnetic Resonance Imaging
NP	Nano Particle

LIST OF ACRONYMS

OCV	Open Circuit Voltage
ORR	Oxygen Reduction Reaction
PA	Phosphoric Acid
PAFC	Phosphoric Acid Fuel Cell
PBI	Polybenzimidazole
PC	Polarization curve
PEM	Proton Exchange Membrane
PEMFC	Proton Exchange Membrane Fuel Cells
PhD	Philosophiae Doctor (doctor of philosophy)
PTFE	Poly Tetra Fluoro Ethylene (Teflon®)
SAXS	Small Angle X-Ray Scattering
SE	Sterling Engine
SEM	Scanning Electron Microscopy
SOFC	Solid Oxide Fuel Cells
TEM	Transmission Electron Microscopy
TPB	Three Phase Boundary
USCAR	US Council for Automotive Research
USFCC	US Fuel Cell Council
WGS	Water Gas Shift

List of symbols

CO   Carbon monoxide

CO_2 Carbon dioxide

CH_4 Methane

γ_x Activity of the species x

e^- Electron

F   Faraday constant

G   Gibbs free energy

η Efficiency

η_{act} Activation losses

η_{Ohm} Ohmic losses

η_{conc} Concentration losses

H   Enthalpy

H^+ Proton

H_2 Hydrogen

H_2O Water

H_3PO_4 Phosphoric Acid

i $\sqrt{-1}$

J   Current

j Current density

n   number of electrons

N_{Av} Avogadro number

O_2 Oxygen

P   Pressure

p_x Activity of the species x expressed as partial pressure in atmosphere

Pt   Platinum

Pt/C   Platinum to Carbon ratio

q   Electrical charge

R   Perfect gas constant

S   Entropy

T   Temperature

U   Internal energy

V   Electrical Potential

W_{el} Electrical work

υ_x Stoichiometric coefficient of the species x

1.Introduction

In this chapter a general introduction of the scientific context of this PhD activity is given in §1.1. The main objectives of the research activity carried out during this three years of activity and the research question of this PhD work are highlighted in §1.2. Afterward, in §1.3 a plan of this thesis is reported to give to the reader a brief overview of the subjects described in each chapter and understand the general structure of the thesis.

1.1.   Scientific context

Even if global community is trying to promote greenhouse gasses reduction, limitation of the fossil fuel depletion and improvement of the efficiency of the energy production systems in order to reduce the primary energy consumption; the world primary energy consumption is increasing with a growth rate of 1.8% and coal consumption is increasing at a rate of 2.5% [1].

Nowadays, more than 40% of the total electrical energy is still produced by coal and gas power plant [2]. In these power plants about 60% of the primary energy is lost as waste heat and, after transportation through the grid, almost 30% of total end-used electrical energy is used for space heating [3]. This means that, actually, if the waste heat lost at the production plant could have been used to cover the household heat needs there would have been a total reduction of the electricity consumption of 30% and a very consistent reduction of heat dispersal in atmosphere. In addition to this, it must be highlighted that 40% of energy-related CO_2 emissions is from electricity generation and 25% to 40% of the electricity cost is due to network services [4].

It is hence evident that decentralizing the production and coupling the electricity production with a heat recover system that could cover the household thermal need would bring an extremely positive effect from the economic and environmental point of view.

Micro Combined Heat and Power (micro-CHP) systems are integrated energy production systems allowing simultaneous production of electrical power and heat.

Micro-CHP technologies allow high system efficiency, low emissions, reduction of primary energy consumption and minimization of power distribution losses thanks to the decentralization of the energy production.

Micro-CHP technologies suitable for residential buildings should have a size ranking from 5 to 10 kWe. Nowadays exist mainly four types of micro-CHP technologies: internal combustion engine (ICE), micro gas turbines (MGT), micro Rankine cycles (MRC) and Stirling engines (SE). Some countries like Denmark, Finland, Russia, and Netherlands

have expanded the use of micro-CHP up to about 30-50% of the total power generation demonstrating that a similar result could be achieved worldwide [5].

In addition to these micro-CHP systems, in the past few years a very important role on the micro-CHP scenario has been played by fuel cell based micro-CHP systems reaching in 2012 the 64% of the global sales of micro-CHP [6]. Fuel cells have the great advantage to maintain extremely good electrical efficiencies for small size plants and during partial load operation. For this reason, for domestic application, fuel cell system can reach electrical efficiencies higher than other micro-CHP technologies. Moreover, the increasing of available renewable energies brings the need for long term storage solutions. Hydrogen can be one of the best long-term renewable energy storage solutions and micro-CHP based on fuel cells can be a suitable technology for the use of hydrogen.

Six types of fuel cells exist: Alkaline Fuel Cells (AFC), Phosphoric Acid fuel cells (PAFC), Molten Carbonate Fuel Cells (MCFC), Solid Oxide Fuel Cells (SOFC), High temperature Polymer Electrolyte Fuel Cell (HT-PEM) and Low temperature Polymer Electrolyte Fuel Cell (LT-PEM). However, for cogeneration systems, some of them have been nowadays almost completely abandoned; in particular AFC did not reach commercialisation due to their low durability and CO_2 contamination issues, PAFC did not reach large scale commercialisation mainly because of high cost and corrosion issues of the fuel cell materials while for MCFC the high operating temperature and the corrosive nature of the electrolyte accelerate the component breakdown and corrosion, decreasing lifetime [1].

Nowadays, fuel cells based micro-CHP available technologies are: SOFC, HT-PEM and LT-PEM.

SOFC systems, thanks to their high operational temperature can operate directly with hydrocarbons such as CH_4 since an internal reforming process can occur; moreover, in stationary operation, they can reach very good electrical efficiency up to 60%. However, they encounter difficulties in variable operation due to their slow transient response (15 minutes vs 10 seconds for PEM) and long start-up process (2.5 to 20 h). Moreover, even if SOFC systems due to their very high operational temperature (700-1000°C) produce very high quality heat, their heat recover system is quite complex since it is obtained by supplying the cathode with excess air. Large quantities of air are required for reactant air preheating and for cooling, which needs the use of electrical air blowers that lower the total efficiency [1].

LT-PEM fuel cells are nowadays the most spread out technology since they received a big commercial push up thanks to car industry research activity. Electrical efficiency reached almost the 40% and lifetime is higher than 20 000 h.

The leading Country in the commercial spreading of this technology for micro-CHP is Japan, with the Ene-Farm project started in 2009 that brought to the installation of 120 000 residential fuel cell units by 2015 and aims to a target of 300 000 by 2020 [7]; almost all installed system (85%) of the Ene-Farm project are based on LT-PEM fuel cells, the rest

(15%) are SOFC. After Japan, the second leading country in micro-CHP area is Germany, with the Callux project started in 2008. The German experience has been recently (2013) integrated in the Ene.field European project which aims to install around 1000 fuel cell micro-CHP systems in the European community [8]. HT-PEM fuel cells are under trial in these European projects.

HT-PEM fuel cells, despite their relatively lower electrical performance efficiency and higher degradation rate have many advantages with respect to LT-PEM when installed in micro-CHP systems. The most important advantage is their high tolerance to CO impurities (up to 5%) [9] that allows an important simplification of the fuel processing with a consequent reduction of the energy consumption for the purification system. Another important simplification of the system is obtained thanks to the elimination of the humidification process that for HT-PEM is not needed. This system simplification can fill the gap between the performance efficiency of LT-PEM and HT-PEM. In fact, even if LT-PEMs have a higher electric efficiency, HT-PEMs can reach a higher CHP efficiency (Electric + Thermal) [1]. Moreover, since HT-PEM fuel cells operate at higher temperatures, the heat available for cogeneration is at higher temperature which allows a reduction of exchange surface area of the exchangers improving the efficiency of the heat transfer. The global system simplification can also reduce costs and volume of the system. In [10], a comparative study between LT-PEM and HT-PEM based micro-CHP system has been carried out, and it outlined that the performance of the two solution are quite similar. However, as highlighted by [11] another advantage of HT-PEM that comes with the simplification of the fuel processing and cooling systems is an increased efficiency of HT-PEM systems at partial load; in fact, while fuel cell systems usually increase their efficiencies at partial loads, the other parts of the system are not at optimal operation and hence their performance decays. HT-PEM, eliminating some auxiliaries such as humidifiers, compressors and radiator can maintain very good system performances at partial load.

Simplification of the system and high temperature heat seem to make HT-PEM a preferable solution for micro-CHP systems. Among the existing HT-PEM fuel cells technologies, the Polybenzimidazole (PBI) based (studied in this PhD work) seems to be the most promising technology.

However, two major problems for this kind of fuel cells still hampering the commercialisation: cost and degradation rate that in the case of HT-PEM fuel cell decreases by more than half the life time of the stack with respect to a LT-PEM fuel cell stack.

The high cost is greatly influenced by the platinum-based electrocatalysts needed to facilitate the kinetics of the electrode reactions [12]. In order to increase the specific surface area, the catalyst is made by Pt or Pt alloy Nanoparticles (NPs) mixed with a porous carbon support [13].

Losses in MEA performance associated with fuel cell operation typically occur via processes related to degradation of the catalyst layer [13,14], in particular the re-

distribution of phosphoric acid within the PBI membrane and catalyst layers, and thinning of the membrane itself [15,16]. It is believed that Ostwald ripening [17] and coalescence [18] are the two main mechanisms through which degradation of the catalyst layer occurs, thereby reducing the electrochemical surface area of the carbon-supported platinum electrodes [19]. This loss is exacerbated by particle size: the smaller the particle, the greater the thermodynamic force for its coarsening. Thus, efforts to reduce the loading of expensive Pt by minimizing catalyst particle size (increasing the ratio ECSA/Pt weight) have the major drawback to increase the ECSA (Electro Chemical Surface Area) loss rate [20].

PBI membranes demonstrated a good lifetime under steady state operation, reaching up to 17000 hours of operational life [15,19], but higher performance degradation rates have been measured when HT-PEM fuel cells operate under variable load conditions [13,21–24].

Operating conditions strongly affect durability and hence, optimization of operation strategies is essential in mitigation of fuel cell degradation and many studies are aimed to analyse working parameters affecting MEAs durability.

Performance degradation of a HT-PEM based on phosphoric acid-doped PBI membranes, such as the one considered in this work, is mainly due to undesired reactions and corrosive environment that can be also related to load cycling between low and high cell voltages, operation at low humidity and high temperature, and fluctuations in temperature and humidity [25–32].

Understanding the degradation mechanism of each process is very important in order to implement adapted production or operation procedures able to enhance lifetime of fuel cell. However, the first important step is to manage how to separate each degradation process and determine a hierarchy between them. A remarkable work has been done in this sense by [33] and [34]. Concerning high temperature fuel cells specific degradation mechanisms have be analysed and reviewed [35,36] with the purpose to understand, hierarchize and model the complex multifactor phenomenon. According to these studies, the primary degradation mechanisms of high temperature fuel cells are considered to be carbon corrosion, platinum agglomeration, and acid leaching/flooding. Moreover, many authors agree that the hierarchy of these phenomena depends on the operation time of the fuel cell. As mentioned in [36] and in [37] the platinum agglomeration is dominant in the initial stage, phosphoric acid leaching occurs late in life and also depends on carbon and PTFE corrosion while carbon corrosion occurs during the whole cell life.

The platinum agglomeration mechanism is considered significant at temperatures exceeding 150°C [35] reducing the active electrochemical surface area (ECSA).

A better understanding of the physical process, which leads to the agglomeration of the catalyst particles, is an important step toward the improvement of the PEM fuel cell efficiency and durability. Many studies show the dependence of the catalyst agglomeration on the operating conditions [38].

In the attempt to separate the effect of operating conditions on performance degradation, in this work, different operational conditions have been analysed and compared thanks to electrochemical and nano-morphological diagnostic tools.

Since, at present, the main potential application for HT-PEM FC is distributed micro-cogeneration, literature on HT-PEM durability and performance degradation is mainly focused on steady-state operation [39–41] and its comparison with dynamic start/stop operation [21,42–44]. In these operation modes, many degradation mechanisms of different fuel cell components take place simultaneously and it is difficult to allocate malfunctions and effects. In order to focus on one single ageing phenomenon, it is necessary to develop specific testing procedures that allow forecasting and isolating a specific degradation mechanism. Some researches on HT-PEM FCs have been focused on the effect of temperature cycling [45,46] on fuel cell performance and electrocatalyst degradation, but a limited number of publications deal with catalyst degradation induced by load cycling [43,47]. Specific tests to characterize the electrocatalyst degradation based on load cycling operation are common in low temperature PEMFCs research [48] as dynamic load operation is widely investigated because of its importance for automotive applications. Indeed, carrying out ageing tests based on load cycling on HT-PEM fuel cells is not intended to study their behaviour in real applications, but it could be of great interest in order to isolate the effects of electrocatalyst degradation from other mechanisms that can be favoured during other operation modes. Load cycling has been proved to be a significant stressor for catalyst degradation [34,49–51] and it is possible to perform this operation keeping constant other parameters such as temperature and reactants flow.

Testing the performance degradation of HT-PEM fuel cells is a time-consuming and expensive process especially when the system to test is not just a single cell configuration but a complex micro-CHP system. Modelling becomes hence an indispensable tool to perform system performance analysis, compare configuration and study mitigation strategies.

Some HT-PEM fuel cell degradation models have been developed during the last decades [52–55] with the main purpose to increase the physical interpretation of degradation phenomena and improve the fitting of experimental data in various operational conditions. Deeply understanding the fuel cell operation and being able to model its behaviour in an analytic way it's a very difficult task given the complexity of the system and the enormous number of variables. However, modelling of the degradation process is an extremely useful tool to perform separation of each degradation mechanism and to establish a hierarchy between the degradation phenomena since it allows to perform parametric analysis of degradation processes on a very large scale.

Concerning micro-CHP system modelling, literature is mainly focused on energy performance analysis and system configuration optimization [11,56–58] while very few work has been done on degradation analysis of HT-PEM based micro-CHP systems.

Concerning the energy performance analysis of HT-PEM system considering typical domestic electric and thermal load profile there are, in literature, many examples of

models. For example, in [57] a high temperature PEMFC-based micro-CHP system similar to the one studied in this PhD work is considered. The overall efficiency is higher than 83%, with 28% of net system electrical efficiency and 55% of net system thermal efficiency. Fuel cell stack efficiency is 38%. The same authors, in [59], implemented a genetic algorithm to optimize the system and they improved the electrical efficiency up to 41% while thermal efficiency and total system efficiency were respectively 50% and 91%. As said before, a major problem for this type of HT-PEM FC based micro-CHP systems is the degradation rate that is much higher than the one of LT-PEM FC systems. Hence, when analysing micro-CHP systems, performance over long period, degradation should be considered. In [60] a simulation model of a HT-PEM micro-CHP system has been implemented and validate with experimental data. The model has then been used in [61] to analyse the system performance over one year of operation. As for the system degradation modelling, in [62], both the stack and reformer long term performance have been considered. A multi-objective optimization approach has been introduced in order to find the optimal operating parameters within the first 15 000 hours of operation while considering the impact of the degradation.

The research presented in this PhD thesis contributes to the advancement of knowledge in the field of HT-PEM FC, in particular, to what concerns the experimental analysis and the definition of degradation mitigation strategies, since literature is still poor of experimental data. Moreover, the introduction of degradation issues in the performance modelling of HT-PEM based micro-CHP systems is still in an early phase of development.

1.2. Aim of the research

The aim of this PhD work is to study the contribution of different operating conditions on the HT-PEM fuel cell degradation and identify some mitigation strategies and system configurations that could allow the integration of HT-PEM fuel cells stacks into a micro-CHP system for long term use.

The research question is: "*How does the degradation issue for HT-PEM fuel cells, installed in micro-CHP systems, can be handled to make the system become suitable for long term operation in terms of performance?*"

In this purpose an experimental campaign has been carried out on 8 MEAs subjected to different load profiles and start-stop cycles. To better understand the degradation phenomena involved in PEM fuel cells, several diagnostic tools have been used, in particular: Polarization Curve (PC), Electrochemical Impedance Spectroscopy (EIS) and Cyclic Voltammetry (CV).

Data have been compared with data obtained in previous works effectuated by the research group of the University of Trieste [13,38] and with literature. Additional information has been obtained thanks to SAXS and TEM analysis performed on the studied MEAs.

Afterwards experimental data as well as literature ones have been used to develop a numerical model allowing the performing of forecasting of fuel cell performance degradation as a function of operational time. This model has then been implemented in a previously developed micro-CHP system model obtaining a very useful tool for global system performance analysis of the system.

1.3.   Plan of the thesis

This thesis is divided in five chapters: Introduction, Theoretical background, Methodology, Results and discussion and Conclusions.

In this chapter, **"Introduction"**, the scientific context, the research question of this work and the "Plan of the thesis" are presented.

In the following chapter, **"Theoretical background"**, it is given the basic knowledge needed to understand the study carried out during this PhD activity and to correctly interpret the presented results.

In the third chapter, **"Methodology"**, the experimental methodology used to perform the laboratory tests as well as the electrochemical and Nano-morphological tools procedures are detailed. Finally, the model development approach is reported.

The fourth chapter, **"Results and discussion"**, presents the main results obtained during this PhD activity through experimental analysis based on various diagnostic tools that allowed the identification of some degradation mitigation strategies and the implementation of a degradation model in a micro-CHP system model that allowed obtaining the answer to the research question.

Conclusions and final remarks are discussed in chapter five: **"Conclusions"**

2.Theoretical Background

This chapter presents to the reader a brief overview of the base knowledge needed to understand and interpret the results presented in this thesis.

The fuel cell working principle and an overview of the existing type of fuel cells is given in §2.1, a deeper analysis of the main specificities of PEM fuel cells is given in §2.2 while §2.3 analyses the fuel cell performance from a thermodynamic point of view and gives an overview of the main dissipative phenomena that reduce the real fuel cell performance with respect to the ideal theoretical performance. An overview of degradation mechanisms occurring during the operation of PEM fuel cell is given in §2.4, in particular, the three main mechanisms occurring in high temperature PEM fuel cells are deeper analysed.

In §2.5 are then described the experimental methods used to study degradation as a function of the operational conditions and §2.6 gives an overview of the diagnostic tools used in this PhD activity to carry out the fuel cell performance analysis.

In §2.7 a state of art of modelling of HT-PEM fuel cells and micro-CHP system is given, to contextualize the modelling activity carried out in this PhD work.

2.1. Fuel cell principle and types

Fuel cells are electrochemical devices able to convert the chemical energy of fuels directly to electricity. A fuel cell is composed by an electrons conducting material (electrode) and an ions conducting material (electrolyte) that allows the physical separation of the oxidising agent and the reducing agent. In a fuel cell the chemical energy contained in the fuel (typically hydrogen) is oxidized to produce water. The total overall reaction is the same as the hydrogen combustion reaction:

$$H_2 + \tfrac{1}{2}\,O_2 \leftrightarrow H_2O$$
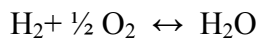
but thanks to the physical separation between reactants performed by the electrolyte, the overall reaction is split in two half reactions:

$$H_2 \leftrightarrow 2H^+ + 2e^-$$

$$\tfrac{1}{2}\,O_2 + 2H^+ + 2e^- \leftrightarrow H_2O$$
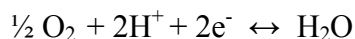
By spatially separating these reactions, the electrons transferred from the fuel are forced to flow through an external circuit (thus constituting an electric current) and due useful work before they can complete the reaction [63].

From the molecular point of view, combustion take place when hydrogen and oxygen molecules collide, and in a time-scale of picoseconds oxygen-oxygen and hydrogen-hydrogen bonds are broken and oxygen-hydrogen bonds are formed producing water and generating heat.

To produce electricity and hence work this heat must before be converted into mechanical work with an unavoidable loss of efficiency.

In fuel cells, by separating the reactants, the electrons transfer necessary to complete the reaction occurs over a greatly extended length scale and hence, the electrons moving from one species to the other can by harnessed as an electrical current. Hence fuel cells have the great advantages of:

- Higher energy conversion efficiency (even at low load)
- Lack of moving parts, hence theoretically highly reliable and long-lasting devices
- Virtually zero emissions
- Independent scaling between power and capacity
- High energy density and quick refuelling

However, major drawbacks still hampering the widespread diffusion of fuel cells, in particular:

- Power density limitation
- High production cost
- Fuel availability and storage
- Susceptibility to environmental poisons
- **Durability under variable load operation** *- our study focus*

Fuel cells are classified according to the electrolyte employed. The six most common technologies are:

- PEMFC (Polymer Electrolyte Membrane Fuel Cells)
    o LT-PEM (Low temperature PEMFC)
    o **HT-PEM (High temperature PEMFC)** *- our study focus*
- AFC (Alkaline Fuel Cells)
- PAFC (Phosphoric Acid Fuel Cells)
- MCFC (Molten Carbonate Fuel Cells)
- SOFC (Solid-Oxide fuel Cells)
- DMFC (Direct Methanol Fuel Cells)

While all six type of fuel cells works on the same electrochemical principle, they differs on temperature regimes, fuel tolerance, performance characteristics and hence application field as summarized in Table 1.

Fuel cell type	Electrolyte	Operating Temperature (°C)	Efficiency (%)	Fuel	Oxidising Agent	Power density mW/cm^2	Application Field
PEM – LT	Proton exchange membrane	50 – 100 LT 150 – 180 HT	50 – 60	Hydrogen	Oxygen / Air	300 – 900	Transportation, portable
PEM – HT	**Proton exchange membrane**	**150 - 180**	**60 – 70**	**Hydrogen**	**Oxygen / Air**	**300 – 900**	**Stationary applications**
AFC	Potassium hydroxide solution	Ambient – 90	60 – 70	Hydrogen	Oxygen / Air	300 – 500	Transportation, portable
PAFC	Phosphoric acid	160 – 220	55	Natural gas / Biogas / Hydrogen	Oxygen / Air	150 – 300	Stationary applications
MCFC	Molten mixture of alkali metal carbonates	600 - 700	65	Natural gas / Biogas / Coal gas / Hydrogen	Oxygen / Air	150	Stationary applications
SOFC	Oxide ion conducting ceramic	600 - 1000	50	Natural gas / Biogas / Coal gas / Hydrogen	Oxygen / Air	150 – 270	Stationary applications
DMFC	Proton exchange membrane	Ambient – 130	60	Methanol	Oxygen / Air	150 – 250	Transportation, portable

Table 1 Type of fuel cells

2.2. PEM Fuel cell

Unlike most other type of fuel cells, PEMFCs use a quasi-solid electrolyte, which is based on a polymer backbone with side-chain possessing acid-based group. Both cathode and anode are made up of a Catalyst Layer (CL) and a Gas Diffusion Layer (GDL). The catalyst layer can be attached to either the electrolytic membrane or to the GDL. A schematic cross section of a typical PEM fuel cell is shown in Figure 1.
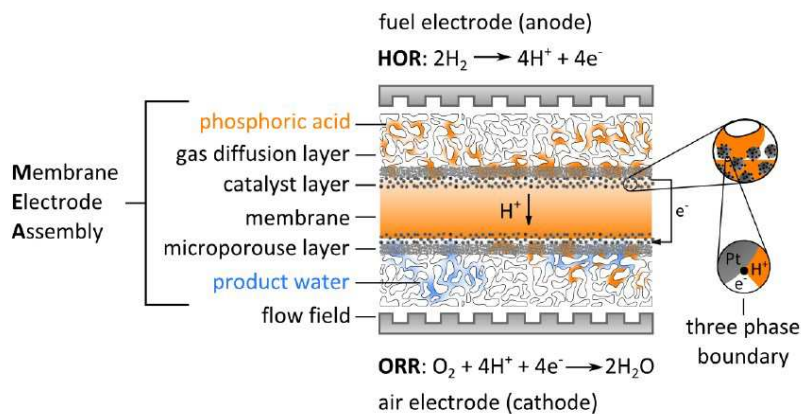
Figure 1 Schematic cross-section of a typical PEM fuel cell: gas diffusion layer, catalyst layer and polymer electrolyte membrane. Gas diffusion layer is constituted by a macro-porous substrate and a micro-porous layer [64]

The task of the gas diffusion layer is to distribute uniformly the reactants on the catalyst layer area, to provide conducting paths for electrons and facilitate the water removal from the MEA to the flow channels. GDL typically consists of two layers, a macro-porous substrate and a micro-porous layer (MPL) or diffusion layer. The macro-porous substrate is made of a carbon fibre matrix with a large void volume, while the micro-porous layer consists of carbon black mixed with fluoropolymer. The catalyst layer or active layer is constituted by catalyst nanoparticles of platinum or platinum alloys deposited on a high-surface-area carbon support. The electrocatalyst usually is in the form of nanoparticles of about 3 nm in order to maximize the active catalytic surface area per unit mass of platinum [49]. Particles size is normally not further decreased because smaller platinum particles start to be significantly unstable. The stability of platinum, platinum alloys, carbon support and the interaction between platinum nanoparticles and carbon support strongly affect PEM fuel cells durability [65]. The polymer electrolyte membrane material choice is crucial and differs for each fuel cell type. PEM fuel cells are divided in two main groups: Low Temperature PEM (LT-PEM) and High Temperature PEM (HT-PEM). The main difference between these two types of PEM fuel cell consists in the material of the polymer electrolyte membrane that in the case of LT-PEM is a perfluorinated sulfonic acid polymer (usually Nafion[®]) while for HT-PEM is a polybenzimidazole polymer (PBI) usually doped with phosphoric acid. These two materials behave in a very different way concerning ion transfer, indeed, as for LT-PEM the ion transfer is performed thanks to the water contained in the Nafion[®] membrane; for phosphoric acid (H_3PO_4) doped PBI membranes, this role is played by the phosphoric acid eliminating the hydration problems of LT-PEM membranes; however, the higher vapour pressure required in HT-PEM FCs results in a somewhat lower Nernst potential [55] with a consequent performance reduction.

The differences between the two membranes influence the operating conditions of the fuel cells in terms of fuel characteristics requirements, water management system and of course operating temperature. While for LT-PEM the ideal operating temperature range from 60 to 80 °C, HT-PEM optimum operation temperature is 160°C-180°C which makes product water to be in vapour state.

The oxidation/reduction reaction takes place at the so called Three Phase Boundary (TPB) which is the triple contact point between the Pt catalyst layer, the electrolyte membrane and the gas phase pores. In order to maximize the reaction surface area, highly porous, nanostructured electrodes are fabricated to achieve intimate contact between gas phase pores, electrically conductive electrode and ion-conductive electrolyte membrane [63]. The membrane also inhibits electrons conductivity which are hence transferred externally from the fuel electrode (anode) to the air electrode (cathode) [64].

The proton conductivity of the H_3PO_4 PBI membranes depends on the phosphoric acid doping level, relative humidity, and temperature [9]. Even though the proton conductivity of the H_3PO_4 PBI membranes increases with increasing relative humidity, the dependence is much weaker than that of Nafion[®] [55]. Current studies regarding H_3PO_4 PBI HT-PEM FCs electrolyte membranes have focused on the membrane conductivity [66] the optimum amount of H_3PO_4 content of the electrolytes [67], the resistance of the membrane varying with temperature [68] and the effect of porosity on power generation [69].

2.3. Fuel cell performance

2.3.1. Fuel Cell thermodynamics

The work produced by a fuel cell is:

$$W_{el} = q \times V$$

Where W_{el} *(Joule/mole)* is the electrical work per mole of hydrogen, q *(Coulomb/mole)* is the transferred charge and V *(Volts)* is the electrical potential.

Hence, the total electrical charge transferred for each mole of hydrogen consumed is:

$$q = n \times N_{Av} \times q_{el}$$

Where n is the number of electrons per molecules, N_{Av} is the Avogadro number corresponding to the number of molecules per mole *(6.022x10²³)* and q_{el} is the charge of the electron *(1.602x10⁻¹⁹ C)*. It is, hence, possible to rewrite the work produced by a fuel cell per mole of consumed hydrogen as:

$$W_{el} = n \times F \times V$$

With $F = N_{Av} \times q_{el} = Faraday\ Constant = 96485\ ^{C}/_{mol}$

Starting from the first principle of thermodynamics:

$$dU = \delta Q - \delta W = \delta Q - \delta W_{el} - PdV$$

where for reversible transformation $\delta Q = TdS$ and considering the definitions of enthalpy and Gibbs free energy:

$$H = U + PV$$

$$G = H - TS$$

It can be written:

$$dH = dU + VdP + PdV = TdS - PdV - \delta W_{el} + VdP + PdV$$

And

$$dG = dH - SdT - TdS = TdS - PdV - \delta W_{el} + VdP + PdV - SdT - TdS$$

That for isothermal and isobaric transformations can be written:

$$dG = -\delta W_{el}$$

Moreover, for adiabatic transformation it can be written:

$$dG = dH$$

And hence the maximal potential for adiabatic and reversible transformations can be written:

$$V_{max} = -\frac{dH}{n \times F}$$

This is called the Thermal Voltage and corresponds to the maximal potential obtainable if all the chemical energy would be transformed in electrical work with no variation in entropy.

Since fuel cells can produce water either in liquid or in gaseous state, the thermal voltage is dependent on the state of the product water [70].

For a hydrogen/oxygen fuel cells producing liquid water:

$$\Delta H = \left(h_f\right)^{liq}_{H_2O} - \left(h_f\right)_{H_2} - \frac{1}{2}\left(h_f\right)_{O_2} = -285{,}83 \; kJ/mol$$

And hence:

$$\boldsymbol{V_{max}} = \frac{286 \; kJ/mol \times 1000}{2 \times 96485 \; C/mol} = \boldsymbol{1{,}48 \; V}$$

While for a fuel cells producing gaseous water:

$$\Delta H = \left(h_f\right)^{gas}_{H_2O} - \left(h_f\right)_{H_2} - \frac{1}{2}\left(h_f\right)_{O_2} = -241{,}82 \; kJ/mol$$

And hence:

$$\boldsymbol{V_{max}} = \frac{241{,}82 \; kJ/mol \times 1000}{2 \times 96485 \; C/mol} = \boldsymbol{1{,}25 \; V}$$

Obviously, it is impossible to convert the total heating value of the hydrogen into electrical work. The thermodynamic electromotive force (EMF) or reversible Open Circuit Voltage (OCV) E^0 of any electrochemical device is defined as:

$$E^0 = \frac{\Delta G}{n \times F}$$

It is the expression of the maximum voltage that can (theoretically) be obtained from the electrochemical reaction taking into account entropy variations and hence considering non-adiabatic transformations.

In this case for isothermal transformations

$$\Delta G = \Delta H - T\Delta S$$

Hence, considering the entropy variation in the case of liquid water:

$$T\Delta S = T \times \left(s_f\right)_{H_2O}^{liq} - \left(s_f\right)_{H_2} - \frac{1}{2}\left(s_f\right)_{O_2} = 298,16\,K \times -163,23\frac{J}{mol \cdot K} = -48,67\frac{kJ}{mol}$$

$$E^0 = \frac{\Delta G}{n \times F} = \frac{-285,83 + 48,67\,kJ/mol \times 1000}{2 \times 96485\,C/mol} = \mathbf{1,23\,V}$$

While in the case of water in gaseous state:

$$T\Delta S = T \times \left(s_f\right)_{H_2O}^{gas} - \left(s_f\right)_{H_2} - \frac{1}{2}\left(s_f\right)_{O_2} = 298,16\,K \times -44,34\frac{J}{mol \cdot K} = -13,22\frac{kJ}{mol}$$

And hence:

$$E^0 = \frac{\Delta G}{n \times F} = \frac{-241,82 + 13,22\,kJ/mol \times 1000}{2 \times 96485\,C/mol} = \mathbf{1,18\,V}$$

2.3.2. <u>Nernst equation</u>

While $\mathbf{V_{max}}$ depends only on the temperature, the theoretical electromotive force $\mathbf{E^0}$ depends also on the pressure; this dependency is in general described by the Nernst equation.

Considering the generic formulation of redox chemical reaction:

$$v_a A + v_b B \longleftrightarrow v_c C + v_d D$$
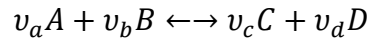
Where v_x are the stoichiometric coefficients of the species x.

From the thermodynamic of the system at equilibrium it can be written:

$$E(T,P) = \frac{-\Delta G(T)^0}{nF} + \frac{RT}{nF}\ln\left(\frac{\gamma_A^{v_a}\gamma_B^{v_b}}{\gamma_C^{v_c}\gamma_D^{v_d}}\right)$$

Where n is the number of exchanged electrons, F the Faraday constant and $\gamma_X^{v_x}$ the activity of the species x. And hence:

$$\mathbf{E(T,P) = \frac{-\Delta G(T)^0}{nF} + \frac{RT}{nF}\ln\left(\frac{(P_A/P^0)^{v_a}(P_B/P^0)^{v_b}}{(P_C/P^0)^{v_c}(P_D/P^0)^{v_d}}\right)}$$

Where P_x/P^0 are the partial pressures of the species x.

This last formulation is known as **Nernst Equation** for a perfect gas and allows to determine the maximum theoretical electromotive force deliverable by a fuel cell at a given temperature and pressure.

2.3.3.   Dissipative phenomena

The real performance of a fuel cell is affected by various dissipative phenomena that reduce the theoretical performance calculated through the Nernst equation following the procedure detailed in the previous paragraphs.

Fuel cell performance losses are classified in five categories listed in Table 2 and better described further below in this paragraph:

Type of loss	Definition	Expression
Cross-over losses and mix potential	They are due to internal currents generated by the mass transfer throughout the electrolyte or other contaminations or impurities	$j = j_0 - j_{corss-over}$
Activation losses	Correspond to the electrical potential needed to overpass the activation threshold energy of the electrolytic reaction on the catalytic surface	Bulter-Volmer equation Tafel equation $$\eta_{act} = a + nlog\,j$$
Ohmic losses	Losses due to the electrical conduction through the electrolyte, the catalytic layer, the connections and the links	Ohm's law $$\eta_{Ohmic} = j(R_{elec} + R_{ionic})$$
Concentration losses	They correspond to a limitation of mass transport of reactants to the electrodes due to a decrease of the surface concentration of reactants with a consequent loss in thermodynamic potential	Nernst equation and Bulter-Volmer equation $$\eta_{conc} = cln\frac{j_L}{j_L-j}$$
Entropy losses	Due to thermodynamics irreversibility	Thermodynamic second law $$\frac{dS}{dT} = \frac{1}{T}\frac{\delta Q}{dt} + \frac{dS_{irr}}{dt}$$

Table 2 Dissipative phenomena

In an ideal fuel cell, only hydrogen oxidation and oxygen reduction would occur. In reality, cross-over of hydrogen from anode to the cathode and the presence of intermediate substances such as H_2O_2 at the cathode reduce the potential difference between anode and cathode. A third process contributing to the reduction of the theoretical potential is the

oxidation of platinum with water at the air electrode. These three phenomena caused the so called mixed potential losses [64].

At low current densities, the working potential is diminished mainly by the kinetic of the charge transfer, which depends on the oxygen reduction and hydrogen oxidation reactions rates at the electrode surface. The exchanged current density can be expressed through the Bulter-Volmer equation in the following way:

$$j = j_0 \left\{ exp\left(\frac{\alpha nF\eta_{act}}{RT}\right) - exp\left(\frac{\beta nF\eta_{act}}{RT}\right) \right\}$$

Where η_{act} represents the activation losses, α and β are the transfer coefficients ($\alpha + \beta = 1$) and n is the number of electrons involved in the oxidation-reduction reaction which differs from the total exchanged electron number. For high η_{act} values Bulter-Volmer equation can be rewritten as shown in Table 2:

$$\eta_{act} = a + b \log(j)$$

At medium current densities, the working potential is mainly affected by ohmic losses due to contact electrical resistance of the fuel cell components and the ion conductive resistance of the electrolyte membrane.

At high current densities the working potential is mainly affected by the mass transport losses. Mass transport losses are caused by the fact the reactant convection and diffusion rate becomes slower than reaction rate, causing a decrease of the surface concentration of reactants with a consequent loss in thermodynamic potential. To calculate the voltage loss due to reactant depletion at catalyst layer, it is necessary to calculate how much the Nernst potential changes when the partial pressure of reactants changes. To do so, it can be written:

$$\eta_{con} = E_{Nernst}^0 - E_{Nernst}^* = \left(E^0 - \frac{RT}{nF}\ln\frac{1}{c_R^0}\right) - \left(E^0 - \frac{RT}{nF}\ln\frac{1}{c_R^*}\right) = \frac{RT}{nF}\ln\frac{c_R^0}{c_R^*}$$

Where c_R^0 is the bulk reactant concentration, c_R^* is the catalyst layer reactant concentration.

The calculation of effective diffusivity (D^{eff}) of reactants allows the definition of a limiting current density j_L which corresponds to the fuel cell current density for which reactants concentration fall to zero [63]:

$$j_L = nFD^{eff}\frac{c_R^0}{\delta}$$

Where δ is the electrode (diffusion layer) thickness.

Introducing the expression of j_L in the concentration losses expression, it can be rewritten as:

$$\eta_{con} = \frac{RT}{nF} \ln \frac{j_L}{j_L - j}$$

The reduction of reactant concentration also affects the reaction rate, but this effect only modifies the previous expression of η_{con} by adding a multiplying constant: $\frac{1}{\alpha nF}$ [63].

2.4. Degradation mechanisms

Understanding the degradation mechanism and establish a hierarchy between them is a very important issue in order to implement adapted production or operation procedures able to enhance lifetime of fuel cell.

Degradation of fuel cell can involve all the component of the fuel cell:
1. Catalyst layer degradation
2. Membrane degradation
3. Gas Diffusion Layer degradation
4. Bipolar plate degradation
5. Other component degradation (seals, endplates, and bus plates)

Many authors tried to identify and classify the degradation processes of HT-PEM fuel cells through experimental testing and numerical simulations [35,71,72]. According to these studies, the primary degradation mechanisms are considered to be:
1. Carbon corrosion
2. Platinum agglomeration
3. Acid leaching/flooding.

Moreover literature seems to agree that different degradation phenomena occur at different stages of the fuel cell lifetime. As mentioned in [36] and in [37], in general operation conditions, the platinum agglomeration is dominant in the initial stage, phosphoric acid leaching occurs late in life and also depends on carbon and PTFE corrosion while carbon corrosion occurs during the whole cell life.

Degradation modes of HT-PEM PBI-H_3PO_4 membranes have been summarized in a remarkable work carried out by [35]. In this work the degradation mode related to the membrane degradation has been identified in the possible formation of pin-holes due to the thinning of the membrane that can cause H_2 cross-over from anode to cathode and to phosphoric acid evaporation. Experimental test performed on MEA Celtec P-1000 (the same used in this PhD work for the experimental tests) showed no significant impact of acid evaporation on cell lifetime due to a very low acid evaporation rate due to the specific properties of the studied membrane. Concerning catalyst degradation, three main

degradation mechanisms have been identified: corrosion of the catalyst metal (both particle growth and dissolution), corrosion of the carbon materials in electrodes (catalyst support and GDL materials) and PTFE degradation. The first two modes seem to be strongly influenced by operational conditions, in particular temperature and electrochemical potential.

In literature, several degradation mechanisms have been suspected of being responsible for the faster degradation of HT-PEM FCs with respect of LT-PEM.

Suzuki et al. [55] showed that the overall cell voltage deterioration was a combined result of the PA evaporation and loss of electrochemical active surface area (ECSA) in the cathode electrode; [73] demonstrates that the rate of carbon corrosion was significantly increased at an elevated cell temperature, which implied that the effect of carbon corrosion and catalyst aging must be substantial during HT-PEMFC operations.

Moreover, as stated in [65] the kinetics of carbon corrosions are substantially enhanced at the higher potential near the OCV and higher operating temperature. Therefore, the catalyst degradation is more exacerbated during start-stop and load cycling compared to a constant current load, while PA evaporation driven by temperature rise and PA dilution by water condensation during the shut-down and subsequent cool-down procedures are significant contributors to the PA loss [73].

In particular the high potential at the cathode, introduced by the hydrogen/air interface at the anode, is the major cause of performance degradation during start-up process [74]. In fact the first step of the start-up process consists in the introduction of air or oxygen into the cathode and hydrogen into the anode. Because of the presence of air in the anode, a hydrogen/air interface is formed into the flow field at the anode. In addition, if in the fuel cell there is a bad gas flow distribution during the start-up process (called local fuel starvation), oxygen could cross the membrane from the cathode to the anode due to a pressure or concentration gradient, creating again a hydrogen/air interface.

The same situation can also occur in the shutdown process. In fact when reactant supplies are shut off, residual gas will remain in the channels and oxygen or air can flow from anode to cathode though the membrane thanks to concentration gradient, moreover atmospheric air can also permeate due to seal failure.

The platinum agglomeration mechanism is considered significant at temperatures exceeding 150°C reducing the active catalytic surface area (ECSA) [35].

In [36] the degradation modes classifications for HT-PEM membranes carried out by [35] has been upgraded and completed giving a quite exhaustive summary of causes, effects and mechanisms of degradation phenomena of HT-PEM MEAs. It must be underlined that many of these degradation processes are common also in LT-PEM FCs. In Table 3 is reported a summary of the main degradation processes.

Degradation mode	Effect	Cause
MEMBRANE DEGRADATION		
Pin hole formation	H_2 crossover → Decreased fuel efficiency	Creep, fibers, f(compression)
Membrane thinning	H_2 crossover → Decreased fuel efficiency	Creep, fibers, f(compression)
Phosphoric acid leaching from membrane	Loss in proton conductivity → Increased Ohmic-losses	Evaporation, f(T,p)
HO and HO_2 radicals oxidative degradation	H_2 crossover Loss in proton conductivity → Increased Ohmic-losses	
ELECTRODE DEGRADATION		
Pt particles agglomeration	Loss in ECSA → Decreased kinetics	Migration, f(T) Dissolution/recrystallization, f(T,E)
Pt particles dissolution	Loss in ECSA → Decreased kinetics	Dissolution, f(T, E)
Phosphoric acid leaching from catalyst layer	Loss in ECSA → Decreased kinetics	Evaporation, f(T,p)
Carbon corrosion	→ Increased Ohmic-losses Loss in ECSA → Decreased kinetics Flooding →Increased mass transport losses	Electrochemical oxidation, f(T,E,p) Fuel starvation, OCV operation
GDL corrosion	→ Loss of structural integrity → Increased Ohmic-losses Flooding →Increased mass transport losses	Electrochemical oxidation, f(T,E,p)
PTFE corrosion	Loss in hydrophobicity, flooding →Increased mass transport losses	Electrochemical oxidation, f(T,E,p)
Catalyst poisoning	Loss in ECSA → Decreased kinetics	Adsorption, f(T, gas composition)
BIPOLAR PLATES DEGRADATION		
Corrosive pinholes formation	Loss in plates material →Fuel and oxidant mixing	F(E,T, gas composition)
Micro Pores and cracks formation	Loss in plates material →Fuel and oxidant mixing	Thermal cycling
Electrocatalyst poisoning	Loss in ECSA → Decreased kinetics	F(E,T, gas composition)
Passive layer formation	Loss in proton conductivity → Increased Ohmic-losses	F(E,T, gas composition)
Cracking	→Fuel and oxidant mixing → Loss of structural integrity	Mechanical shocks Thermal cycling

Table 3 Review of HT-PEM degradation modes. T: Temperature, p:Partial pressure of water, E: Electrochemical potential [36]

Even if some consensus seems to emerge regarding the main degradation pathways, some observed phenomena are still not fully understood such as the strong degradation increase at open circuit voltage (OCV) reported by many authors or the degradation increase at low relative humidity [75].

A typical voltage degradation rate for HT-PEM FCs operating in a temperature range of 150-190 °C is of around 5 - 60 mV/h while the degradation of LT-PEMFCs is much slower, usually 2-10 mV/h [76].

As mention above, for HT-PEM, the three main degradation mechanisms are considered to be: carbon corrosion, platinum agglomeration and acid leaching/flooding. The following paragraphs briefly describe these three main degradation processes.

2.4.1. Carbon corrosion

Carbon support of the catalyst layer has the function to anchor the catalyst platinum nanoparticles and to provide electrical conductivity to the GDL and bipolar plates. The electrochemical corrosion of the carbon support materials causes electrical insulation of the catalyst particles which can results in accumulation of charge in the porous electrode and GDL structure. This is due to the brake away of the catalyst particles from the support. Aggregation of platinum particles with consequent ECSA decreasing is also favoured by carbon support structure failure. Carbon corrosion occurs following the reaction indicated here below:

$$C + 2H_2O \rightarrow CO_2 + 4H^+ + 4e^-$$
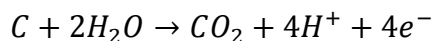
Even if the standard electrode potential of the carbon corrosion reaction (E_0=0.207 V) is in the range of the normal fuel cell operation, the reaction, in this potential range and for low operative temperatures, is very slow and hence negligible for short time operation. On the other hand in long-term operation, or at higher temperatures and higher voltage ranges (higher than 0.8 V), carbon corrosion can strongly affect the durability of the fuel cell [65].

Carbon corrosion depends on voltage and follows the Taefel behaviour, while its dependence with temperature follows the Arrhenius behaviour. During start up and shut down processes, local fuel-starved areas are created at the cathode causing local high potentials that brings to carbon corrosion. OCV operation generalises this situation to the whole cathode active surface causing important corrosion of the catalyst support.

At operating temperatures higher than 160°C carbon corrosion currents can be quite large: currents of 1-10 mA/mg$_{carbon}$ have been observed for Vulcan XC-72 at 180°C and 1.0 V [35,77].

2.4.2.   Catalyst degradation

PEM fuel cell electrodes consist of carbon-supported nanoparticles of platinum or platinum alloys for both anodes and cathodes. The nano-scale particles provide theoretical surface areas of over 100 m^2/g and fuel cell active areas of 25-40 m^2/g [65]. According to literature [78] the Pt/C electrocatalyst suffered from the strong adsorption effect of anions onto the active sites of catalysts in H_3PO_4 solution. Therefore, the strong adsorption effect of anions should be responsible for the lower ECSA of Pt/C electrocatalyst in the H_3PO_4/PBI HT-PEM FC with respect to LT-PEM FC that can have ECSA higher than 60 m^2/g [79].

One of the main causes of PEM fuel cells performance loss is supposed to be the reduction of the electrochemical surface area (ECSA) of the electrocatalyst [80], this occurs especially at the cathode due to high potential. ECSA loss is mainly attributed to three different phenomena related to the electrocatalyst: dissolution, agglomeration and isolation, [49] of platinum nano-particles.

Dissolution is caused by the platinum oxidation in aqueous acid electrolytes. Chemical state of the platinum surface and the platinum species in solution govern the Pt solubility. Solubility is influenced by the electrolyte materials, the nature of the solvent, the pH, the temperature and potential. Pt solubility it's an endothermic reaction and hence increases with temperature following the Arrhenius relationship [65]. The dissolution reaction seems to be more dependent on the oxidation-reduction cycles rather than on the length of the cycle or time at oxidizing potentials. Pt is slowly oxidized during operation at high potential (0.85-0.95 V) [65]. However, the presence of oxygen in a gas-phase accelerates the oxidation at high potentials; fuel cell performance can be halved in just 1 h of operation. The loss has been attributed to the blocking of Pt surface sites to take part in the oxygen reduction reaction by the formation of platinum oxide [81]. The performance loss due to Pt oxidation, however, is completely recoverable with a short excursion of the cathode potential to a value lower than 0.5 V that trigs the reduction of the oxide layer formed at the higher cathode potentials [82]

Platinum dissolved in the ionomer phase can then either deposit on existing platinum particles to form larger particles ("*Ostwald ripening*") or re-deposit on new sites forming new particles with very different statistics of crystallite size distribution ("*Re-precipitation*"). Dissolved platinum can also be transport out of the fuel cell or diffuse and re-deposit into electrochemically inaccessible portions of MEA where the triple-phase boundary is not available and hence lose its functionality.

Another phenomena, known as "*coalescence*" occurs when Pt particles are in close proximity and sinter together to form larger particles.

Isolation occurs when carbon corrosion leads to electrically isolated Pt particles that are detached from the support and hence not available anymore in the three-phase boundary zone

2.4.3.   <u>Acid loss and flooding</u>

Phosphoric acid loss from membrane and electrodes is a peculiar degradation phenomenon of high temperature PBI based phosphoric acid-doped PEMFC. Phosphoric acid loss can occur due to capillary transport, diffusion, membrane compression, evaporation and mainly by leaching due to product water; acid leaching is enhanced at high current densities where more water is produced and during transient modes, such as start-up and shut-down processes where water can condensate into liquid phase [83]. Indeed, in [47] a sharp increase in phosphoric acid loss from the cathode is attributed to liquid water formation caused by a facility event. A reduction of the acid may be responsible of lower conductivity of the electrode along with a reduction of three phase boundary zone [84].

Carbon corrosion/oxidation causes the carbon surface to become more hydrophilic [85]. The increased hydrophilicity of the carbon surface can also increase the phosphoric acid depletion. Indeed a more hydrophilic carbon surface at the anode can induce product steam to condensate.

Flooding of the catalyst support is another consequence of carbon corrosion, indeed increasing the hydrophilicity of the surface it will be more readily flooded by H_3PO_4; this results in higher mass transport resistance [86]. Indeed flooding of pores of the carbon structure obstructs the gas transport.

2.5.   Accelerated Stress Tests

At present, technical characteristics of PEM fuel cell in terms of durability are promising but still quite far from industry expectations. The reduction of aging processes of PEM fuel cell components is still one of the main fuel cells research challenges.

To allow the study of the degradation process research must select a methodology which follows three main requirements:

- **Reduction of test time :** need to estimate life-time of a fuel cell in the shortest time as possible
- **Separation of degradation processes:** the degradation of a fuel cell is a complex process which involves many different components and degradation phenomena. To allow identifying the working parameters affecting each degradation process it is necessary to make the study of each phenomena and component as independent as possible.
- **Reproducibility and uniformity:** To allow the scientific community to evolve, each characterisation of fuel cell working parameter and aging effect should be exploitable from everybody. Compare different studies which have different methodologies and different check parameters it is very difficult. Standardisation of test processing is a huge step forward to the improvement of fuel cell performances

2.5.1. Reduction of test time

Since the beginning of the analysis of fuel cell durability, scientific community started to study a way to allow the life time evaluation of the fuel cells without performing a test lasting as long as the fuel cell life time.

Some working conditions affect durability of the fuel cell more than others. However, the evaluation of the life time of a fuel cell, to be useful, must be done in the respect of the real working conditions.

Therefore, choosing extreme working conditions would drastically reduce time-test but would turn away the results from the real applications.

The purpose is then to reproduce real working conditions that could sensibly affect the durability of the fuel cell and increasing their frequency of occurrence in a controlled way. This should allow reproducing real working conditions during the fuel cell life-time in a much shorter time.

2.5.2. Separation of degradation processes

The purpose of durability studies is not just to characterise fuel cell life time but to increase it in order to meet the market expectations and allow fuel cell diffusion.

In this purpose it is indispensable, firstly, to understand what are the main degradation phenomena and which fuel cell component is affected the most, and secondly, to link the effect of each working condition to its predominant degradation phenomena and component.

This is a hard work which involved many research groups in the last decades. A remarkable work has been done in 2009 by Zhang et al. [33] in this sense.

Literature seems to agree on the methodology which aims to study the degradation phenomena separating them by fuel cell component.

There is a first separation step which provides two different methodologies for the study of single cell degradation and stack degradation.

Afterwards, in literature, it can often be found the following separation by fuel cell components [34]:

1. Catalyst layer degradation
2. Membrane degradation
3. Gas Diffusion Layer degradation
4. Bipolar plate degradation
5. Other component degradation (seals, endplates, and bus plates)

To this separation, is often added an ulterior analysis of special working conditions which affects the durability of the cell in a sensible way [65]:

1. Impurity Effects
   a. Fuel impurities
   b. Air impurities
2. Subfreezing effects
3. Other operating conditions :
   a. Challenging dynamic loads
   b. Fuel Starvation
   c. Start and Stop
   d. Temperature
   e. Relative Humidity

To allow the separate analysis of each component many authors have developed different accelerated stress tests (ASTs) protocols.

The complexity in load cycle profiles is given by the fact that respecting the criterion quoted in the previous paragraph, load cycle should not just tend to improve a specific degradation process but also to respect the real application working parameters.

For this reason different load cycles are aimed to study the same phenomena on the same fuel cell component but for different final purposes in particular:

   o automotive
   o stationary

Moreover there is additional complexity given by the fact that each fuel cell technology needs different standard protocols.

Therefore, for example for PEM FC, there is a quite reach sample of testing protocols for LT PEM FC but quite few has been developed for HT-PEM FC, and some authors still using test protocols of LT PEM for characterise HT-PEM FC or proposing new test protocols for HT-PEM FC [12,13]

2.5.3.   <u>Reproducibility and Uniformity</u>

Following the two main purposes explicated in the previous paragraphs many authors experienced different fuel cell testing protocols.

Scientific literature became than reach in protocols but poor in uniformity and standardisation. The first step toward standardisation has been done by authors who tried to list, reference and compare existing protocols.

A remarkable work has been done by Wu et al. [28] in 2008, where a very large of existing protocols are listed and divided by cell component.

Afterward, institutional research groups such as: US department of Energy (DOE), the US Fuel Cell Council (USFCC), the US Council for Automotive Research (USCAR), Fuel Cell Hydrogen Energy Association (FCHEA), the European Joint Research Centre (JRC), the International Electrotechnical Commission (IEC), started to work in the purpose to standardize the protocols of fuel cells testing.

Each institution published separately their own standard test protocols.

Finally in 2010 the common effort has been done by the US and the EU institutions to standardize and harmonize their different methods. A uniform testing protocol for single cells was then validated in a round-robin experiment in the EU and the US bringing to the publication of the IEC norm TS 62282-7-1 [87].

The next step will be the standardisation and harmonisation of protocols to characterize PEMFC stacks.

However, even on single cell, the harmonisation process is still not completed and some authors keep working on reviewing and comparing existing protocols [34,88] to allow harmonisation.

In literature new suggestions of test protocols [12] continue to by suggested especially for HT-PEM FC for which literature is poor; institutional research group still constantly updating their protocols [89]; however, an important step forward has been done by the JRC for the automotive applications in 2015 with the publication of an harmonized test protocol for PEMFC [90] on which is based the test methodology applied in this PhD work.

2.6. Diagnostic Tools

With the purpose to improve the fuel cell durability and performance, a wide range of diagnostic tools for the analysis of PEM fuel cells have been developed to help gain a fundamental knowledge of fuel cell dynamics, to diagnose failure modes and degradation mechanisms, mitigate performance losses and provide data for modelling of fuel cells. Due to the complexity of the fuel cell environment there are typically multitudes of parameter to be analysed. Diagnostic tools are usually divided in to big families: *in-situ* diagnostic tools and *ex-situ* diagnostic tools [91]; however, some of them can be done in both situations, for example measurement of gas permeability and SAXS can be a priori performed *in-situ* and *ex-situ*. Diagnostic tools can also be divided in electrochemical diagnostic tools and nano-morphological diagnostic tools depending on the type of analysis allowed by the specific method.

Some diagnostic tools, such as Polarization Curve, Cyclic Voltammetry (CV), Electro Impedance Spectroscopy (EIS), Scanning Electron Microscopy (SEM) and Transmission Electron Microscopy (TEM) are nowadays, very common and widely used while some others are more exotics and they have not reached yet the scientific maturity and/or diffusion, such as Transparent Cell, Cathode Discharge, Current Mapping, Magnetic Resonance Imaging (MRI), Atomic Force Microscopy (AFM) and Small Angle X-Ray Scattering (SAXS).

In this PhD activity three diagnostic tools have been adopted for the electrochemical analysis: Polarization Curve, EIS and Cyclic Voltammetry; while for the nano-morphological analysis the SAXS tool has been used and results have been compared with the one obtained with TEM analysis.

In this chapter is given an overview of the diagnostic tools used during this PhD activity.

2.6.1. Electrochemical diagnostic tools

2.6.1.1. Polarization curve

The polarization curve is the standard electrochemical technique for characterizing the performance of fuel cells, and consists in the plot of the cell voltage versus the current density. Polarization curve yields information on performance losses in the cell under operating conditions. By measuring polarization curves, the effect that certain parameters have on fuel cell performance can be characterized and compared systematically [91]. To do so measurement of polarization curves must follow a strict and repeatable test procedure as described in §3.2.1.

As described in §2.3 the theoretical voltage of an electrochemical reaction depends on its Gibbs free energy ΔG_r:

$$\Delta G_r = -nFE$$

Where *n* is the electron transfer number in the reaction, *F* is the Faraday constant and *E* is the theoretical voltage (ie. *nFE* is the electrical work done by an electrochemical reaction).

As already seen in §2.3, the reaction Gibbs free energy can be obtained by the following formula:

$$\Delta G_r = \Delta G_r^0 + RT ln \frac{\prod \gamma_{Products}^{v_i}}{\prod \gamma_{Reactants}^{v_i}}$$

Where ΔG_r^0 is the standard reaction Gibbs free energy, *R* is the gas constant, *T* the is the absolute temperature, γ is the activity of the product and v_i is the stoichiometric coefficient of the species *i*. Thus,

$$E_N = E^0 - \frac{RT}{nF} ln \frac{\prod \gamma_{Products}^{v_i}}{\prod \gamma_{Reactants}^{v_i}}$$

Where E^0 is the standard thermodynamic voltage at 25°C and the activities of both reactants and products are equal to 1 and E_N stands for Nernst Voltage since this is nothing else than the Nernst equation already seen in §2.3 that for a H_2/O_2 PEM fuel cell take the form:

$$E_N = E^0 - \frac{RT}{2F} ln \left[\frac{\gamma_{H_2O}}{p_{H_2}\sqrt{p_{O_2}}} \right]$$

Where E^0 is equal to 1.229 V under standard conditions and water produced in liquid phase; p_x is the activity of the species x expressed as partial pressure in atmosphere.

The Open Circuit Voltage (OCV) is the voltage provided by a fuel cell in the condition of no electrical load. When current approaches to zero, true electrochemical equilibrium can be achieved, which represent the voltage E_N calculated on by Nernst equation and dependent on thermodynamics conditions as shown in Figure 2. In practice, OCV is always lower than theoretical OCV. This difference results mainly from fuel cross-over from the anode to the cathode; sometimes impurities or current leakage can also cause an OCV reduction.
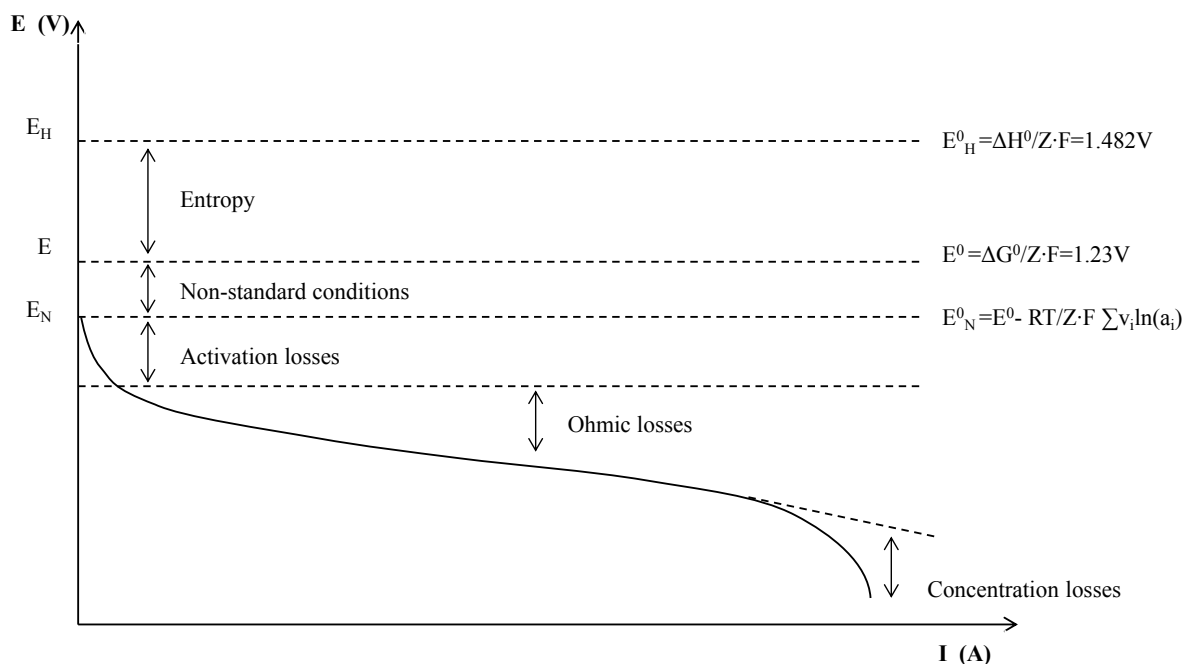
Figure 2 Typical polarization curve of a PEMFC

The OCV is of less practical use because no power output occurs under this condition. It is much more useful the working potential as function of the current density changes, that is the polarization curve. The working potential is always lower than the OCV and decreases

as the current density increases. A polarization curve can be divided into three regions corresponding to activation, ohmic and mass transport dominated voltage losses as shown in Figure 2.

In the low current region the working potential loss is mainly due to the charge-tranfert kinetics, that is, O_2 reduction and H_2 oxidation rates at the electrode surface. In the intermediate current density range, the working potential drop is mainly due to internal resistance, including electric contact resistance and the proton resistance of the proton-conducting membrane. In the high-current density range, the working potential decreases rapidly because the transfer speed of reactants and products is lower than the reaction rate. The transfer of reactants in the fuel cell is called mass transport and consist in convection and diffusion.

Although polarization curve is a useful indicator of overall performance of the cell or stack under specific operating conditions, it fails to produce much information about the performance of individual component within the cell. It cannot be obtained during normal operation of the fuel cell and take significant time to complete. In addition it fails to differentiate mechanisms from each other.

2.6.1.2. Electro Impedance Spectroscopy

EIS is a non-destructive measurement technique that provides detailed diagnostic information about a wide range of electrochemical phenomena including charge transfer reaction at the interface electrode/electrolyte, reaction mechanism, electrode material properties and general state of health of fuel cells. The technique involves applying a low-level alternative current waveform to the electrochemical system under investigation and measuring the response of the cell to this stimulus. Typically, a swept frequency sine wave is used as the stimulus so that the impedance can be evaluated across the frequency range of interest, in most cases from 1mHz to 100 kHz.

Impedance is measure of the opposition that a circuit presents to a current when a voltage is applied. It is given by the ratio between a time-dependent voltage and a time-dependent current:

$$Z = \frac{V(t)}{j(t)}$$

As sad before, the impedance measurement is done by applying a sinusoidal perturbation $V(t) = V_0 cos(\omega t)$ and monitoring the current response $j(t) = j_0 cos(\omega t - \phi)$. Hence,

$$Z = \frac{V_0 cos(\omega t)}{j_0 cos(\omega t - \phi)}$$

That in complex notation can be expressed in terms of an impedance magnitude Z_0 and a phase shift ϕ or a real component $Z_{real} = Z_0 cos\ \phi$ and an imaginary component $Z_{imag} = Z_0 sin\ \phi i$ where $i = \sqrt{-1}$.

Typically, impedance data are plotted in terms of real and imaginary component in a Nyquist plot as shown in Figure 3.
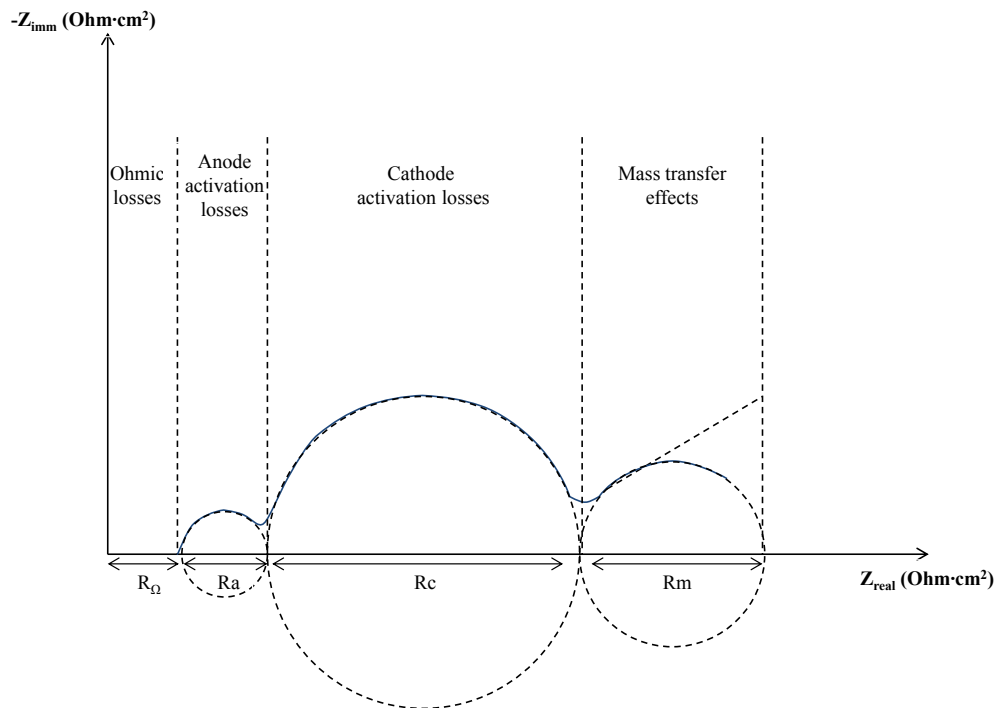
Figure 3 Typical Nyquist plot for a PEMFC

The spectrum can be divided in three zones. At high frequencies the intercept with the x-axis R_Ω represents the Ohmic electrolyte losses, the first small arc R_a represents the anode activation losses, R_c represents the cathode activation losses and R_m represents the mass transport effects.

Ohmic Resistance

The highest contribution to this term is given by the electrolytic resistance (membrane resistance), R_Ω. This can be divided into: contact resistance (R_{cn}) and cell components ohmic resistance R_s.

$$R_\Omega = R_{cn} + R_s$$

The contact resistance and the component resistance are dependent on the clamping pressure [92]. It is hence important that pressure is kept constant during all the cell working period. Other factors that can influence the Ohmic resistance are: humidification (for LT-PEM) and temperature that could cause desiccation or evaporation of proton conducting media.

Charge transport resistance

The resistance associated to the charge transport, derives mainly from the slow oxygen reduction reaction (ORR). Smaller contributions come from the hydrogen oxidation reaction (HOR) and from the accumulation of charge in the porous electrode and GDL structure. This resistance is associated to the first two high frequencies arcs in the EIS spectrum.

Gas transport resistance

The gas transport resistance is associated to the reactant gas transfer into the active sites of the electrodes. This is manly governed by the mass transfer on the cathode side in terms of convection into the bipolar plate channels and in terms of diffusion in the GDL and in the electrodes. Since hydrogen is, by nature, more diffusive and has better transport properties then oxygen, the anodic side is much less affected by these losses. This resistance is associated to the third low frequencies arc in the EIS spectrum and can be modelled by a finite Warburg element in the EIS equivalent circuit as will be hereafter briefly discussed (see Figure 4).

EIS Modelling and equivalent circuit

The processes that occur inside a fuel cell can be modelled using circuit elements. For example, groups of resistors and capacitors can be assigned to describe the behaviour of electrochemical reaction kinetics, ohmic conduction process, and mass transport.

A typical equivalent circuit model and its derived Nyquist plot is represented in Figure 4. From the modelling point of view, cathode mass transport process is usually modelled with and infinite Warburn impedance element as represented in Figure 4 giving a infinite straight line for frequencies tending to zero instead of the third arc represented in Figure 3. The slope of the infinite Warburn element straight-line is usually sufficient to describe the mass transport properties of a fuel cell [63].
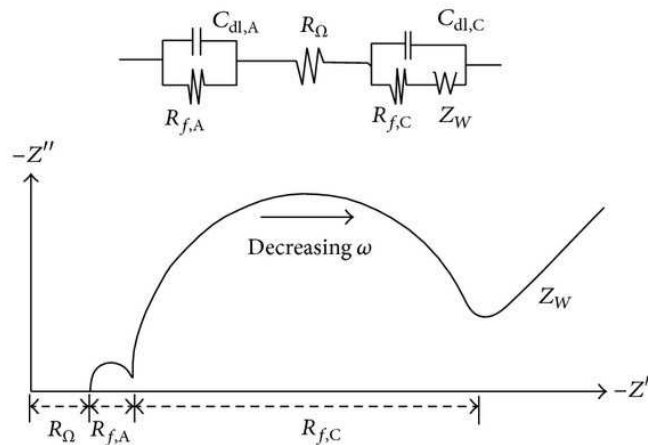
Figure 4 Nyquist plot and equivalent circuit for a simple fuel cell model [93]

EIS measurements of PEM fuel cells are usually carried out by means of two-electrode connections in which both the counter electrode and the reference electrode from the measuring instrument are connected to the fuel cell anode. This is easy to implement compared to a three-electrode connection for PEM fuel cells, because inserting a conventional reference electrode such as SCE or Ag/AgCl into the thin solid polymer electrolyte is difficult [94].

The drawback of the two-electrode measurement is that the impedance of an individual electrode cannot be obtained directly.
But the fact that anode polarization is negligible against to cathode polarization during fuel cell operation means that this drawback has little effect in most of the cases when the anode is a pure hydrogen electrode.
EIS measurements can be performed either in galvanostatic mode or in potentiostatic mode.

The galvanostatic technique consists in applying to the cell a perturbation in current and measuring the voltage response. In opposition to the potentiostatic technique, these measurements allow a constant conversion ratio with respect to all charged species involved in the reaction. Moreover, this technique has the advantage that the constant and alternative current levels can be precisely established by the operator preventing overcharging of the cell and the potentiostat. In this way higher currents can be used and more information can be obtained.

A very important aspect to well perform EIS is the choice of the perturbation amplitude, usually between 5% to 10% of the base current. Wagner at al. [95] in their study of the changes in the spectra with time during CO poisoning of the Pt-anode catalyst, they chose an amplitude of 200mV for a cell operating at constant continuous current at 5A (217 mA/cm2). In the study of Gode et al. [96] a perturbation of 5% of the applied continuous current has been chosen. The amplitude for a galvanostatic mode measurement under heavy duty operation was also chosen to be 5% of the DC current by [94]. In [97] it is demonstrated that while for small amplitudes next to 1% the spectrum is very scattered, there is no considerable difference between the impedance plots in the amplitude range of 5% to 10%.

In general, the galvanostatic technique is more suitable for the analysis of high energy electrochemical devices, where current levels are high.

2.6.1.3. Cyclic Voltammetry

CV is an electrochemical technique that gives information and insight into the kinetic and thermodynamic details of many chemical systems. CV is rarely used for quantitative determination, but is ideally suited for a quick research of redox couples, for understanding reaction intermediates, and for obtaining stability in reaction products.

The characteristics of the picks in a cyclic voltammogram can be used to acquire qualitative information about the relative rates of reaction and reactant diffusion in a given electrochemical system.

Cyclic voltammetry is typically used to characterize fuel cell catalyst activity. In a standard CV measurement, the potential system is swept back and forth between two voltage limits while the current response is measured.

In fuel cells, CV can determine in situ catalyst activity by using a special configuration. In this mode nitrogen is passed through the cathode instead of oxygen, while the anode is supplied with hydrogen.

When the potential increases from 0, a current begins to flow. There are two contributions to this current. One contribution is constant and consists in a simple, capacitive current which flows in response to the linearly changing voltage.

The second current response is nonlinear and corresponds to a hydrogen adsorption reaction occurring on the electrochemical active anode catalyst surface. As the voltage increases further, this reaction current reaches a pick and then falls off as the entire catalyst surface becomes saturated with hydrogen [63].

The active catalyst surface can be obtained by quantifying the total charge provided by the hydrogen adsorption/desorption on the catalyst surface. The total charge essentially corresponds to the area under the hydrogen adsorption or desorption reaction peak (see Figure 5) in the CV after converting the potential axis to time and making sure to exclude the capacitive charging current contribution.

If the electrochemical reactions are reversible the position of the oxidation and reduction peaks do not change with the potential scan rate and the peak height is proportional to the square root of the potential scan rate.

The reversibility of an electrochemical reaction is always a relative term, related to the potential scan rate, a reaction that is reversible at low scan rates may become irreversible at high scan rates.

In this case, the anodic peak become more positive and the cathodic peak becomes more negative [91]. The result is likely to be more accurate if average of cathodic and anodic peak areas is used [49].
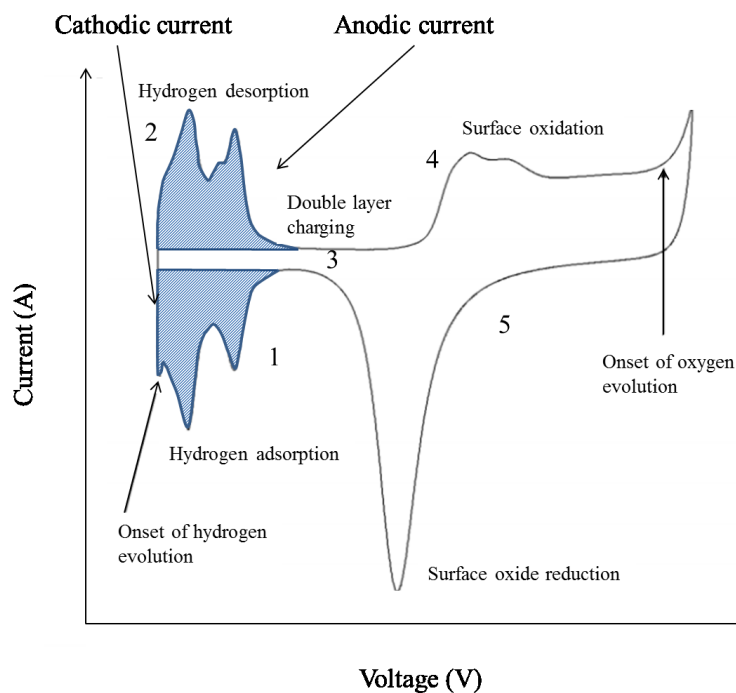
Figure 5 Typical result of a CV for a fuel cell cathode. Highlighted areas correspond to hydrogen adsorption and desorption peaks

As highlighted in [98] and [99], different actions at the catalyst particles corresponds in the 5 points shown in the voltammogram:

1. Protons absorb to the Pt particles and thereby creating a monolayer
2. The potential is low and the hydrogen desorption from the Pt particles takes place
3. At this point the platinum yields no specific current and the existing current is due to the double layer capacitance
4. Due to the oxygen in the water inside the membrane, the Pt particles start to oxidize to PtO
5. The PtO is reduced to Pt

2.6.2. Nano-morphological diagnostic tools

2.6.2.1. Transmission Electron Microscopy

The Transmission Electron Microscopy (TEM) is an important nano-morphological diagnostic tool allowing to see objects to the order of few Angstroms (10^{-10} m). TEM operates on the same basic principles as the light microscope but uses electrons as "light source" and, hence, since their wavelength its much lower than the light wavelength, they make possible to get a resolution 1000 times better than with a light microscope [91].

In TEM the electron beam passes through the sample and the transmitted electrons are detected. The interaction between the electron beam and the atoms of the sample emits several types of radiations, in particular: secondary electrons coming from the sample, backscattered electrons due to the collision of the beam with the nuclei of the atoms of the sample, electrons transmitted through the sample, X-rays, light and heat. X-rays are emitted when an electron from the core level of an atom leaves a vacancy that can be filled by an electron from a higher energy level. This radiation can be used to investigate the composition of the volume penetrated by the electron beam since the energy gap between electron levels is specific of a particular atom [100].

TEM technique has been firstly used by Knoll and Ruska in 1931 [101]. Only four years later TEM was developed by commercial companies.

The application of TEM to fuel cell electrocatalyst degradation analysis is, nowadays, a very common technique allowing to observe Pt catalyst nanoparticles changes in the PEM fuel cell electrocatalyst layer. In [102] TEM has been used to analyse Pt catalyst variation on a PBI HT-PEM fuel cell subjected to 600h of operation at constant load.

TEM indicated an increase of the Pt/C nanoparticles from 3.72 nm to 7.40 nm in anode and 8.39 nm in cathode. In [78], TEM is used to investigate the sintering of the electrocatalyst at the cathode in order to evaluate the stability of Pt/C catalyst in a single cell configuration of a HT-PEM FC operated at high temperature. The mean nanoparticles size increased from 4.02 nm to 5.73 nm, 8.30 nm and 8.95 nm after 100h, 300 h and 520 h respectively. The results suggested that Pt particles agglomeration occurred via coalescence mechanism on carbon.

In [45] the effect of operating temperature on HT-PEM cell performance and durability has been investigated. TEM analysis showed a growth of mean particle size from 3.8 nm, to 4.1 nm and 6.0 nm for the samples operated for 1000 h at 150°C and 190°C respectively.

2.6.2.2. Small Angle X-ray Scattering

In addition to the typical electrochemical diagnostic tools described in the above paragraphs, other very useful diagnostic tools allow to establish a correlation between performance degradation and electrocatalyst structure variation.

An efficient class of instruments employs X- rays to observe the structure of materials and its changes during operation in PEM fuel cells. X-rays methods have the great advantages to be usually non-intrusive and offer accurate data regarding the structure of the sample. Furthermore, the information they give is averaged on a relatively wide area, unlike the one obtainable by microscopy, in which just a single point is observed. Small-angle X-ray scattering (SAXS) is a suitable method to characterize the MEA of a fuel cell and its degradation since it is able to give information about size, shape and distribution of objects in the nm-range of sizes. Moreover, SAXS allows both time-resolved and in-situ

measurements [100]. SAXS is a well-established technique, perfect for examination of state-of the-art fuel cell electrocatalysts with particle sizes ranging from 2 to 4 nm [20].

In SAXS analysis normally X-rays are sent through the sample (transmission mode) and every particle that happened to be inside the beam will interact with them. Thus the averaged structure of all illuminated particles in the bulk material is measured. The SAXS method is accurate, non-destructive and usually requires only a minimum of sample preparation. The particle or structure sizes that can be resolved range from 1 to 100 nm in a typical set-up but can be extended on both sides by measuring at smaller (Ultra Small-Angle X-Ray Scattering USAXS) or larger angles (Wide-Angle X-Ray Scattering, WAXS also called X-Ray Diffraction, XRD).

In SAXS the sample is invested by a monocromated and collimated x-ray beam and the resulting scattering is recorded in the range between 0.1° and 10°. This angular range contains information about the shape and size of macromolecules, characteristic distances of partially ordered materials, pore sizes, and other data. When X-Rays are scattered at atoms, every atom emits spherical waves emanating from the position of the respective atom. Because the outgoing light waves from Thomson-scattering processes are synchronized with the incoming plane waves, they produce interference patterns at the detector's position. The interference pattern is characteristic to the internal structure of the material [103].

A schematic of the experimental setup is shown in Figure 6.
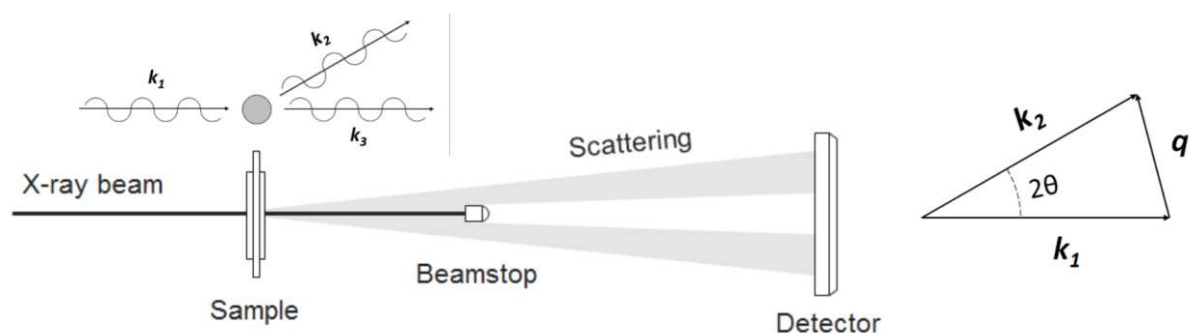
Figure 6 Schematic of SAXS test configuration

After the interaction with the sample, part of the parallel x-ray beam deviates from its path and photons scatters in other directions. The theory employed to correlate the scattering patterns with the nanometric structure of the sample usually assumes pure elastic scattering, photon absorption and inelastic scattering are neglected [100]. The scattering angle is related with the particle size by a reciprocity relationship, the Bragg's law:

$$n\lambda_x = 2dsin\theta$$

Where n is an integer number, λ_x is the x-ray wavelength, d is the characteristic length (i.e. lattice spacing) and θ is the scattering angle shown in Figure 6. This states that the

larger the scattering angle the lower is the dimension measured. The dimensions in the scattering patterns (inverse space) are thus inversely proportional to the dimensions in the sample (real space) [100]. It is possible to convert the information measured in the inverse space into the real space by means of the Fourier transform. It is not possible to derive uniquely the electron density distribution in the real space from the scattering pattern because only the intensity of the scattering is measured while the phase information is lost. This information loss complicates the data analysis and allows different possible interpretation of the scattering patterns [104].

[105] pioneered the use of SAXS to investigate growth and transformations of carbon-supported Pt nanoparticle electrocatalysts. Later, [106] used ex situ SAXS to determine Pt PSDs. More recently, in situ SAXS studies revealed a time-resolved look at Pt particle growth under potential cycling [107].

In [20] small-angle X-ray scattering (SAXS) is used to examine, in situ, a carbon-supported PEFC cathode electrocatalyst. They observed that particle size increased rapidly for 20-Pt over the first 8 h before reaching slower growth at ~3.2 nm. Contrarily, 40-Pt, whose particle size starts at 3.2 nm, exhibited a steady particle growth from the start. Pt particle growth with potential cycling of a PEFC cathode has been observed as well by [107] using ex situ X-ray diffraction (XRD) and ECA loss measurements in fuel cell environment showing a particle growth from 1.9 to ~4 nm after 300 cycles between 0.1 and 1.2 V; estimated from ECA loss and the ECA loss-particle size relationship.

In [107] has been showed through experiments and computations that above a particle diameter of 3–5 nm, Pt particles showed a significantly enhanced stability.

In [108], recently, has been carried out an analysis of Pt agglomeration thought in-operando ASAXS that showed for all tests a general trend for the evolution of the particle size distribution during cycling which is a loss of smaller particles, less than 3.0 nm, and an increase in the number of particles larger than this diameter. They manage to demonstrate that Pt nanoparticle surface area loss resulting from potential cycling can be inhibited by reducing the number of particles smaller than a critical particle diameter (CPD), which was found to be 3.5 to 4 nm.

2.7.   Modelling of HT-PEM FC and micro-CHP systems

2.7.1.   <u>HT-PEM fuel cell modelling</u>

Fuel cell modelling, as any other modelling approach, is an endless evolution domain that starts from very simple statements and can reach extreme complexity depending on the phenomena scale analysis and the development of theoretical knowledge.

Usually the first approach to modelling of a phenomenon is an empirical model based on a reference analysis tool.

In fuel cell domain, the main performance analysis tool is the polarization curve and hence the first pioneers of fuel cell modelling started their work form a simple 0-dimensional empirical model of the polarization curve.

The first effort in this direction has been done in 1988 by Srinivasan et al. [109] who developed an empirical formula to describe the relationship between working potential and current density in the low and mid-current density range where the cell overpotential is dominated by activation and ohmic losses:

$$V_{cell} = E + blog(j_0) - blog(j) - Rj$$

Where V_{cell} is the working potential j is the current density, j_0 the exchange current density and b the Tafel slope for oxygen reduction. The third terms represents the cathodic activation overpotential.

Starting from here, in 1995 Kim J. et al. [110] suggested the addition of an exponential term in order to fit the high current density region where predominate mass transport losses:

$$V_{cell} = E + blog(j_0) - blog(j) - Rj - mexp(\xi j)$$

Where m and ξ are parameters liked to mass transport limitations.

This polarization curve model reached and excellent fitting of the polarization curve, however, was missing the theoretical interpretation of the exponential term.

Since there, many works [111–113] have been published bringing to increasing the physical interpretation of the terms and improving the fitting of experimental polarization curves in various operational conditions.

Recently more complex models based on computational fluid dynamics tried to take into account and optimise the interpretation of the most tricky part of the polarization curve which is the high current density part dominated by mass transport losses. Mass losses are

mainly dominated by reactant concentration at the reactive sites and water transport in porous electrodes, it is hence indispensable to take into account the convection and diffusion in flow channels, as well as transport in porous gas diffusion layer. With this purpose many 1-D [114,115], 2-D [116,117] and 3-D [52,118–120] models have been developed and literature is still evolving in this direction. However, the main problem with all of these models is the assumption that proton conductivity is constant, which, actually, has been shown to vary with both relative humidity and temperature [55].

Deeply understanding the fuel cell operation and being able to model in an analytic way its behaviour it's a very difficult task given the complexity of the system and the enormous number of variables. A complete model should be able to analyse factors, such as: gas transport channel configuration, porous layers configuration, catalytic layer loading, sulphuric acid doping level, catalytic composition and particle size, reactant humidity, reactant pressure and temperature, reactant poisoning, operating temperature of the fuel cell, clamping pressure etc.

In order to understand the performance variation as a function of each of such parameters, in literature can be found many independent models suggested by authors to analyse the specific influence of each parameter.

Very important conclusions on performance effects on HT-PEM have been suggested by [121] through a numerical simulations carried out thanks to a three-dimensional non-isothermal model that has been developed to investigate the effects of operating temperature, phosphoric acid doping level of the PBI membrane, inlet relative humidity (RH), stoichiometry ratios of the feed gases, operating pressure. In their work, numerical results indicate that increasing both the operating temperature and phosphoric acid doping level are favourable to the improving of the cell performance. Humidification of the feed gases at room temperature has negligible improvement on the cell performance while pressurising the cell and using oxygen instead of air have significant improvements on the cell performance. Increasing the stoichiometry ratios only helps to prevent the concentration loss at high current densities.

In addition to the performance optimization, the other big challenge of PEM fuel cell and especially for high temperature fuel cell is the improving of lifetime. The understanding and modelling of degradation process is a very active research domain with many open issues.

In this PhD work the focus of the analysis is the degradation modelling of HT-PEM.

As already highlighted in §2.4, understanding the degradation mechanism of each process and establish a hierarchy between them is very important in order to implement adapted production or operation procedures able to enhance lifetime of fuel cell. Modelling of the degradation process is an extremely useful tool to perform this separation and to establish

a hierarchy between the degradation phenomena since it allows to perform parametric analysis of degradation processes on a very large scale.

Hu et al. [72] performed a five hundred hours continuous aging test at constant discharge current ($640mA/cm^2$) on PBI/H_3PO_4 high temperature PEMFC and attribute the main reason of performance degradation to the decrease of ECSA caused by platinum sintering. Based on this assumption they developed a one dimensional mathematical model to simulate polarization curves [122].

The model was developed based on the following assumptions:

1. The operation of the cell was in steady state.
2. The temperature was evenly distributed in electrode.
3. The reactant gases mixture was incompressible, ideal fluid.
4. The GDL and membrane were isotropic and homogeneous.
5. Catalyst layer was treated as an interface rather than a region.
6. Butler–Volmer kinetics governed the electrochemical reaction.
7. The water produced by electrochemical reaction at cathode
side was in vapor state.
8. The membrane was impervious for reactant gases.
9. The anodic overpotential was ignored.

The model was based on these three governing equations:

$$E = E_r - \eta_c - \eta_{ohm}$$

$$\eta_{ohm} = iR_{hf}$$

$$i = i_{0,area} \left(\frac{C_{O_2}}{C_{O_2,ref}}\right)^{\gamma_c} \left[exp\left(\frac{\alpha_c F \eta_c}{RT}\right) - exp\left(\frac{\alpha_a F \eta_c}{RT}\right)\right]$$

Where E_r is calculated through the Nernst equation. In their model, firstly, the current density was set; then, the one-dimensional concentration distributions of oxygen and gaseous water were calculated. Afterwards the concentrations of the oxygen and gaseous water at catalyst layer site was obtained by their concentration distributions, in this way cathode overpotential (η_c) could be determined; then, the steady state cell voltage can be calculated simulating in this way the whole polarization curves.

In Korsgaard et al. [54] a semi empirical model of cell voltage versus current density, cathode stoichiometry and temperature was derived and it showed excellent agreement with the experimental data.

The very simple expression of this model makes it ideal for system modelling, control design and real-time applications:

$$E_{cell} = E_0 - \eta_{act} - \eta_{ohm} - \eta_{diff}$$

$$E_{cell} = \frac{E_0 - RT}{4\alpha_c F} ln\left(\frac{i + i_0}{i_0}\right) - \frac{R_{ohm}i - R_{conc}i}{\lambda - 1}$$

However, in the form developed by [54] they did not take into account degradation effects. This model has then been upgraded in 2009 by Nielsen [36] who developed a 1-dimensional, non-isothermal, and semi-transient (considering degradation with time) model to describe Pt agglomeration and carbon corrosion processes. In their previous experimental analysis they had considered that these two degradation phenomena were the two main ones in HT-PEM fuel cells. On the basis of this conclusion a mechanistic model has been suggested. Using the proposed model, information about optimum operational temperatures was derived.

For the modelling of the ECSA reduction they suggested the following simple formulation:

$$ECSA\,(t) = \left(w_{pa} \cdot e^{-\frac{\alpha_{pa}}{A}t} + w_{cc} \cdot e^{-\frac{\alpha_{cc}}{A}t}\right) \quad with \; w_{pa} + w_{cc} = 1$$

In this formulation α_{pa} [V/h] is the degradation rate due to Pt agglomeration and α_{cc} [V/h] is the agglomeration rate due to carbon corrosion, w_{pa} and w_{cc} are weights reflecting the impact of individual phenomena. This correlation was then implemented in the already existing model developed by [54] through a modified time dependent version of the Tafel equation and the model was then fitted according to experimental data from single cell experiments.

An important step forward in the modelling of degradation process has been done by Suzuki et al. [55] studying the sintering of electrocatalysts and its effect on voltage drops trough a three-dimensional kinetic Monte Carlo method coupled with Ultra Accelerated Quantum Chemical Molecular Dynamics (UA-QCMD) method. The multi-scale modelling presented in this study allows to investigate various phenomena at different scales and to find a correlation between platinum sintering and fuel cell operating temperature.

This model allows local analysing of the phenomena considering temperatures variations on the MEA. This model have been developed applying the UA-QCMD to clarify the energetic or electronic structures of electrocatalysts. Afterwards, the three-dimensional kinetic Monte Carlo method allowed tracing the sintering progress of electrocatalysts over time. Finally a specific algorithm of polarization loss was developed to predict the impact of the morphological change over time inside of the catalyst layer. Their simulation results, compared with experimentally measured voltage drops, brought them to conclude that the voltage loss during the long-term experimental cell was caused by both aggregation of the electrode catalyst particles and evaporation of acid. Moreover they stated that since the

amount of voltage loss caused by the depletion of specific surface area of electrocatalyst was smaller than that caused by both sintering of electrocatalysts and the evaporation of acid, sufficient controlling of the evaporation of acid is the key to achieving long-term power generation of HT-PEMFCs for practical application.

Based on the fact that in literature several groups have reported that the durability of the high-temperature PEMFC decreases rapidly with the increasing of temperature whereas its performance improves, Kim J. et al. [37], in the attempt to resolve this problem, developed a model to predict the performance and durability of the high temperature PEMFC as a function of operating temperature. To develop this model experimental data reported by Oono et al. [45] have been used. The objective of this work was to optimize the operating temperature through a method that balanced the performance and lifetime of the MEA without using different materials or designs. The optimal operating temperature was then determined for a variety of lifetimes. Theoretical model to estimate cell performance and empirical model to predict the degradation rate of cell performance were constructed based on the work of [117,122] (the work effected by [122] have been previously presented in the above paragraphs). The development of the prediction model for the cell voltage drop consists of two steps. In the first step, three draft models are used to estimate the cell voltage drop using only the operating time, not the temperature. In the second step, the modelling coefficients in the draft models are estimated using the operating temperature. Finally, the final model predicts the voltage drop using both operating time and temperature.

In 2014 Kim M. et al. [53] developed an hybrid model based also on the work of [117,122] and [123]. Their model have been then validated with experimental data as well as literature data obtained by [45]. In this model are taken into account the effects of: membrane, catalyst layers, gas diffusion layers, bipolar plates and current collector but not gas channels. The model has been built based on the following assumptions:

• Single phase flow
• Ideal gas mixture
• Ignore contact resistance between components
• Isotropic macro-homogeneous porous media
• Negligible activation and concentration over-potential at anode side

Governing equation used in the model are referred to [114].

Since Oono et al. [45] reported that activation overpotential of HT-PEM during long term continuing operation has been mostly increased due to agglomeration of Pt, and reduction of an active surface area they defined that the reference exchange current density parameter is the function of time and operating temperature. They hence developed an empirical equation for the reference exchange current density parameter (j_{ref0}) :

$$j_{ref_0} = (a \cdot e^{b \cdot T}) \cdot t + (c \cdot T + d)$$

That implemented in the Butler–Volmer equation :

$$j_r = i_{ref}\xi \left[exp\left(\frac{\alpha_c F \eta_c}{RT}\right) - exp\left(\frac{\alpha_a F \eta_c}{RT}\right) \right]$$

With

$$j_{ref} = i_{ref_0} exp\left(-\frac{E_c}{R}\left(\frac{1}{T} - \frac{1}{T^{ref}}\right) \right)$$

Allows to obtain the variation of the activation overpotential over time.

The simulation results demonstrated that the durability of HT-PEMFC is changeable with respect to current density and PA doping level. In addition, the lifetimes have been predicted according to different operating conditions and thus they found whether any conditions were helpful to improve lifetime of HT-PEM or not.

While at specific extreme conditions, dominant degradation phenomenon can be identified, the identification of dominant degradation process during constant load operation seems to not be trivial. Seongyeon et al. [76] carried out a numerical analysis of the effects of phosphoric acid (PA) loss and electro chemical surface area (ECSA) reduction on the voltage degradation of high temperature proton exchange membrane fuel cells (HT-PEMFCs) during long-term operations, placing their major focus on elucidating the dominant degradation mechanism of HT-PEM FCs during constant current operations and concluding that the loss of ECSA is the major contributor to the long-term voltage degradation of HT-PEM FCs under constant-load operations.

Given the complexity of the degradation mechanisms that involves simultaneous process that, as elucidated here above, are often difficult to separate, the modelling approach can follow two main paths: either resolve a specific mechanism in depth as it has been done by most of authors cited before or describe a more general effect. An uncompromised approach would lead to detailed information but a very high number of parameters and an important computational complexity. This kind of approach have been chosen by [55] and briefly presented before. The opposite approach have been chosen by [124] drastically reducing the level of detail. Such models are favourable if only a restricted set of information is available or a more general answer is preferred, which better fits with the purposes of our PhD work.
In this approach the modelling of degradation effects requires suitable key variables that take into account the properties of the fuel cell subjected to degradation. Variation of these variables is than a function of operating parameters such as voltage, temperature and time which are the driving force for degradation. In [124] a list of the most representative reactions related to catalyst dissolution, carbon corrosion and membrane degradation is derived from literature and hence a specific potential range is individuated for each

degradation process as reported in Table 4. However, this range can vary with respect to the specific mix of electrode materials and other operating conditions. Therefore, at first, the limits of each degradation reaction are calculated through thermodynamic values.

The standard voltage E_0 is calculated as:

$$E_0 = \left| \frac{-\Delta G}{zF} \right|$$

The absolute value operator is introduced to avoid the changing of sign of ΔG during electrolysis which would bring to inconsistently high degradation when water is found at the anode.

Number	Reaction	ΔG/kJ mol^{-1}	E_0/V
1	$CO + 0.5\ O_2 \leftrightarrow CO_2$	-257	1.33
2	$H_2 + 0.5\ O_2 \leftrightarrow H_2O$ (liq.)	-237	1.23
3	$Pt \leftrightarrow Pt^{2+} + 2e^-$	228	1.18
4	$C + O_2 \leftrightarrow CO_2$	-394	1.02
5	$Pt + 2H_2O$ (liq.) $+ PtO_2 + 4H^+ + 4e^-$	386	1.00
6	$C + 0.5\ O_2 \leftrightarrow CO$	-137	0.71
7	$H_2 + O_2 \leftrightarrow H_2O_2$ (liq.)	-120	0.62
8	$0.5\ H_2O_2$ (liq.) $+ 0.5\ H_2 \leftrightarrow H_2O$ (liq.)	-117	0.61
9	$C + H_2O$ (liq.) $\leftrightarrow CO + H_2$	100	0.52
10	$C + 2H_2O$ (liq.) $\leftrightarrow CO_2 + 2H_2$	80	0.21
11	$CO + H_2O$ (liq.) $\leftrightarrow CO_2 + H_2$	-20	0.10

Table 4 Extracted from [124] **- Reactions and corresponding voltages**

The model is developed based on the assumption that a degradation reaction occurs when the cell voltage is equal or above the value of E_0.

In the use of Table 4 it must be taken care to correct the voltage values for the influence of temperature and local concentration since the values in table are given at standard conditions (25°C and 101.325 kPa).

Starting from these considerations in [124] they developed a model based on two degradation modes: catalyst degradation and electrolyte degradation.

E_{cell} is calculated in the following way:

$$E_{cell} = E_0 - R_\Omega j - \eta_{act} - \eta_{trans}$$

Where:

$$\eta_{act} = \frac{RT}{\alpha F} ln \frac{j}{j_0}$$

$$\eta_{trans} = \frac{RT}{\alpha F} \ln \left(\frac{j_{lim}}{j_{lim} - j} \right)$$

This model contains three parameters which could be subject to degradation: j_0, R_Ω, $j_{lim.}$ The first one is linked to the activity and the ECSA. Catalyst degradation as well as carbon corrosion would make decrease the value of j_0 while the increase of the R_Ω would indicate a loss in proton conductivity and hence a membrane degradation process. The change of morphology of the catalyst or a change of phosphoric acid distribution (for example the increasing of the electrolyte film thickness) would limit the oxygen diffusion affecting the parameter j_{lim}.

Defining the vector of degradation parameters $X = [j_0, R_\Omega, j_{lim}]$ and assuming a single time constant for all degradation processes (first order reaction), for each time step the value of X would change by a magnitude of B multiplied by the time interval Δt.

$$X_{t=n+1} = X_{t=n} + X_{t=n} \cdot B \cdot \Delta t$$

Which leads to:

$$\frac{dX}{dt} \approx \frac{X_{t=n+1} - X_{t=n}}{\Delta t} = X_{t=n} \cdot B$$

From where it can be found the solution for *X(t)*:

$$X(t) = X_{t=0} \cdot \exp(B \cdot t)$$

As explained before each degradation reaction should be related to a certain cell voltage (uniform voltage across the active cell area is assumed). It is, hence, needed to introduce a switch on/switch off function that in the work of [124] has been suggested in the following form:

$$F(E) = \frac{1}{1 + exp\left(-a \cdot \left(\frac{E_d}{E_{cell}} - b\right)\right)}$$

Where *a* and *b* are model parameters chosen to be fix (*a=10.0; b=1.5*) while E_d represents the onset of degradation. In this way, degradation "intensity" is spread over a certain voltage range.

The degradation model can hence be rewritten as:

$$X_{t=n+1} = X_{t=n} + X_{t=n} \cdot B \cdot \Delta t \cdot F(E)$$

$$X(t) = X_{t=0} \cdot \exp(B \cdot t \cdot F(E))$$

Afterwards experimental data are fitted by the model considering the least square procedure, i.e. the best fit is the combination of B and E_d that minimize the error S:

$$S = \sum_t \left(E_{cell,exp}(t) - E_{cell,model}(t, B, E_d) \right)^2$$

The model algorithm is based on the following steps:

1. Load profile j *(t)* is obtained experimentally.

2. One degradation parameter is selected from $\{ j_0, R_\Omega, j_{lim} \}$.

3. For each $E_d \in [0.2; 0.5]$ V and $B \in [1 \cdot 10^{-4}; 1 \cdot 10^{-2}]$ s^{-1} the following steps are performed (brute force method):

  (a) The cell voltage is calculated based on the load profile j (t) from model governing equations
  (b) The error S is calculated

4. The combination of B and E_d which minimise S is chosen as best fit.

In their work [124], the same procedure is then applied considering heat as driving degradation force instead of voltage.

Results brought them to two different interpretations. Degradation could be explained both by carbon corrosion or phosphoric acid redistribution and loss. But since considering the heat as driving degradation force they were obtaining a better fit they suggested that degradation could be explained by a combination of effects.

In particular the loss of phosphoric acid could be explained by a local temperature increase on the catalyst caused by high current with a consequent decrease of viscosity and enhanced mobility of phosphoric acid. Afterwards, the high water production rate at high currents may dilute the phosphoric acid.

2.7.2.   Micro-CHP modelling

Concerning micro-CHP system modelling, literature is mainly focused on energy performance analysis and system configuration optimization [11,56–58] while very few work has been done on degradation analysis of HT-PEM based micro-CHP systems

A first remarkable work has been done by [56] who proposed a novel model of HT-PEM-based micro-combined heat and power fuel cell system based on the HT-PEM models previously developed by [114] and described in §2.7.1. The purpose of its work was to study a system layout allowing to obtain a global system efficiency higher than 45-50% in order to be competitive with combined cycle central power plants. Their model allowed the comparison of different layout of the systems and brought to the definition of a novel layout of the micro-CHP allowing to obtain 45% of electricity efficiency and 90% to 100% of total CHP efficiency.

Their work has than be used by [57] who investigated in greater detail and precision a similar high temperature PEMFC-based micro-CHP system focusing on the design of key system components, such as the reactors, heat exchangers and combustor. For their study they analysed a micro-CHP unit of approximately 1 kWe and based on three loads profiles: electrical load, space heating and hot water production. The system performance is analysed in terms of efficiencies defined as follow:

The thermal efficiency of the cogeneration is defined as the recovered heat over the input fuel low heating value (LHV):

$$(\eta_{th})_{cogen} = \frac{\left(\dot{Q}_{Ex}\right)_{cogen}}{\dot{m}_{CH_4,in} LHV_{CH_4}}$$

The electrical efficiency is defined as the ratio of the net power output of the system and the input fuel LHV:

$$(\eta_{elc})_{net} = \frac{\left(\dot{W}_{El}\right)_{net}}{\dot{m}_{CH_4,in} LHV_{CH_4}}$$

While the combined CHP efficiency is defined as the sum of the two efficiencies defined above.

Their model is based on six main simplification assumptions: natural gas behaves as methane, reformate gas is provided to the stack at operating temperature, heat losses are neglected, complete oxidation is assumed at combustor, performance is calculated at steady-state, inverter losses are not considered. The modelling of the fuel cell stack has been done through the governing equations presented in [56]. As highest combined cogeneration system efficiency they obtained 83.08% corresponding to 27.62% of net system electrical efficiency and 55.46% of net system thermal efficiency, while the fuel cell stack efficiency was 37.74%.

In another study [59], the same author used a genetic algorithm to optimize the system, and obtained an improvement of the electrical efficiency up to 41.2% while thermal efficiency and total system efficiency were respectively 49.7% and 91%.

In 2014 [11] developed a AspenOne Hysys model of a 1kWe methanol FC micro-CHP system consisting of three main components: a combustor, a methanol reforming reactor and an HT-PEM FC. Pumps, centrifugal fans and heat exchangers have as well been integrated in the system. The simulation of the HT-PEM equipment has been carried out taking into account the same semi-empirical model developed by [56]. The influence of several operating variables in the power and global CHP efficiency has been studied, in particular they analysed the influence of CO concentration and temperature.

In [58] a previously existing LT-PEM micro-CHP system has been modified in order to implement a HT-PEM FC stack, allowing an important system simplification. Detailed mathematical models for the fuel processor components, PEM fuel cell stack, the heat exchangers, and all other auxiliary components of the plant have been developed. The steam methane reformer reactor have been modelled through a Langmuire – Hinshelwood realistic kinetic model [125]. The modelling of the MEA has been done employing a quasi 2D model while for the ejectors an isobaric mixing single phase thermodynamic model has been used and, finally, for heat exchangers they performed a logarithmic mean temperature difference iteration method. As well as in the work of [11] they performed a sensitivity analysis on the key system parameters in order to study the behaviour of the system from an efficiency point of view. In the new HT-PEM system it was demonstrated that due to the advantages of this type of PEM fuel cells, the obtained electrical efficiency of the previous LT-PEM FC system (21.2%) can be increased up to 29.2%. This confirmed that, as already highlighted by [10], in spite of the lower electrical efficiency of the HT-PEM stack with respect to HT-PEM stack, the hole micro-CHP system based on HT-PEM FC can reach higher efficiencies then LT-PEM based micro-CHP systems.

While literature is quite rich in micro-CHP performance analysis models, very few of models have been developed in order to take into account the performance degradation of the system.

However, taking into account degradation it is an extremely important issues since as shown by [126] techno-economic studies that ignore degradation can overestimate the marginal value of a micro-CHP system with respect to the conventional alternative by up to 45% and the CO_2 emissions reduction potential by up to 57%, for performance degradation rates of 2% per MWhe output.

A remarkable work in this sense has been recently done in 2017 by [62] who introduced degradation issues of both the stack and reformer on the system model. In this work they performed a multi-objective optimization approach in order to find the optimal operating parameters within the first 15 000 hours of operation while considering the impact of the degradation. Stack degradation has been modelled through a previously developed degradation model suggested by [53] and already analysed in §2.7.1.

3.Methodology

In order to answer to the research question, the methodology developed during this PhD consists in the steps described hereafter.

After the literature review carried out on the test procedures and degradation results for HT-PEMFC, as well as on existing fuel cell numerical models; it has been chosen to carry out a long term experimental campaign on commercial HT-PEM MEAs, in a single cell configuration, subjected to different operating conditions. The single cell configuration has been chosen in order to separate the degradation processes induced by different operating load profiles. Indeed, single cell configuration with respect to stack configuration, even if does not reproduce the real operating configuration of a micro-CHP system, has the great advantage to allow a better control of the operating conditions and to isolate the possible parameters influencing a specific degradation process. Moreover cost of experiments is much lower allowing in this way to perform more tests.

Performance degradation analysis has been carried out, *in-situ,* through electrochemical diagnostic tools (Polarization Curves, EIS and CV) allowing to quantify performance degradation over time as a function of the operating condition. These tools allow, as well, a first qualitative analysis on the dominant degradation process occurring during operation. However, it is often very difficult to separate contributions of each degradation process through the analysis of the results obtained with these electrochemical diagnostic tools.

For this reason, some deeper analyses have been carried out, *ex-situ,* at the end of the ageing test, considering the nano-morphology of the catalyst layer. Two techniques have been used: TEM and SAXS.

The experimental data collected during this PhD activity allowed to identify the performance degradation of the fuel cell over all the load conditions and allowed to infer a degradation law as a function of the operational time. This information has been used to develop an empirical degradation model based on a linear hypothesis, with variable coefficients, as a function of the current density.

In this chapter, in §3.1 the test bench set-up and the degradation experimental test procedure are described; Paragraph 3.2 explains the procedures used to perform the electrochemical diagnostic analysis: polarization curve, Electro Impedance Spectroscopy and Cyclic Voltammetry. In §3.3 the methodology used to perform the nano-morphological analysis on the MEAs subjected to the ageing test is presented.

The numerical model assumptions and architecture are described in §3.4.

3.1. Experimental test procedure

The test bench used for this work has been developed following the JRC recommendations [127] and it is schematically presented in Figure 7. Two pressure transducers are used to measure the reactants inlet pressures. The cell temperature is measured using K-type thermocouples fitted on the anode and cathode endplates. Reactants flow rates are measured and controlled using two mass flow controllers: a Sierra$^®$ SmartTrack M100 for the air circuit (accuracy $\pm1\%_{\text{reading value}}$) and a Bronkhorst$^®$ El-Flow F201 for the hydrogen circuit (accuracy $\pm0,5\%_{\text{reading value}}$ plus $\pm0,1\%_{\text{full scale}}$).
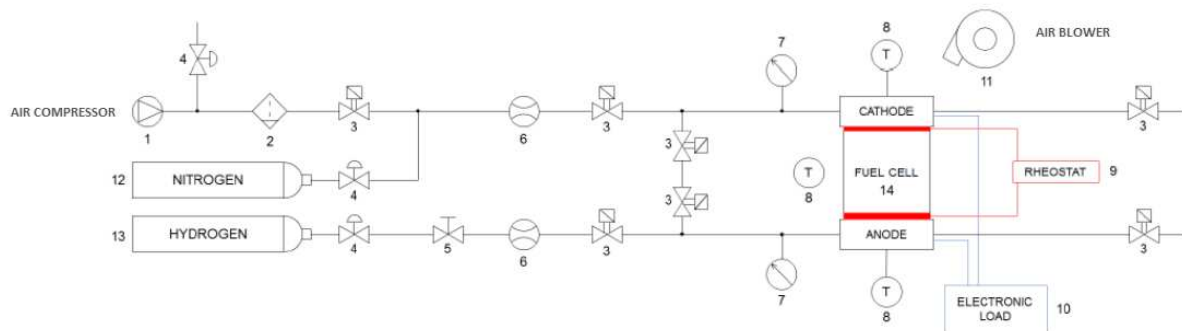
Figure 7 Simplified schematic of the test bench: (1) air compressor, (2) air filter, (3) solenoid valve (4) pressure regulator, (5) valve, (6) flow meter, (7) pressure transducer (8) thermocouples, (9) rheostat, (10) electronic load, (11) air blower (12) nitrogen cylinder, (13) fuel cylinder and (14) fuel cell

An image of the fuel cell assembly is shown in Figure 8. The steal bipolar plates guaranty the mechanical stability and contain the gas inlets and outlets. Two warming plates of 200 W of nominal power are inserted on each steal plate. The current collector provided with golden coating allows the reduction of the contact resistance between the warming plate and the bipolar plate. Two thermocouples are mounted on the terminal plates to measure cathode and anode temperature. Two PTFE gaskets avoid gas dispersion through the bipolar plates.
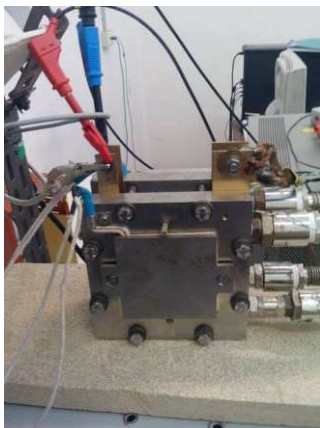
Figure 8 Fuel cell used for experimental tests

The test bench is controlled by two real time systems: a home-made LabView® control system and Nova® Metronorm software. The first one allows the monitoring, recording and controlling of all test bench variables, allows the performance of the polarization curves and manages the accelerated stress tests in automatic mode. The second one is the control software of the Autolab® Potentiostat/Galvanostat and allows the performing of EIS and cyclic voltammetry through specifically developed procedures.

The instrument used as electronic load is the Agilent® N3300A shown in Figure 9. It is provided with two spaces for two load modules; in this case the module N3304A and the module N3306A. The module used during this experimental campaign was the N3306A. The accuracy of the instrument at low range (12A) is $\pm$ ($0.05\%_{reading\ value}$ + 10mA), while for high range (120A) the accuracy of the instrument is $\pm$ ($0.05\%_{reading\ value}$ + 20 mA), The case contains a processor, a GPIB connector, a RS-232 connector with an interface circuit, trigger circuits, display and keyboard on the front panel in addition to other circuit common to all electronic loads. Each module can operate independently in constant current mode, constant voltage mode and constant resistance mode. Moreover each inlet and output can be activated or deactivated.

Figure 9 Electronic load Agilent N3300A

The instrument used to perform EIS and cyclic voltammetry is the potentiostat/galvanostat Autolab® PGSTAT302 shown in Figure 10. It is a high power and high speed instrument

with potentiostatic and galvanostatic functions. It accepts a maximum current of 2A and a maximum voltage of 30V. It can operate in a band width of more than 1MHz and can be equipped with all Autolab® modules available. In this case it is equipped with the FRA32M module; this module allows electro impedance spectroscopy analysis over a wide range of frequencies, from 1µHz to 10MHz. The potential and current accuracy are both $\pm$0.2%$_{reading\ value}$. In order to perform EIS measurements at currents higher than 2A, an external circuit allows the use of the electronic load in parallel with the PGSTAT avoiding high current to destroy the instrument.

Figure 10 PGSTAT302 Potentiostat/Galvanostat

The Labview homemade acquisition system allows remote monitoring and control of the entire test bench. Cell voltage, cell current, ambient temperature, anode temperature, cathode temperature, air pressure, air flow, hydrogen pressure and hydrogen flow are recorded in continuous during the cell operation time with an acquisition frequency of 1Hz.

To allow continuous operation, an UPS unit has been installed to avoid data acquisition interruptions due to frequent grid defaults encountered during the initial tests.

During this PhD work 8 MEAs have been subjected to different load cycles. All tests have been performed on commercial 45.16 cm^2 BASF Celtec-P1000 HT-PEM MEAs operated with hydrogen and air. Technical characteristics of Celtec-P1000 MEAs are reported in Table 5.

Property	Value
Active cell area (cm^2)	45.16
Electrode thickness (µm)	340
Electrode material	woven graphite
Catalyst	Pt-alloy
Cat. loading anode (mg cm^{-2})	0.75
Cat. loading cathode (mg cm^{-2})	1.0
Cat. layer thickness anode (µm)	60
Cat. layer thickness cathode (µm)	60
Membrane material	PBI/H$_3$PO$_4$
Membrane thickness (µm)	120

Table 5 Celtec-P1000 properties

The carbon support in the catalyst layer is Vulcan XC-72, while the electrocatalyst material is Pt-alloy (0.75 mg$_{Pt}$ cm^{-2}) at the anode and Pt (1 mg$_{Pt}$ cm^{-2}) at the cathode [21,23]. Graphite based plates with serpentine flow fields have been used to distribute the reactants on the MEA surfaces. PTFE gaskets of 320 μm (anode side) and 345 μm (cathode side) have been used to assemble the MEAs in the fuel cell hardware that has been subjected to a compression given by six screws tighten at 7 Nm in order to obtain a reduction of 20% of the gaskets original thickness, as suggested by the producer [128].

From the beginning of the research activity it has been chosen to name the MEAs in the following way: "MEA XXX", where "XXX" is the progressive number in chronological order of the tested MEA. In particular, data considered in this thesis concerns MEA 263 to MEA 278. Before starting the degradation tests, all MEAs have been conditioned for 100 hours under reference conditions as suggested by the manufacturer (T= 160°C, j=0.22 A/cm^2).

MEA 271 has been subjected to 125 000 triangular load cycles between Open Circuit Voltage (OCV) and 0.5 A/cm^2 corresponding to 440 h of operation. MEA 272 and MEA 273 have been subjected to 440 h of constant load operation at 0.2 A/cm^2, MEA 274 have been subjected to constant OCV for 126 h, MEA 275 have been used as reference membrane and no ageing test have been performed on this MEA. MEA 276 have been subjected to 300 start and stop cycles corresponding to 440 h of operation while MEA 277 have been subjected to constant OCV for a duration of 400h. MEA 278 has been conditioned for 100 h and then underwent to a three month stop period followed by 100 h of conditioning.

As explained in §2.5, the load cycles chosen in this activity are Accelerated Stress Tests (ASTs) specifically designed to accelerate the stress of a singular component of the MEA. The choice of the load profiles used in this PhD activity has been done with the purpose to highlight the operating conditions that most affect catalyst layer and catalyst carbon support.

The proprieties of electrodes materials such as degree of oxide coverage of catalyst and carbon support change when they are subjected to potential variations [100]. Moreover, during the operation at high cathode potentials, platinum can dissolve very fast until the formation of a protective oxide layer on the platinum surface. For this reason load cycles are considered to be a major stressor for the catalyst layer.

High potential are, as well, an important stressor for both catalyst layer and carbon corrosion; for this reason the OCV permanence during the load cycle and the constant OCV permanence have been suggested as load profiles in this experimental activity. The purpose of these testing procedures is thus to quantify the effects of periodic OCV permanence during dynamic operation on performance and state of the electrocatalyst comparing the results of the two loading cycles and constant permanence at OCV.

Lastly, start and stop cycles and prolonged shut down are supposed to be major stressor for catalyst carbon support corrosion. Degradation due to start and stop operation implies

different transient mechanisms that can affect the proper performance of the single components. Differently than in LT-PEMFCs, start and stop cycling in HT-PEMFCs leads also to a significant temperature cycling that can favour several degradation processes such as the delamination of the different layers of the MEA and the phosphoric acid leaching

Results obtained have been compared with previous data obtained for MEA 263, MEA 264, MEA 265 and MEA 266 by the research group of the university of Trieste [13,100]. All tested MEAs and the ageing profiles to which they have been subjected are synthetized in Table 6.

During the ageing test, MEAs temperature has been kept constant at 160 °C. Air flow has been kept constant at 2.5 sl/min and no backpressure applied to the cathode outlet. Anode was maintained in dead end operation with a purge every 3 min only during the ageing test, while when measurements were performed, hydrogen flow was set to 0.5 sl/min and no back pressure was applied.

In order to measure cell performance degradation, fuel cell potential variation with time, Polarization Curves (PC), Electro Impedance Spectroscopy (EIS) and Cyclic Voltammetry (CV) have been recorded periodically during all ageing tests.

Polarization curves have been carried out following a specific procedure based on JRC recommendations [127,129] described in §3.2.1. EIS has been carried out according to the methodology used in [22] and described in §3.2.2. Cyclic Voltammetry has been carried out according to the methodology used in [19] and discussed in §3.2.3.

Afterward, all MEAs have been subjected to SAXS analysis. SAXS have been performed following the methodology already used by the research group in a previous work [13] and described in §3.3.2. For MEA 263, MEA 264, MEA 265, MEA 271, MEA 273 and MEA276 SAXS data have as well been compared with the ones obtained by TEM analysis. TEM has been performed during this PhD activity on MEA 263, MEA 271, MEA 273 and MEA 276 following the methodology used by [100] and described in §3.3.1. While data of MEA 264 and MEA 265 have been obtained by [100] with a previous TEM analysis.
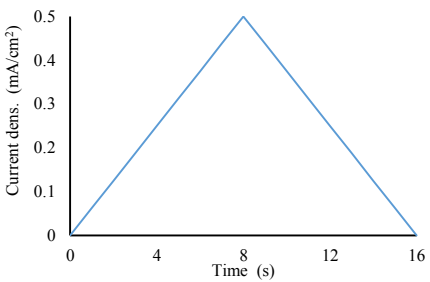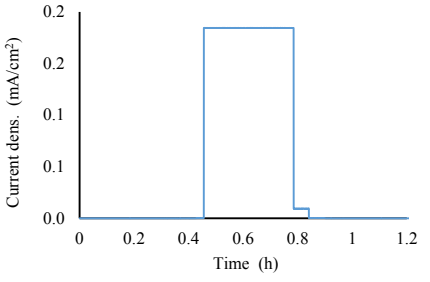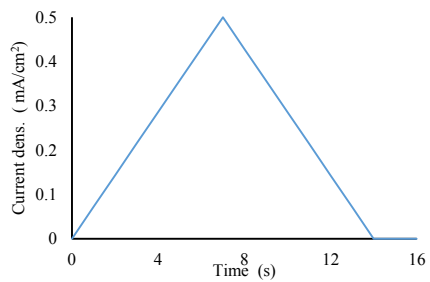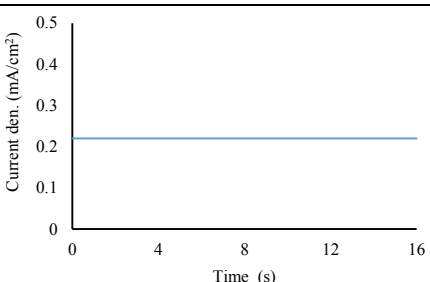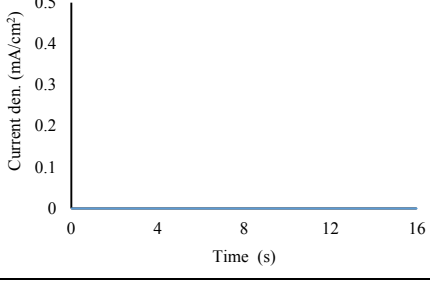
	Test Parameters	Load Profile
MEA 264	100 000 triangular sweep cycles between Open Circuit Voltage (OCV) and 0.5 A/cm^2 corresponding to 440 h of operation	
MEA 266 **MEA 276**	1000 start and stop Cycles	
MEA 265 **MEA 271**	100 000 triangular sweep cycles (MEA 265); 125 000 triangular sweep cycles (MEA 271); between Open Circuit Voltage (OCV) and 0.5 A/cm^2 with 2 seconds of permanence at OCV corresponding to 550 h of operation	
MEA 272 **MEA 273**	550 h of constant load operation at 0.2 A/cm^2	
MEA 274 **MEA 277**	MEA 274 - 126 h of constant OCV MEA 277 – 400h of constant OCV	
MEA 275 **MEA 263**	No test have been performed on thiese MEAs	
MEA 278	100 h conditioning 3 moths stop period 100 h conditioning	

Table 6 Test parameters and load profile of all analysed MEAs

3.2. Electrochemical diagnostic tool procedures

3.2.1. Polarization curve

In this work all measurements of polarization curves have been performed following a methodology based on the JRC recommendations [90,127,129,130] and described here below.

Differently from stack, JRC procedure for single cell test prescribes to keep constant fuel and oxidant flow rate during the entire polarization curve. In the procedure used in this experimental activity, a fixed air flow of 2.5 sl/min and a H_2 flow of 0.5 sl/min have been set.

All tests have been performed in galvanostatic mode at constant reactant gases flow and constant temperature. All inputs and outputs have been measured in continuous during the whole test with a frequency of 1Hz.

From the set value of the operating condition, current was increased up to maximum current density value of 500 mA/cm^2 by steps of 22 mA/cm^2. Since each step must have a sufficient duration to reach stationary state, the duration of the step (T_{hold}) has been chosen to be 2 minutes for all steps. Stabilization time is usually twice longer than measure time (T_{acq}) as shown in Figure 11. Hence T_{acq} has been chosen to be 1 minute.
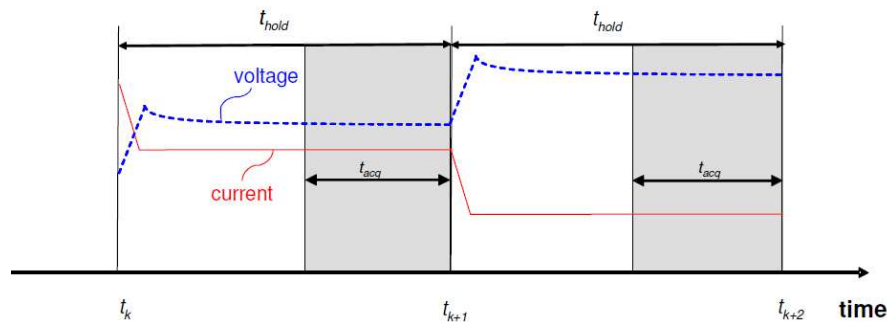
Figure 11 Data acquisition criteria [127]

Potential is acquired during T_{acq} with a 1Hz sample rate and output value is calculated as the average of the registered values.

Once the maximum current density value has been reached, current is made decrease down to OCV by steps of 22 mA/cm^2 and duration equal T_{hold} except for the current density value of 22 mA/cm^2 and at OCV for which, a T_{hold} of 1 minute and 30 seconds respectively has been chosen in order to minimize degradation due to high potential operation; T_{acq} was respectively 30 seconds and 15 seconds. Data for the recording of the polarization curve are acquired during the current density decreasing phase as shown in Figure 12.
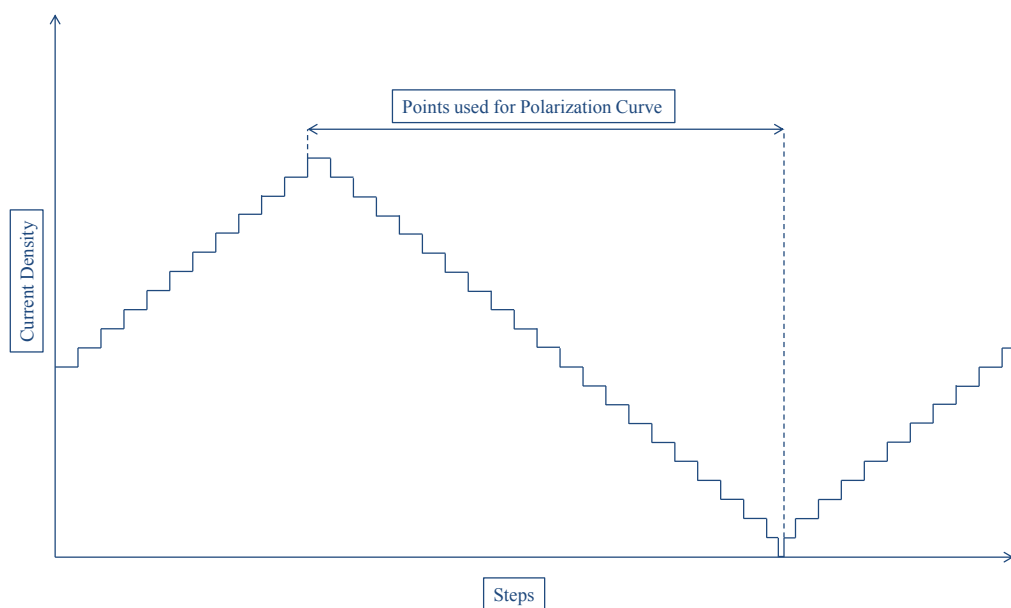
Figure 12 Polarization curve procedure for data acquisition

3.2.2. Electro-impedance spectroscopy

EIS has been carried out based on methodology described in [22] and reported here below.

EIS is carried out in galvanostatic mode without interrupting the fuel cell power generation. The amplitude of the perturbation sinusoidal function has been chosen to be of 10% of the base current. The EIS spectrum has been measured for 100 frequencies from 0.1 Hz to 1,000 Hz with a logarithmic distribution. EIS has been performed at three different current density levels: 22 mA/cm^2, 220 mA/cm^2 and 330 mA/cm^2.

EIS measurements are carried out by means of two-electrode connections in which both the counter electrode and the reference electrode from the measuring instrument are connected to the fuel cell anode.

Measures are performed with a Metronorm Autolab® Potentiostat/Galvanostat PGSTAT302. In order to measure the impedance of a fuel cell the frequency response analyser (FRA32M) was connected to the programmable load. A sinusoidal wave generated by the FRA and applied on the fuel cell through the load is added to a direct current signal. The response signals are then sent back to the FRA. In this way the impedance spectrum could be obtained.

Data were then automatically recorded and plotted by Nova® Metronorm software and then analysed in an Excel® sheet.

3.2.3. Cyclic Voltammetry

The aim of the CV measurements was to evaluate the order of magnitude of ECSA changes with the aging treatment since, as reported in literature, for this kind of membrane the interaction with the adsorbed acid may hamper a precise quantification of ECSA [22,78].

As described in §2.6.1.3 the ECSA is evaluated at cathode side and calculated from the H_2 adsorption/desorption peaks applying the methodology suggested by [131]:

$$ECSA(cm^2_{Pt}/g_{Pt}) = \frac{q_{Pt}}{\Gamma \cdot L}$$

where q_{Pt} $(C/cm^2_{electrode})$ is the charge density obtained from the CV experiment, $\Gamma = 210$ $\mu C/cm^2_{Pt}$ is the charge required to reduce a monolayer of protons on Pt and $L(g_{Pt}/cm^2$ electrode) is the Pt content or loading in the electrode.

Cyclic Voltammetry has been carried out with a constant H_2 flow of 0.4 sl/min at the anode side and a constant N_2 flow of 0.5 sl/min at the cathode side. The anode is taken as reference and counter electrode, while the anode is taken as working electrode [22]. The minimum applied voltage was 0.03 V and the maximum voltage was 0.6 V, with a scan rate of 0.2 mV/s.

Data were then automatically recorded by Nova® Metronorm software; afterwards, the cyclic voltammograms have been analysed by an Excel® procedure developed to calculate the integral of the hydrogen adsorption and desorption peaks. Average of the two peaks has been used for the calculation of the ECSA as suggested by [49].

3.3. Nano-morphological diagnostic tools procedures

3.3.1. Transmission Electron Microscopy

TEM has been performed on MEA 263 and compared with the data of [100] obtained for the same MEA with a slight different procedure of sample preparation and a different model of microscope. Comparison of results is shown in §4.1. Afterwards, TEM has been carried out on MEA 271, MEA 273 and MEA 276 with the purpose to confirm results of SAXS analysis.

TEM analysis of the samples has been carried out at the Electronic Microscopy office of the Life Sciences Department of the University of Trieste. The microscope used for the analysis was a Philips EM208 electron transmission microscope with a line to line

resolution of 0.35 nm. The microscope has been operated at 100 kV and the images were acquired with an Olympus Quemesa 2500 x 2500 kbit camera. Maximum magnification obtained was 200 000 times.

The samples have been prepared with the following procedure: a portion of few cm^2 has been cut from the MEA, the GDL has been peeled out manually and the catalyst layer has been scratched to obtain a powder that has been dissolved in isopropyl acid. For each MEA the anode and the cathode side have been analysed separately. The obtained solution has been deposit over a FCF 100H-Ni 50/pk Formvar Carbon Film on 100 Hex Mesh Nickel Grids and let dry under vacuum for two days.

The sample has then been introduced in the TEM and the obtained images have been analysed with the software ImageJ in order to determine the average Pt particle size. Firstly a portion of the sample where the nanoparticles could be found attached on the carbon support was detected (see Figure 13); afterwards, an evenly illuminated portion of the image was selected to perform image analysis.
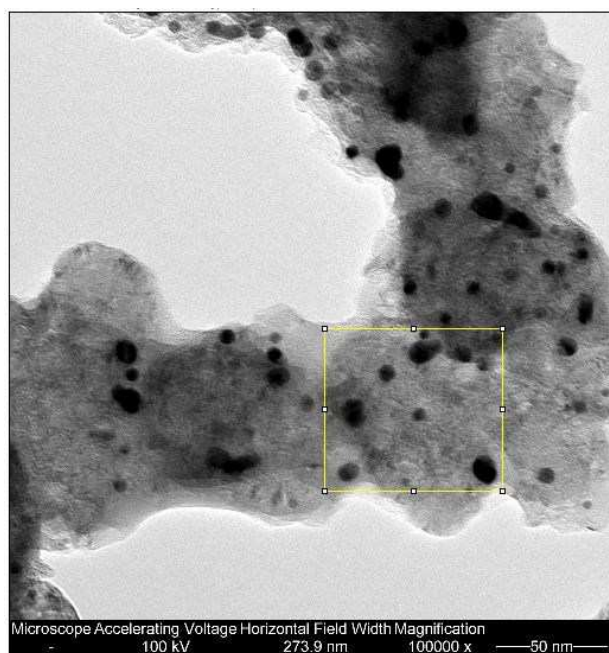
Figure 13 TEM image of MEA 276 cathode. Magnification x100000

Image was treated with a FFT bound pass filter in order to eliminate too large and too small structures and afterwards a threshold adjustment was performed to individuate the particles (see Figure 14). A minimum and a maximum size particle, as well as a circularity criteria, were then imposed to the ImageJ automatic particle detection to eliminate image artefacts. The obtained particles areas were then use to determine the average radius of the particles.
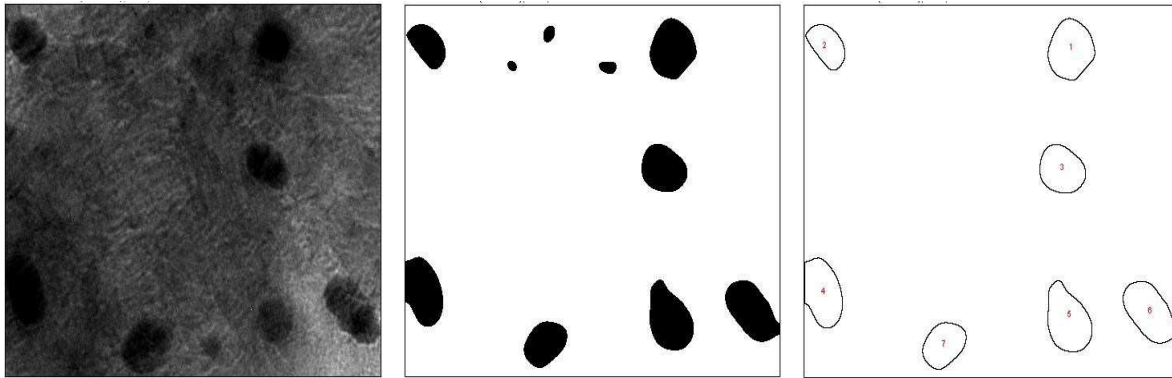
Figure 14 Example of TEM analysis - MEA 276 cathode - a) TEM image before treatment b) ImageJ treated image c) ImageJ particles selection

3.3.2. Small Angle X-ray Scattering

Small angle X-Ray Scattering analysis has been performed for all MEAs (except for MEA 278) following the procedure described hereafter.

<u>Setup of the beamline</u>

The experiments have been carried out at the synchrotron radiation source Elettra in Trieste, Italy, at the Austrian SAXS beamline [132]. The beamline has been set to have a beam dimension of about 1mm x 0.5mm, sample to detector distance of 80 cm and an X-ray wavelength λ of 1.54 Å. The SAXS images have been collected using a 2D detector (Pilatus 1M, Dectris Ltd. Swiss) with a typical exposure time of 3 s. To calibrate the angular scale of the detector silver behenate has been used. All the images obtained by the detector have then been integrated over the azimuthal angle to obtain 1D scattering pattern with respect to the scattering vector $q = 4\pi \sin\theta / \lambda$ (θ is the half-value of the scattering angle and λ is the X-ray wavelength) with the software FIT2D [133]. The final q-range was from 0.1 to 4 nm^{-1}. All integrated scattering pattern have been normalized to the primary beam intensity and corrected for transmission using the transmitted beam intensity measured by a photodiode in the beamstop. Moreover, the air scattering has been subtracted from each scattering pattern. Figure 15 shows the Setup of the SAXS beamline at Elettra in Trieste, where measurements have been performed.
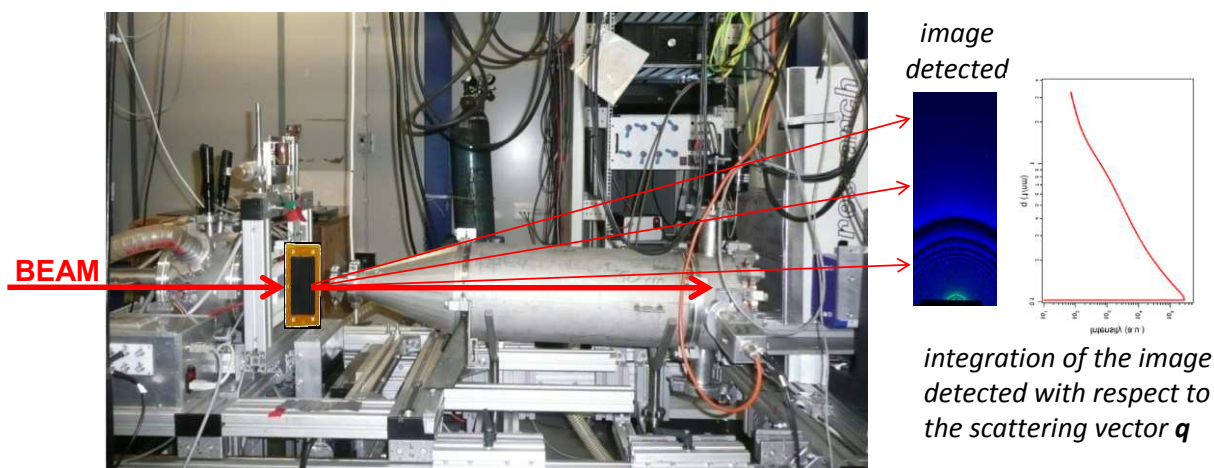
Figure 15 Setup of SAXS beamline at Elettra, Trieste

In the Figure 16 are shown the intensity curve of silver behenate and a general aged MEA.
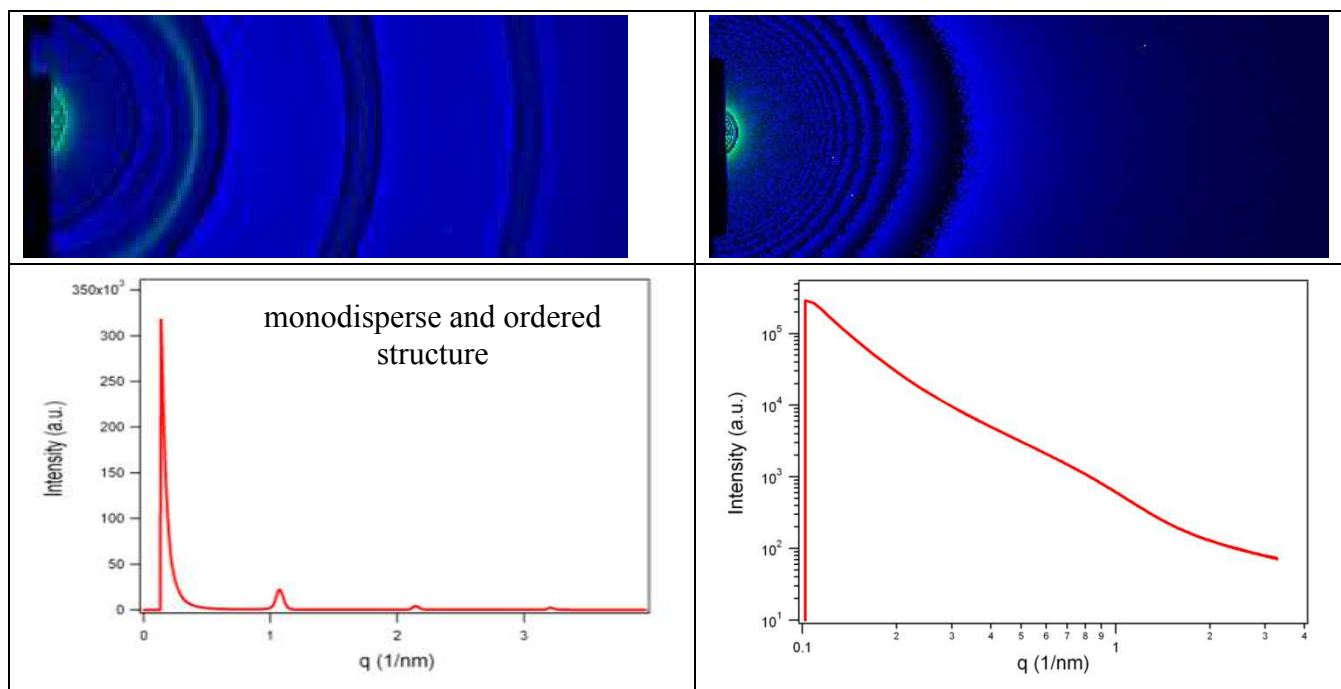
Figure 16 Intensity curve of silver behenate and a general aged MEA

Fitting of the intensity curves

The model describing the NPs within the catalyst layer considers a polydispersed system of spherical adhesive particles with a narrow and deep attractive inter-particle potential and a log-normal volume distribution of the particle sizes, as described by Pontoni et al.[134]. Figure 17 shows the parameters of the model and the inter-particles potential described by hard-sphere repulsion with an attractive square-well.
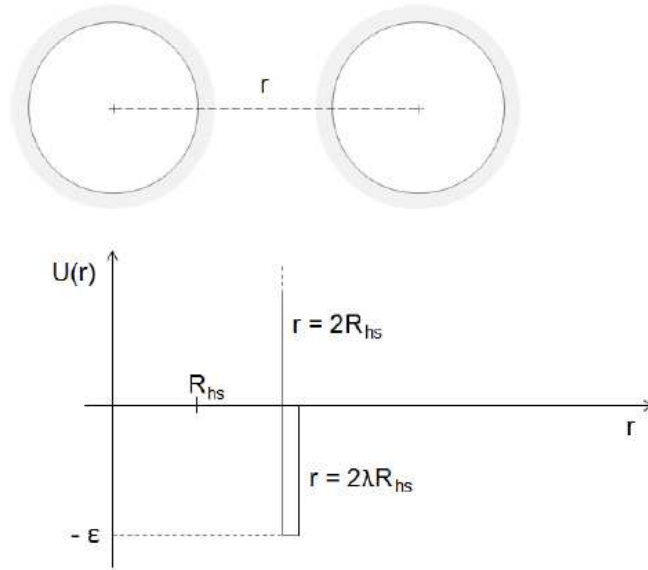
Figure 17 Schematic of the inter-particle potential assumed in the model employed to describe the Pt nanoparticles interactions. R_{hs} is the hard-sphere radius, U(r) is the inter-particle potential and r is the inter-particle distance [100]

The volume size distribution has been considered to improve the stability of the fitting. The contribution of the carbon present in the GDL and the catalyst layer has been modelled with a generalized Porod law Porod law [135]. The main parameters introduced in the model are the mean radius of the particles R, the root mean square deviation of the radius s_R, the volume fraction of the particles surrounding every single particle V_f, the width l, and depth e of the square-well of the inter-particle potential. The fitting of the experimental scattering intensity curve with the analytical curve, derived from the model, allowed the determination of these parameters. In the used model the total scattered intensity $I(q)$ from an interacting distribution of spherical particles is proportional to the form factor averaged on all the particles $\tilde{P}(q)$ which is dependent on the size and shape of each single particle, and the structure factor $S(q)$, which is a measure of the inter-particle interference:

$$I(q) \propto \tilde{P}(q) \cdot S(q)$$

Where

$$\tilde{P}(q) = \int_{r_{min}}^{r_{max}} f_R(r) \cdot V_P(r)^2 \cdot P(q) dr$$

$f_R(r)$ is the log-normal distribution function of the particles size and V_P the volume of the single particle. For uniform spherical particles, $P(q)$ may be obtained with:

$$P(qr) = A(qr)^2 = \left\{ \frac{3[sin(qr) - qr \cdot cos(qr)]}{(qr)^3} \right\}^2$$

where $A(qr)$ is the scattering amplitude of a sphere of radius r.

The structure factor *S(q)* can be obtained by solving the Ornstein-Zernicke integral equation [134] using an appropriate interaction potential *U(r)*. The calculated structure factor can then be compared with the experimental data and information on the microscopic interactions in the system can be obtained. The particle interaction potential *U(r)* can be approximated by a square-well for colloidal systems with short ranged attraction as seen in Figure 17.

$$U(r) = \begin{cases} \infty, & r < 2R_{hs} \\ -\varepsilon, & 2R_{hs} \leq r \leq 2\alpha R_{hs} \\ 0, & r > 2\alpha R_{hs} \end{cases}$$

In addition to the scattering of the particles, two terms have been added: a generalized Porod scattering that accounts for large particles in the sample (like Pt aggregates, carbon fibres and polymers) and a constant that accounts for additional diffuse scattering [134]. The whole expression of the intensity scattering used to determine the structural parameters of the sample is:

$$I(q) = I_0 \cdot P(q) \cdot S(q) + \frac{c_p}{q^p} + c$$

Where I_0 is the fitting constant for the scattering intensity of the particles, c_p is the Porod constant, p the Porod exponent and c a constant due to the diffuse scattering. The parameters have been determined by a non-linear weighted least square fitting of the model to the experimental curve with the program IGOR Pro® (Wavemetrics®, USA) [13].

3.4. Micro-CHP simulation model implementation

Experimental data obtained during this PhD activity, allowed to measure the performance degradation at each current density level as a function of the operating conditions. Literature rarely reports degradation data for the entire polarization curve; indeed, usually, only one or few values are reported for the central part of the polarization curve allowing to determine an average value but not managing to model in a proper way the performance variation over time as a function of the operational conditions. For this reason, the experimental campaign carried out in this PhD has been useful in order to implement a complete degradation model over the entire operating range of the fuel cell stack. However, degradation data have been collected for a single cell configuration working with pure hydrogen. Implementing this data directly in a micro-CHP system model would not be correct; indeed, as explained in §4.2.5, fuel stack degradation in a micro-CHP system differs by single cell configuration fed with pure hydrogen on a specifically developed test bench. For this reason different hypothesis of degradation values have been implemented in the model based on experimental results and literature data for micro-CHP

systems. This degradation model has then been implemented in an existing micro-CHP system model already developed by the research group of the University of Trieste in [61] and described here below.

The system modelled by [61] consisted in a 1kWe high temperature fuel cell system coupled with a 3kWh lithium battery pack and a water boiler used to compensate the heat power peak demand in the case it exceeds the heat power provided by the fuel cell heat recover system. The schematic of the system is reported in Figure 18.
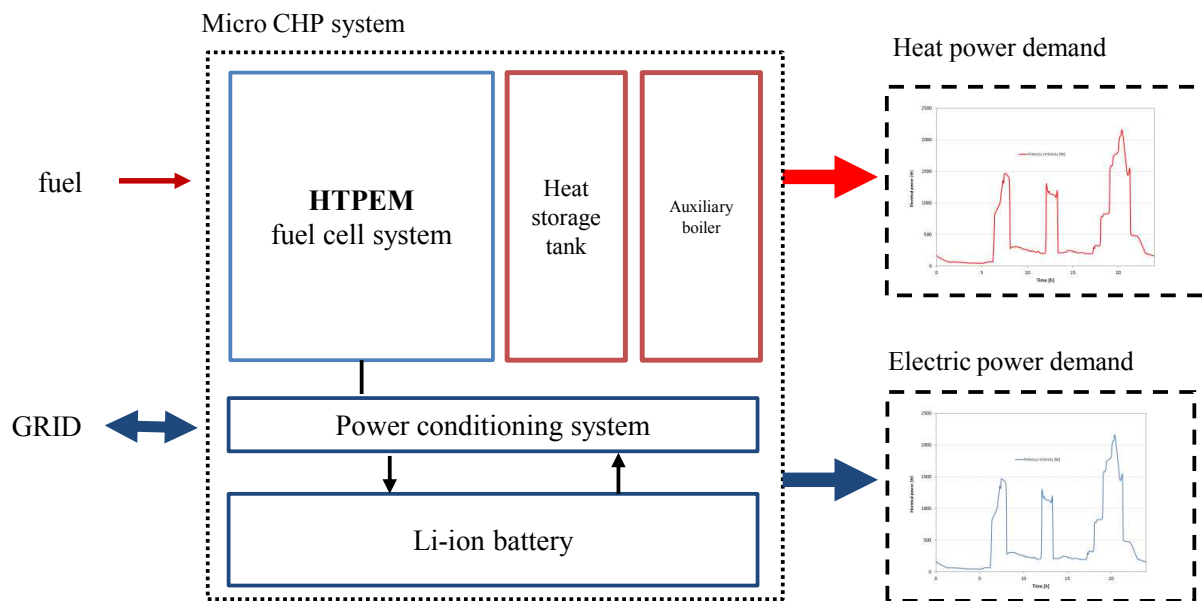
Figure 18 Schematic of the micro-CHP system – *modified from* [136]

The fuel cell system is composed by the fuel cell stack, the fuel processor and the BOP components: The fuel cell stack is an air cooled 100 cells stack based on PBI membranes with 45.16 cm^2 active area; The fuel processor is composed by a Nickel catalyst reformer reactor, a water gas shift (WGS) reactor and a desulphurisation unit, while the BOP components consist in a water pump providing the water to the steam reformer, three air blowers for anode air delivery and air cooling system, and the system controllers such as mass flow controllers and solenoid valves.

The fuel cell system, the battery pack and the grid are electrically connected through a power conditioning system which consist in a multi converter system that allows the power output of each source to be properly controlled and to fully control battery charging and discharging operations. A Battery Management System (BMS) protects the battery from over charge/discharge current and balances cells during charging operations, as shown in Figure 19.
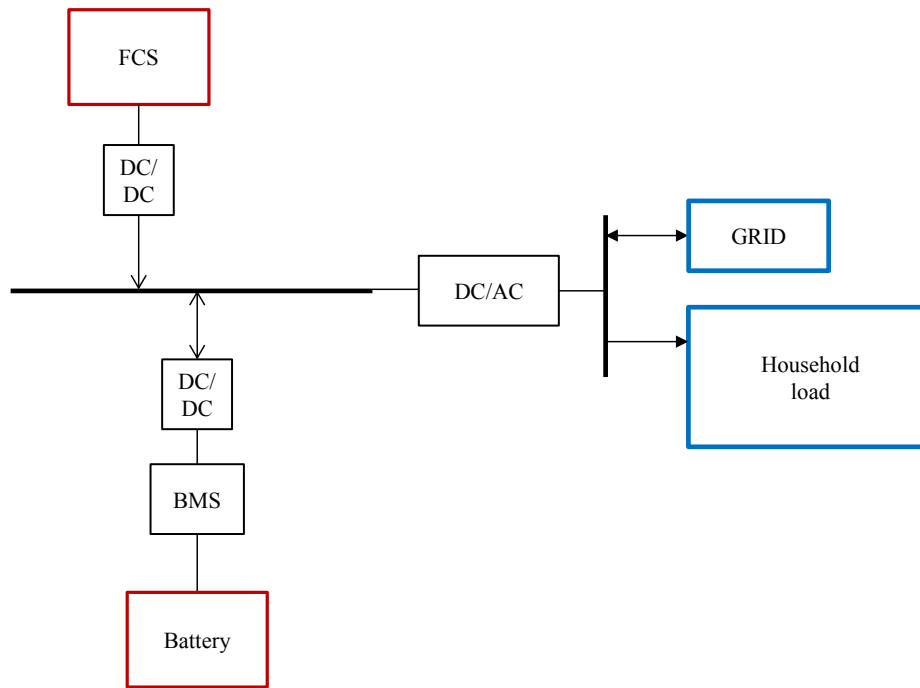
Figure 19 Schematic of the power conditioning system – *Modified from* [136]

An empirical degradation model of the fuel cell stack system has been develop based on literature data and data collected during these three years of experimental tests [137]. The model has been developed in Matlab® environment. The first step has been done by implementing the average *time-zero* polarization curve and attributing an average degradation rate for each current density level. Afterwards, it has been suggested a linear behaviour for the degradation array over time as indicated in the following governing equation:

$$V_{cell}(j,t) = V_{0,cell}(j) - DR_{cell}(j) \times t$$

Where j is the current density, *DR* is the degradation rate, t is the operational time.

Data has then been fitted with a polynomial curve whose equation can be used to extrapolate fuel cell performance for each current density values as shown in Figure 20. The fitting has been performed with the polynomial Matlab® *"polyfit"* fitting function.
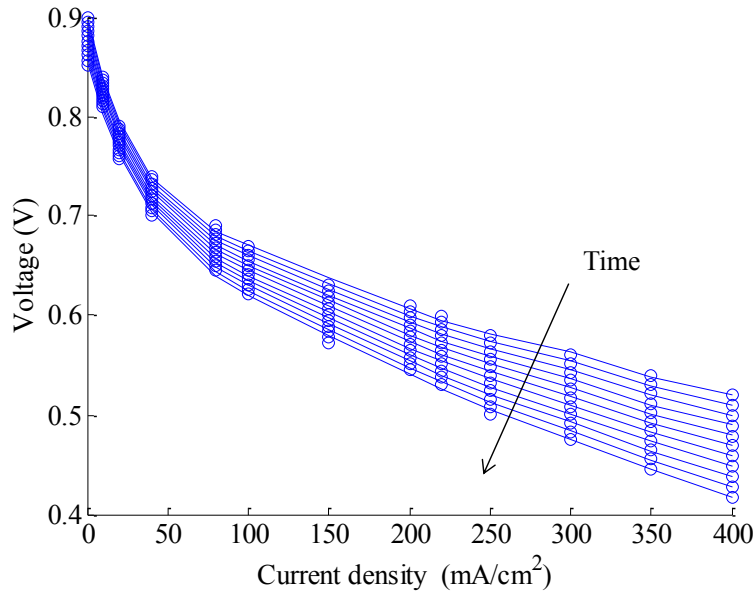
Figure 20 Cell performance degradation model. Cell polarization curves over one year of operation. Each curve represents fuel cell performance after 796 h of operation [137]

In Figure 20 the dots on the plot corresponds to the V(*j,t*) matrix calculated by the model and do not corresponds to experimental data.

Afterwards the obtained time-dependent polarization curves have been used to develop a global CHP system efficiency model.

Considering that:

$$V_{0,stack}(j) = V_{0,cell}(j) * n_{cell}$$

$$J_{stack}(j) = j \times A_{cell}$$

$$DR_{stack}(j) = DR_{cell}(j) * n_{cell}$$

Where $V_{0,stack}$ is the fuel cell stack potential at time 0, $V_{0,cell}$ is the single cell potential at time 0, n_{cell} is the number of cells, J_{stack} the current, j the current density, A_{cell} is the cell active area and DR_{stack} and DR_{cell} are respectively the stack and single cell degradation rates.

It can be written:

$$V_{stack}(j,t) = V_{0,stack}(j) - DR_{stack}(j) \times t$$

$$P_{stack}(t,j) = J_{stack}(j) \times V_{stack}(j,t)$$

83

Where V_{stack} is the stack potential at time t and P_{stack} is the power of the stack at time t.

From here, it is possible to derive the expression of the stack efficiency (η_{stack}) based on the definition given by [61]:

$$\eta_{stack}(j,t) = \frac{J_{stack}(j) \times V_{cell}(j,t)}{J_{stack}(j)}$$

This allows us to obtain a degradation model of the entire micro-CHP system efficiency by defining the net electric efficiency (η_{net}) and net delivered power (P_{net}) of the system in the following way:

$$\eta_{net}(j,t) = a \times \eta_{stack}(j,t) \times \eta_{BOP}(j) \times \eta_{FP}(j) \times \xi_{REC}(j)$$

$$P_{net}(t,j) = P_{stack}(t,j) \times \eta_{BOP}(j)$$

Where a is a constant, η_{BOP} is the balance of plant efficiency and η_{FP} is the efficiency of the fuel processor (reformer).

The coefficient ξ_{REC} is a coefficient that takes into account the effect of anode off gas flow recirculation on the efficiency of the reformer and is defined in as follows:

$$\xi_{REC} = \frac{1}{1 - \dfrac{m_{REC} \cdot LHV_{REC}}{m_{Burn}^* \cdot LHV_{m_{Burn}^*} + m_{ref} \cdot LHV_{m_{ref}}}}$$

Where m_{REC} is the mass of the anode off recirculating gas, m^*_{burn} the mass of the fuel going to the burner and m_{ref} the mass of the fuel going to the reformer as shown in the schematic of the fuel cell system reported in Figure 21.
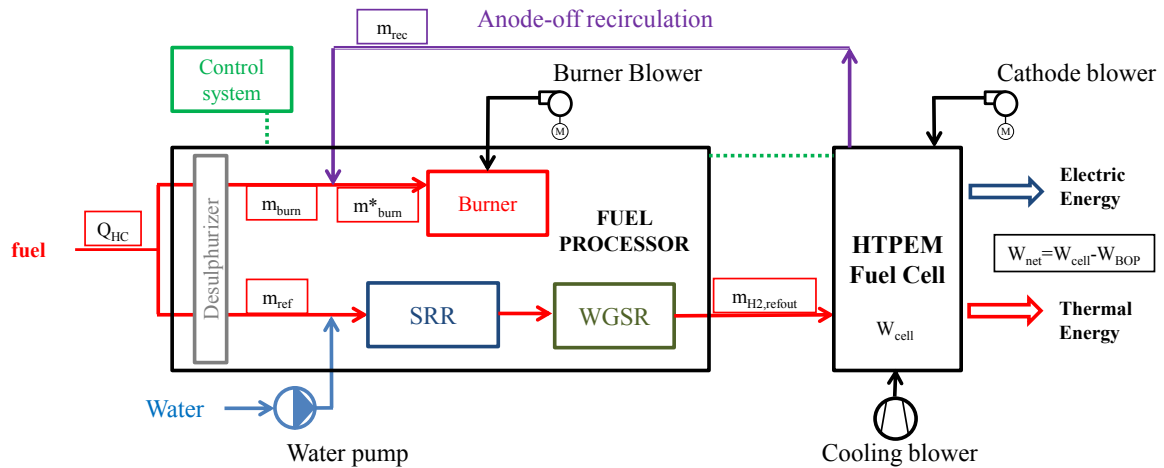
Figure 21 Schematic of the fuel cell system [61]

Also in this case, the same approach developed for the polarization curve modelling has been followed and a polynomial fitting time-dependent expression has been obtained, allowing to determine the system net power and efficiency for each current density level as shown in Figure 22. The fitting has been performed with the polynomial Matlab[®] *"polyfit"* fitting function.
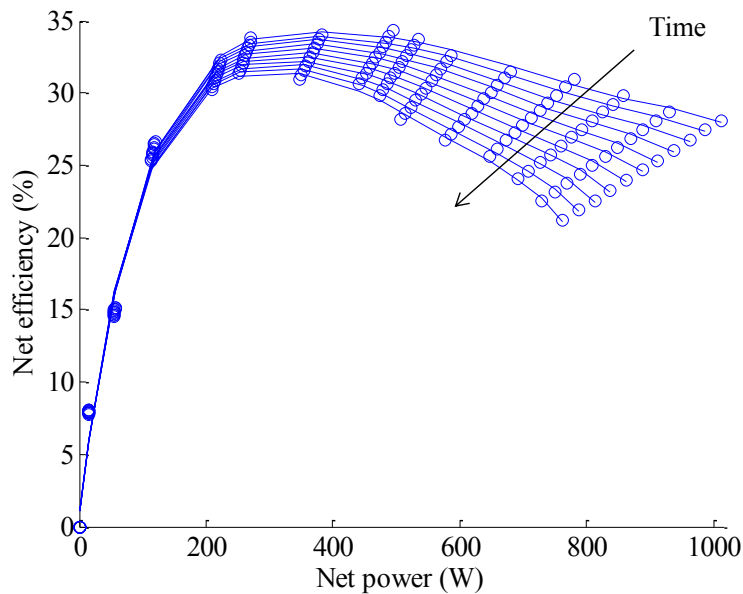
Figure 22 Cell performance degradation model. CHP system efficiency variation over one year of operation. Each curve represents fuel cell performance after 796 hours of operation. [137]

In Figure 22 the dots on the plot corresponds to the $\eta(W,t)$ matrix calculated by the model and do not corresponds to experimental data.

This time-dependent polynomial fitting expression of the CHP system efficiency could hence be implemented in the existing model developed by [61].

4. Results and discussion

In this chapter, paragraph 4.1 is dedicated to a general discussion on the repeatability and reproducibility of experimental ageing test performed on HT-PEM MEAs, highlighting the main difficulties encountered in performing experimental tests on this type of MEAs.

Experimental results obtained during the ageing tests performed during this PhD activity are presented and discussed in §4.2. To allow an easier comparison between the results, it has been chosen to present and discuss the results dividing them by operational test conditions as already reported in Table 6. Hence § 4.2.1 presents data obtained for MEA 272 and MEA 273 operated at constant load, §4.2.2 presents data obtained for MEA 271, MEA 265 and MEA 264 operated with different load cycles. Paragraph 4.2.3 presents results obtained for MEA 274 and MEA 277 operated at OCV while §4.2.4 presents results of MEA 266 and MEA 276 that have been subjected to start and stop cycling. Paragraph 4.2.5 analyses the results of degradation of this type of MEAs installed in a micro-CHP systems.

Literature and experimental data have been used to develop the degradation model following the methodology described in §3.4. Performance analysis in terms of energy balance of plant and primary energy saving (PES) has been performed thanks to the developed model. Main results are reported in §4.2.6.

4.1. Experimental reproducibility and repeatability

Definitions of terms related to the measurements uncertainty used in this PhD thesis refers to definitions given by the Joint Committee for Guides in Metrology (JCGM) in the Guide to the expression of Uncertainty in Measurement [138], in particular, reproducibility and repeatability are defined as follows:

Reproducibility is the closeness of the agreement between the results of measurements of the same measure and carried out under changed conditions of measurement.

Repeatability is the closeness of the agreement between the results of successive measurements of the same measure and carried out under the same conditions of measurement.

Performing degradation measurement on HT-PEM MEAs over a long period is a complex task. In this paragraph, an overview of the main difficulties for this kind of experimental

test will be given in order to improve the interpretation of results reported in the following paragraphs.

Difficulties on degradation measurements come from many factors, in particular: fabrication differences, cell assembly differences, history of the MEA and operating conditions that affect reproducibility of the measurements.

First of all, fabrication differences exist even for MEAs of the same producer and coming from the same production series. These differences influence the initial performance of the MEA and also its repose to degradation test.

A second important issue consists in the reproducibility of the mounting of the MEA in the test bench hardware. Hardware layout can influence performance of the fuel cell. For example as reported in [139] bipolar plates perform critical functions on fuel and oxidant distribution, on electrical current conduction from each cell and on the cell cooling in the stacks. Moreover, the same membranes installed in a single cell configuration or in a stack do not have the same performance and degradation [14] since, position of the cell in the stack can influence its performance and degradation. As reported by [92] another important parameter that can strongly influence performance of the fuel cell is the clamping pressure which must hence be very carefully controlled. Even gasket property can influence performance, for example, some impurities deposited on the gasket could cause anode – cathode crossover. Only the experience of the person performing the test can guaranty a good reproducibility.

Lastly, the history of the MEA can have an important effect on performance measurement of the MEA. Accidents during the test, which are almost unavoidable for long term experiments, can have a non-negligible effect on degradation. Unfortunately, this is not just caused by the start and stop cycle caused by an accidental switch off of the test bench or accidental permanence at OCV and temporary fuel starvation conditions but can also be influenced by the age of the membrane, the duration of the test [86] and by the duration of the stop time.

As an example of this last mentioned condition, the MEA 278 has been conditioned for 100 hours following the same procedure as for the other membranes, but afterwards, instead of begging the ageing test it has switched off and left in the test bench for three months. After this stop period it has been switched-on again and, as reported in Figure 23 and it showed a very strong degradation which corresponds to about 26 μV per stop period hour calculated at 0.22A/cm^2. The conditioning procedure has then been repeated to check if performance could be recovered.
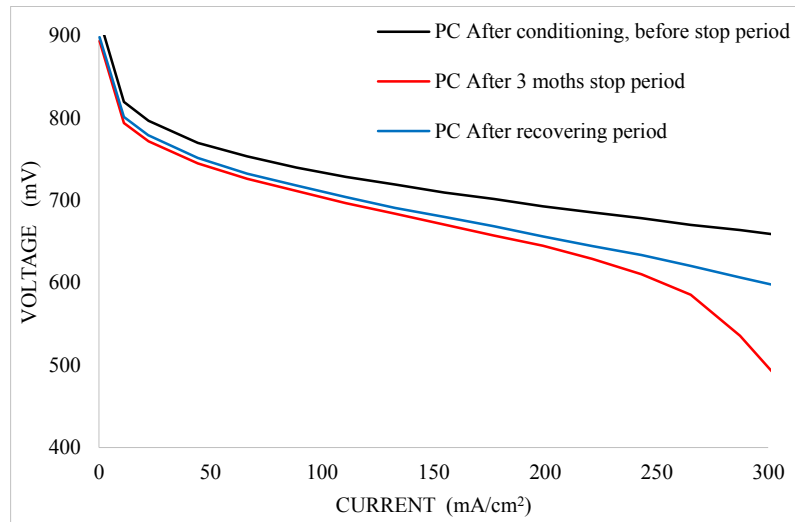
Figure 23 Polarization curves of MEA 278 before and after stop period and recovering period

An improvement of the performance has indeed been obtained, but performance do not went back to initial values of the MEA before the stop period. This highlights the importance of the effect of the MEA history on its performance analysis.

In addition to these reproducibility issues, repeatability of measurements for each diagnostic tool is influenced by measurement uncertainty and procedure of measurement. Indeed as explained in §3.2 precise procedures in performing electrochemical analysis of fuel cell is indispensable to allow repeatability of measurements due, as well, by hysteresis problem highlighted in [140]. Estimating the repeatability of measurements is indispensable to understand if a variation of the measured performance can actually be interpret as a MEA degradation effect or it must be attributed to one or more of the aforementioned uncertainties.

For this reason, the reference performance measurements, before the begging of the ageing test, were repeated twice and, during the entire ageing test, measurements were performed periodically in order to verify the trend of performance evolution.

Figure 24 shows the first two polarization curves performed before the ageing test for MEA 272 and Figure 25 shows the first two polarization curves performed before the ageing test for MEA 273. These two results allow the analysis of two important aspects of the polarization curve measurement. First of all, it can be notice that for MEA 273 the two measurements are in good agreement confirming the repeatability of the polarization curve as diagnostic tool. Indeed, for MEA 273 differences between the first and the second measurement is less than 0.5% for the low and medium current density region but it grows up to 1.8% at high current densities. In the polarization curve analysis of MEA 272 it is interesting to notice the strong sensibility to operating condition and MEA history of the high current densities region. Indeed, while for the low and medium current density region, the repeatability is quite good, in the high current density region, the difference between the first and the second measurement goes up to 5,7% with the second

89

measurements showing an increased performance. This can be possibly explained by variation on mass transport that could actually be caused by the first polarization curve. In fact, variation of current levels can allow the elimination of some local flooding, eventually reducing mass transport losses [86]. This highlight the complexity of analysing the performance and the degradation of fuel cell in the high current density region dominated by mass transport losses that are very sensible to air pressure, humidity variation and local phosphoric acid distribution.
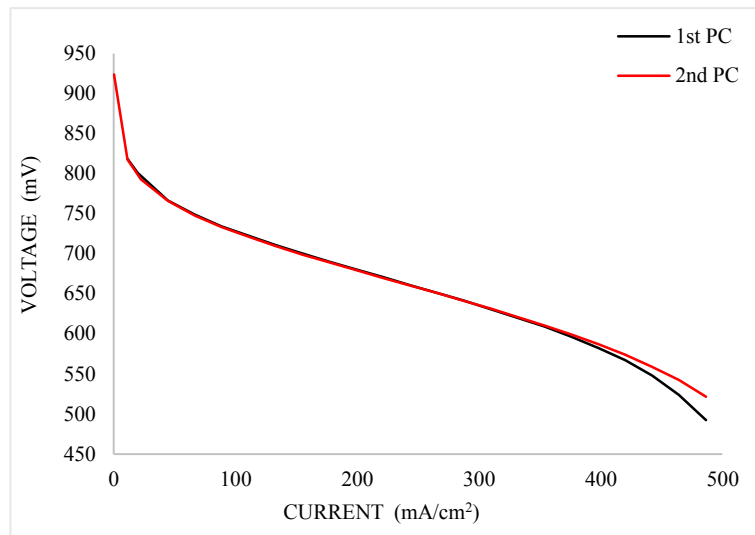
Figure 24 Polarization curves of MEA 272 after conditioning
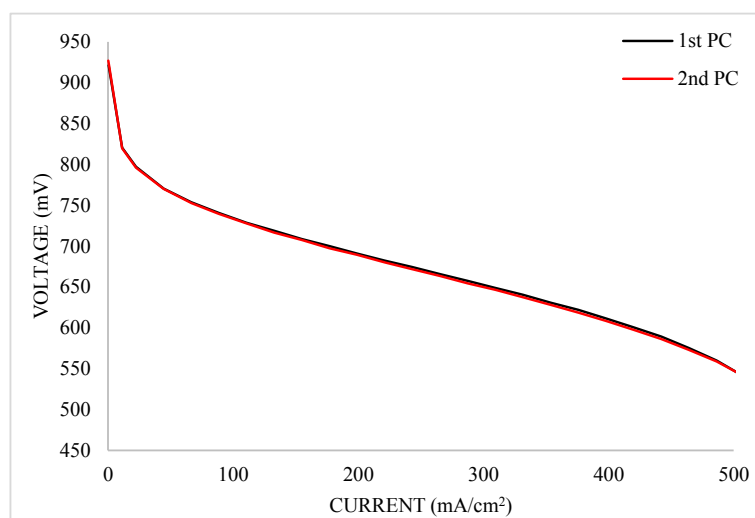
Figure 25 Polarization curves of MEA 273 after conditioning

Figure 26 compares the initial polarization curves of MEA 272 and MEA 273. The presented data are the average of the first two subsequent measurements for the two

MEAs. It is evident that even if the two MEAs are exactly of the same type, their behaviour differs. This is attributable to fabrication differences that, as said before are still unavoidable due to the low scale production of this type of membranes that makes the production procedure remain quite artisanal.
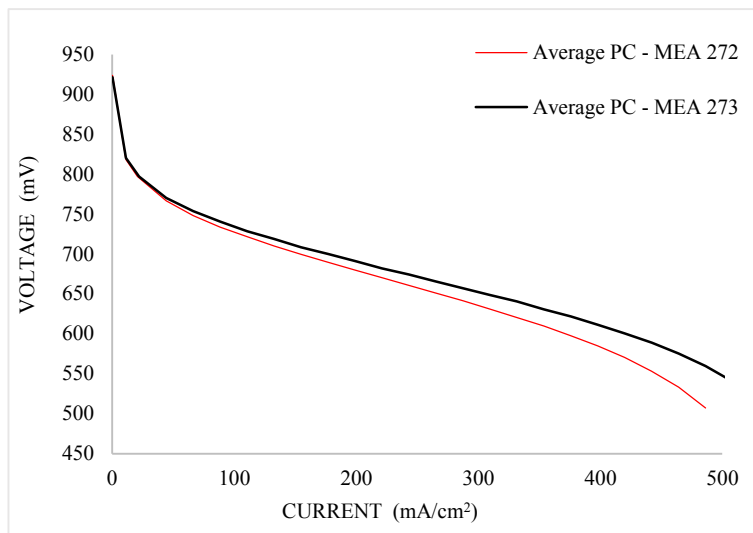
Figure 26 Comparison between initial PCs of MEA 272 and MEA 273

As for the polarization curves, also the EIS measurements has been repeated twice to verify the repeatability. The EIS measurements are performed at three different current levels: 1A, 10A and 15A. The measurements effectuated on MEA 272 confirm that something occurred between the first polarization curve measurement and the second one at a mass transport level. Indeed, while at low and medium current densities (1A and 10A) the first EIS measurement and the second show a very good agreement, at high current level it can be find again a difference in the mass transport arc of the EIS spectra as shown in Figure 27.
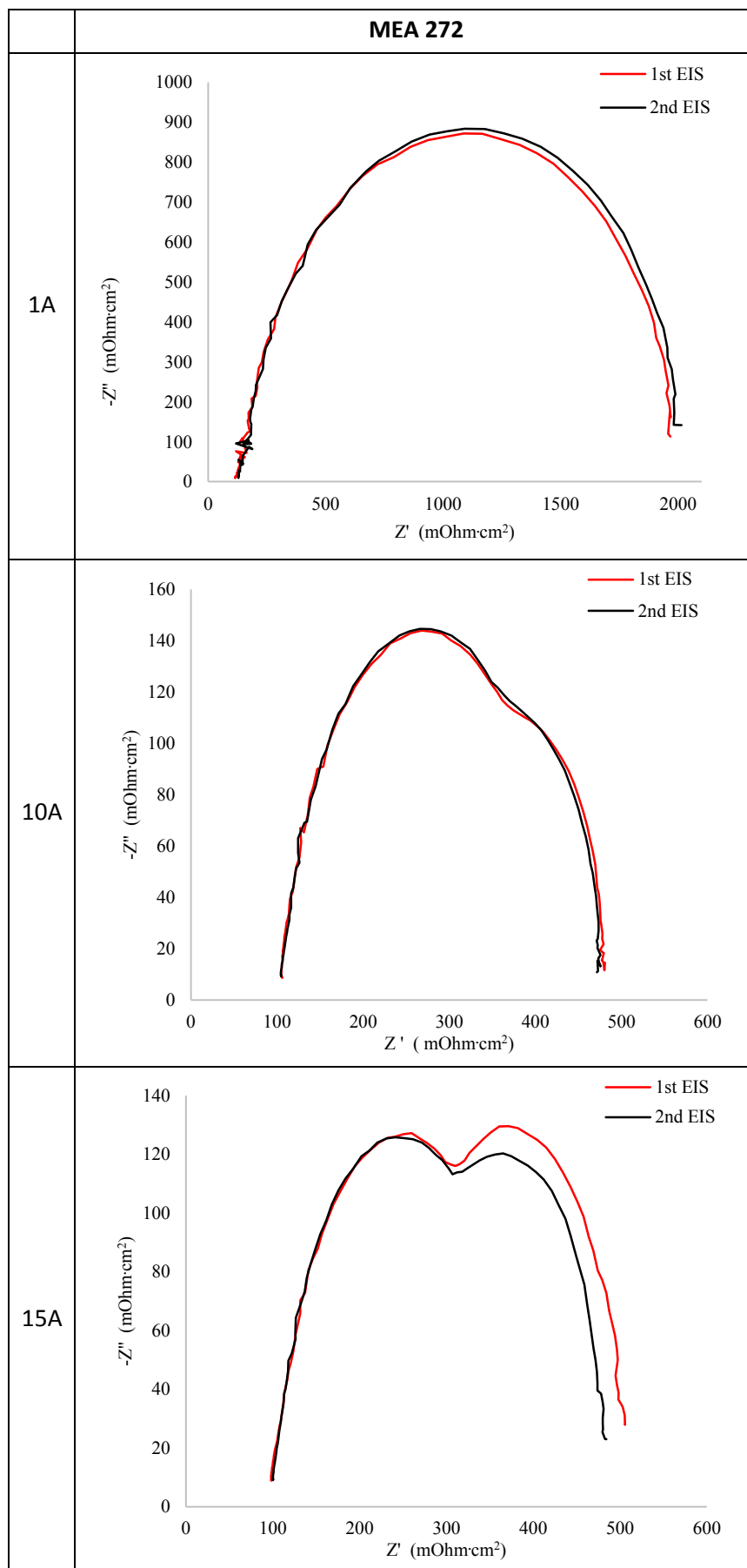
Figure 27 EIS spectra of MEA 272 at the beginning of the test

Afterwards a CV measurement has been performed following the methodology described in §3.2.3. The CV measurement has been repeated three times. Results for MEA 272 and MEA 273 are shown in Figure 28.
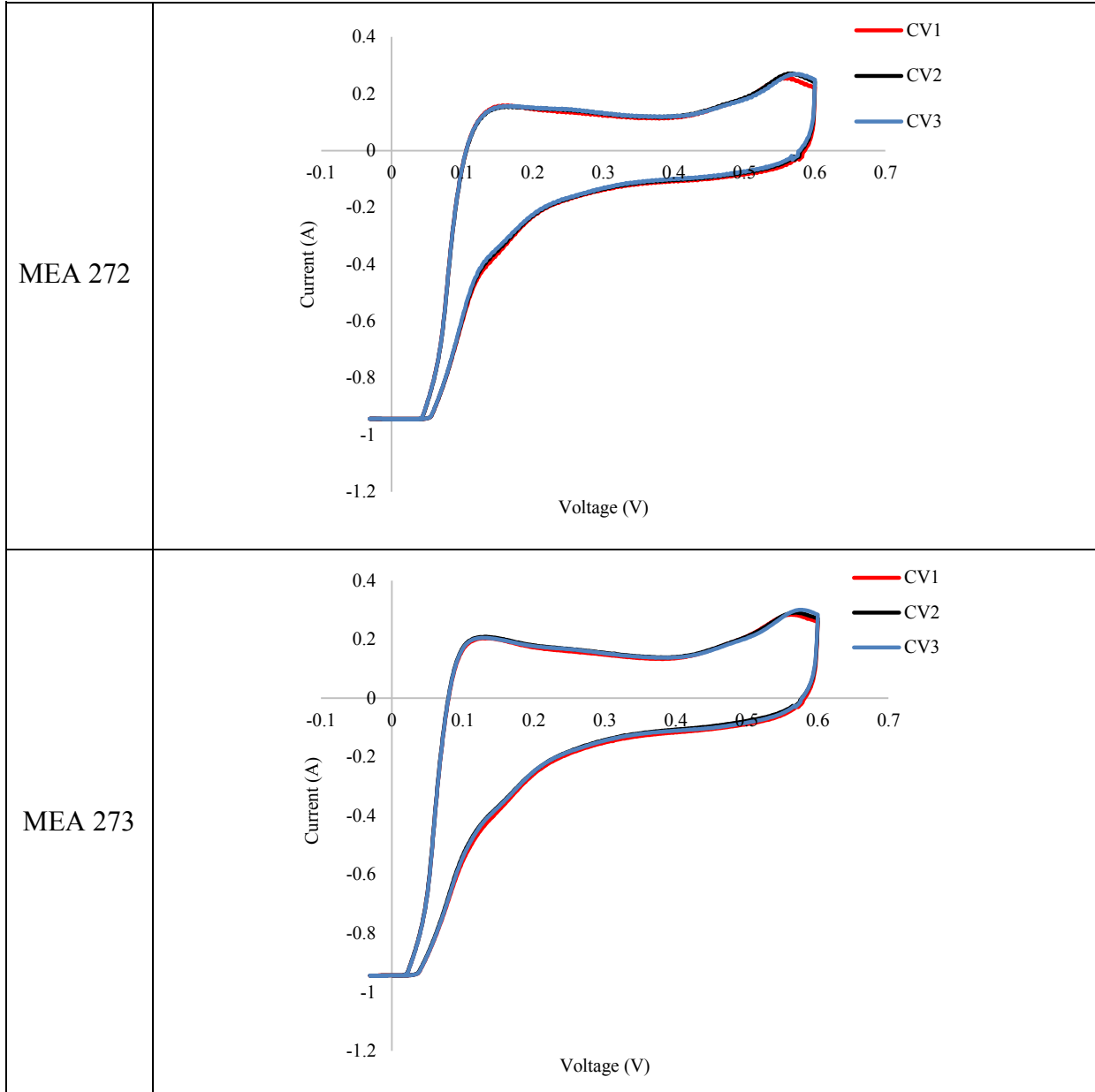
Figure 28 CV measurement before the ageing test for MEA 272 and MEA 273

As described in §3.2.3 the voltammograms have been used to calculate the Electro Chemical Surface Area (ECSA) which correspond to the Pt catalyst active surface. The calculation has been performed estimating the area under the hydrogen adsorption and desorption peaks and averaging them as reported in §3.2.3. For MEA 272 an initial average ECSA of 23.2 m^2/gPt has been found, while for MEA 273 an initial average ECSA of 26.2 m^2/gPt has been found; these values are in accordance with results obtained by [22,78] for similar MEAs. The

difference encountered between MEA 272 and MEA 273 can be attributed to construction differences confirmed as well by the higher initial performance of MEA 273 found during the polarization curve measurement (see Figure 26).

The same slight increase in performance found for MEA 272 at high current densities between the first and the second measurement has been noticed as well in the first set of measurements performed on MEA 271 and shown in Figure 29.
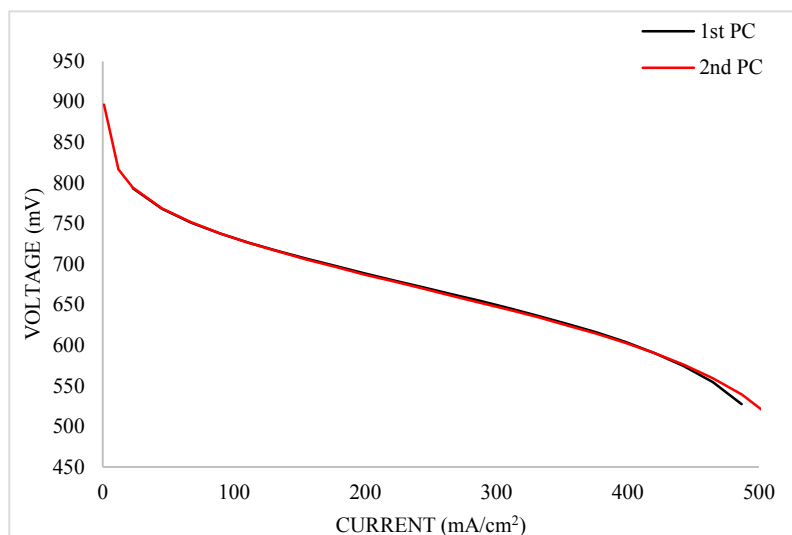
Figure 29 Polarization curves of MEA 271 after conditioning

In this measurement a supplementary precaution had been taken, choosing to not reach OCV in the first polarization curve in order to avoid possible effects on the second measurement. But this precaution seems to not have influenced the results. Difference between the two measurements is less than 1% for low and medium current densities while reaches 4.9% of difference at high current densities.

EIS measurement has been performed at three different current levels as for MEA 272 and MEA 273. The first measurement has been repeated twice. In this case the repeatability was not very good as shown in Figure 30. However, this difference is understandable since, after the first EIS measurement the fuel cell has been switched off and the second EIS has been performed after some days. This important issue has already be underlined by the analysis of MEA 278, in fact, while measurements are very repeatable if performed one after the other with a small time interval (i.e. 4 hours), as it has been done for example for the polarization curve measurements shown in Figure 29, at the opposite, even if no operation time has passed from one measurement to the other, just one start-stop cycle with some day of operating pause can sensibly influence the second measurement as noticeable in Figure 30.
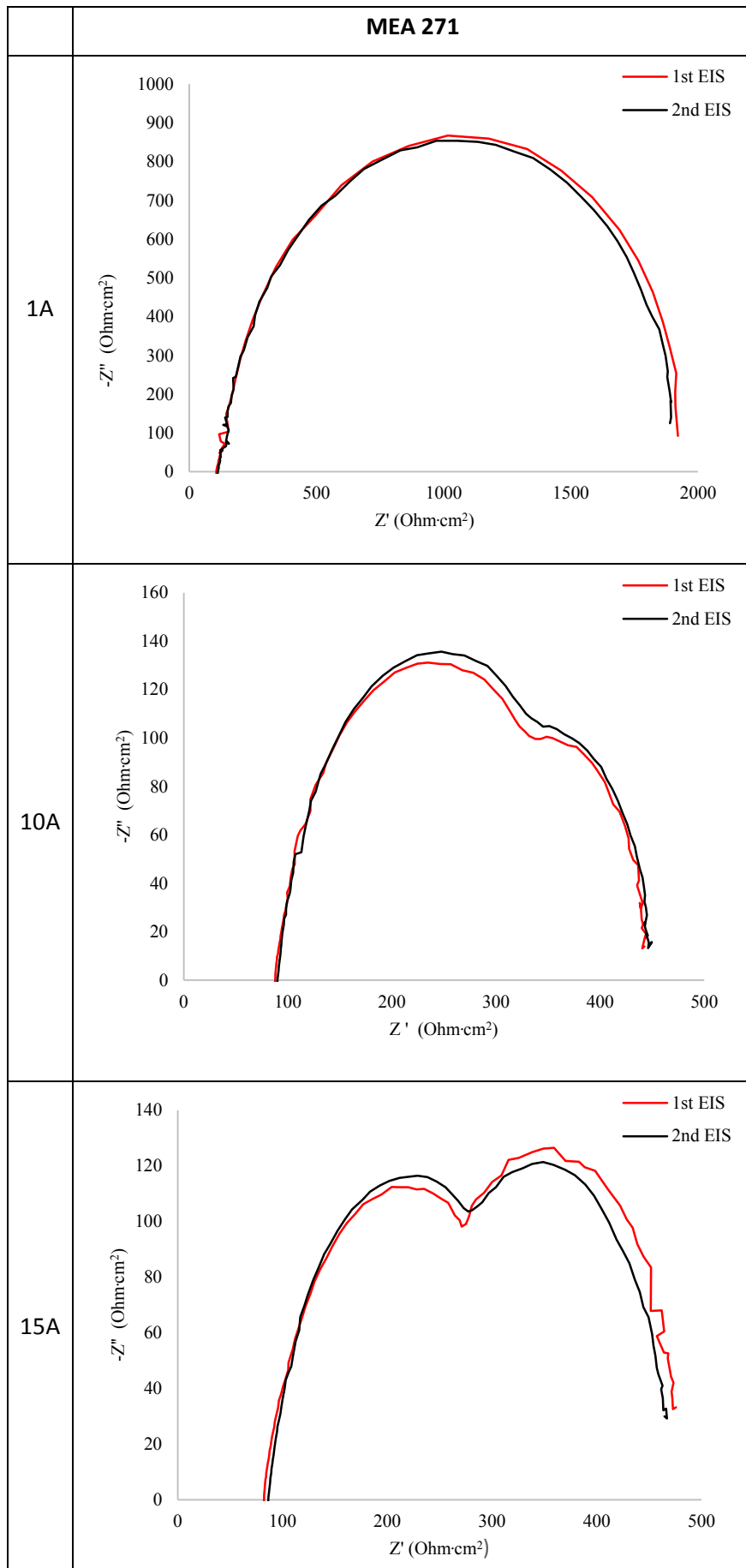
	MEA 271
1A	
10A	
15A	

Figure 30 EIS spectra of MEA 271 at the beginning of the test

Cyclic voltammetry has then been performed following the methodology described in §3.2.3. The CV measurement has been repeated three times as for MEA 272 and MEA 273. Results are reported in Figure 31.
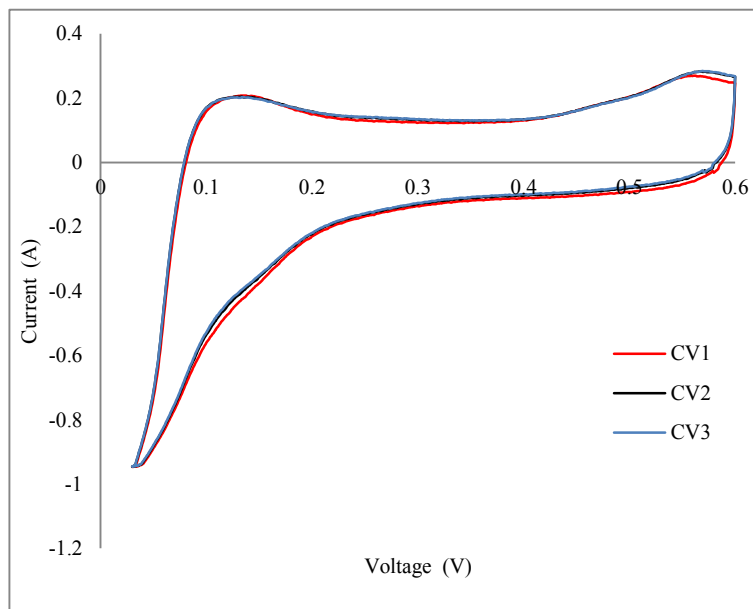
Figure 31 CV measurement before the ageing test for MEA 271

Concerning SAXS analysis a new membrane, MEA 275, has been analysed. A first Pt mean radius measurement has been performed on the untouched MEA 275, these data have, then, been compared with the one obtained for MEA 263 in a previous SAXS analysis [13] to check the reproducibility of the test. The Pt mean radius values of these two MEAs were, 2.78 nm (st. deviation 0.64) for MEA 263 and 2.38 nm for MEA 275 (st. deviation 0.59). A second SAXS measurement has been carried out removing the GDL from the MEA 275. This has been done with the purpose to evaluate if the presence of the GDL could influence the SAXS results. The difference between this two Pt mean radius measurements is about 0.17 nm (2.38 nm with GDL and 2.55 nm without GDL). Figure 32 shows the comparison between the 3 different log-normal volume distributions obtained by the SAXS analysis results of the two membranes: MEA 263 and MEA 275.
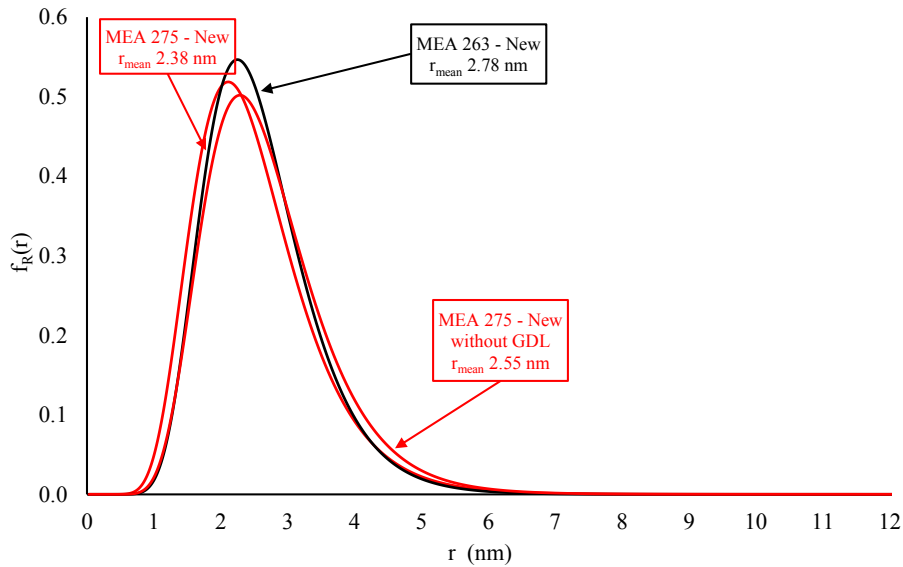
Figure 32 SAXS analysis. Volume size distributions of MEA 263 (black line) and 275 with and without GDL (red line)

Concerning TEM analysis, MEA 263 has been analysed with the purpose to check the reproducibility of the technique. MEA 263 had already by analysed with the TEM technique by the research group [100] and results showed for the cathode a mean radius of 2.85 nm (st. deviation of 0.81), while, for the anode a mean radius of 2.26 nm (st. deviation 0.81) has been found. The weighted average was of anode and cathode Pt particles radius was 2.55 nm (st. deviation 0.86).

In the analysis performed in this PhD activity, a mean radius of 2.33 nm (st. deviation 1.2) has been found at the cathode (see Figure 33), and a mean radius of 2.17 nm (st. deviation of 0.72) at the anode (see Figure 34). The weighted average of anode and cathode Pt particles radius is 2.30 nm (st. deviation 1.13).
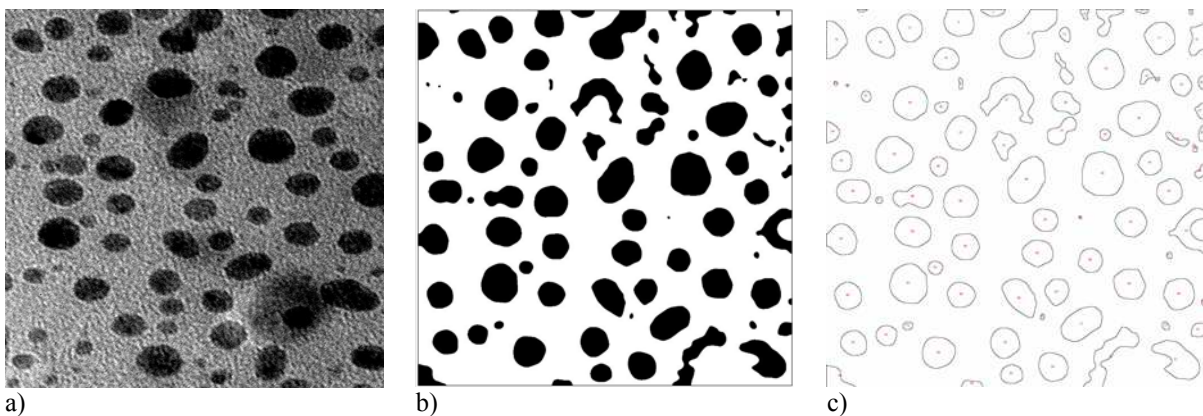
Figure 33 TEM analysis of MEA 263 cathode - a) TEM image before treatment b) ImageJ treated image c) ImageJ particles selection
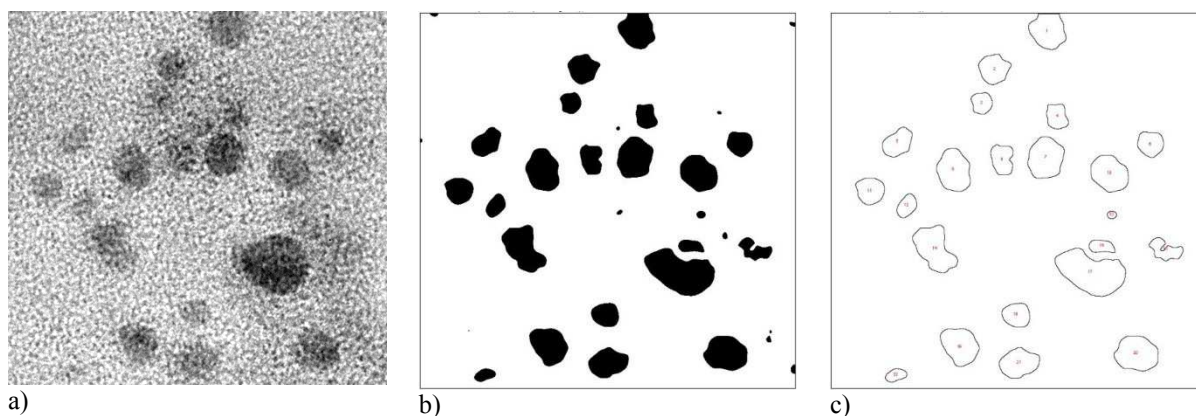
Figure 34 TEM analysis of MEA 263 anode - a) TEM image before treatment b) ImageJ treated image c) ImageJ particles selection

Even if the number of analysed samples is limited, results suggest that TEM analysis has a good reproducibility. However, as already highlighted by [100], the comparison between SAXS and TEM data showed that there is a difference in terms of mean radius detected by the two techniques. Indeed, the mean radii of Pt particles obtained by SAXS are bigger than the one obtained by TEM analysis. This difference can be attributed to different reasons: higher sensitivity to bigger particles of the SAXS technique, the fact that probably not all the catalyst layer thickness can be analysed by TEM technique and the difference in the analysed portion of the MEA (area covered by SAXS is 10^6 higher than TEM analysed area).

4.2. Degradation tests

4.2.1. Constant load operation

In order to study the effect of constant load operation on MEA degradation, a literature review has been carried out. In a second phase, an experimental analysis has been performed on two MEAs: MEA 272 and MEA 273.

Here below, in Table 7, literature degradation values are reported for HT-PEM fuel cells in a single cell configuration operated at constant load. In grey are highlighted the data referred to Celtec P1000 membranes which correspond to the ones used for the experimental test carried out in this PhD activity.

Type of membrane ---	PA doping level	Operating current density	Operating temperature	Operating stochiometry	Duration of the test	Current density for degradation measure	Degradation rate	Ref.
type	PA/repeat unit	A/cm2	°C		h	A/cm2	μV/h	
para-PBI	27.7	0.2	80	λH_2=1.2 λair=2	800-1000	0.2	45	[47]
			160				4.9	
			190				60	
2OH-PBI	25.4	0.2	80	λH_2=1.2 λair=2	800-1000	0.2	14	
			160				5.8	
			190				39	
Homemade PBI/ H_3PO_4	85	0.64	150	100 ml/s H_2 100 ml/s air	100 conditioning + 500	0.64	150	[72]
Homemade PBI/ H_3PO_4	85	0.2	160	λH_2=1.3 λair=1.8	780	0.2	25	[42]
m-PBI membranes (Dapozol®)		0.24	160	λH_2=1.5 λair=2.5	17000	0.24	9	[19]
BASF Celtec-P2100		0.2	160	λH_2=1.2 λair=2	950	0.2	8.6	[22]
BASF Celtec-P2100		0.2	160	λH_2=1.2 λair=2	540	0.2	6	
BASF Celtec-P2100		0.2	160	λH_2=1.2 λair=2	210	0.2	7	

(Dapozol®)-G55	8-9	0.3	160	$\lambda H_2=1.5$ $\lambda air=2$	10000	0.3	**57**	[141]
				$\lambda H_2=1.5$ $\lambda O_2=9.5$			**70**	
				$\lambda(78\%H_2+22\%CO_2)=1.5$ $\lambda air=2$			**63**	
H_3PO_4/PBI HT-PEMFC	-	0.2	-	$\lambda H_2=1.2$ $\lambda air=2$	1000	0.2	**33**	[142]
Homemade PBI/ H_3PO_4	-	-	150	$\lambda H_2=1.2$ $\lambda air=2$	17800	0.2	**3.6**	[45]
Homemade Co-20%SO_2PBI	11	0.3	160	-	2400	0.3	**2.4**	[143]
			180	-			**6.4**	
H_3PO_4/PBI HT-PEMFC	85% H3PO4 at 60 °C for 20 min	0.714	150	H_2 = 100 mL/min O_2 = 100mL/min	510	0.714	**81.6**	[102]
Celtec®-P 1000	-	0.4	160	λref (70% H_2 + 29% CO_2+ 1% CO) = 1.4 $\lambda air=2$	70 conditioning + 505	-	**41**	[14]
Celtec®-P 1000	70	0.2	160	-	18000	0.2	**6**	[35]
Celtec®-P 1000	70	0.2	160	$\lambda H_2=1.2$ $\lambda air=2$	6000	0.2	**5**	[21]
Celtec®-P 1000	70	0.2	150	$\lambda H_2=1.2$ $\lambda air=2$ .2	1640	0.5	**15.3**	[23]
Celtec®-P 1000	70	-	-	-	-	-	**<6**	[144]
Celtec®-P 1000	70	-	180	$\lambda(60\%H_2$ 2% CO and 5-ppm	3500	-	**17**	[77]

Table 7 Degradation rates in literature of HT-PEM single cells operated at constant load

Experimental testing of MEA 272 and MEA 273

The experimental testing of the MEAs has been carried out following the methodology described in chapter 3. The membranes have both been installed in the hardware following the same procedure and with the same clamping torque of 7Nm. The membranes have then been activated with 100h of constant load operation as suggested by the manufacturer.

After the first set of measurements reported in §4.1 the membranes have been operated at constant load of 220mA/cm^2 for 550h. Periodically polarization curves and EIS measurements were performed to evaluate the trend of the degradation and the main parameters were recorded in continuous. Unfortunately, it was not possible to perform the measurements of polarization curves and EIS at constant interval of time for MEA 272 and MEA 273. Figure 35 and Figure 36 show the polarization curves recorded during the ageing test respectively for MEA 272 and MEA 273.
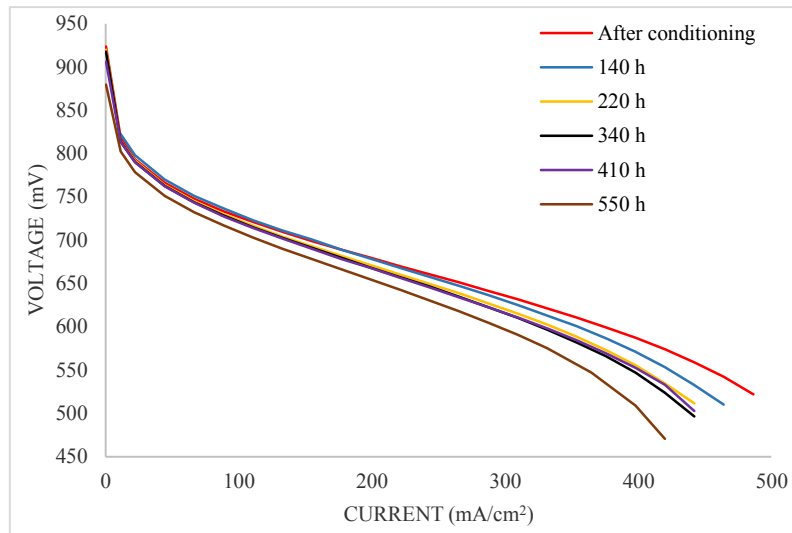
Figure 35 Polarization curves recorded during constant load degradation test of MEA 272
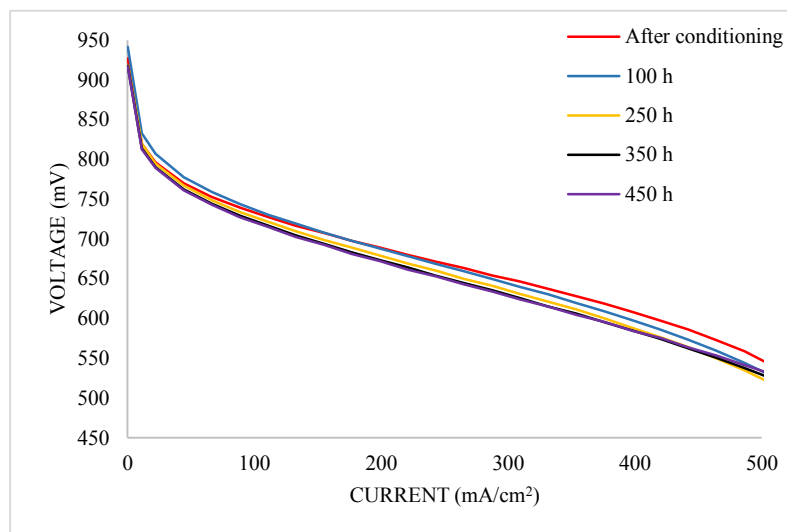
Figure 36 Polarization curves recorded during constant load degradation test of MEA 273

Degradation values for each current density have been calculated over the entire degradation test period and reported in Table 8 for the two MEAs.

| Current density | MEA 272 | | | MEA 273 | | | Average |
	Voltage after conditioning	Voltage after 440 h of ageing test	Degradation rate	Voltage after conditioning	Voltage after 440 h of ageing test	Degradation rate	Degradation rate
A/cm^2	mV	mV	$\mu V/h$	mV	mV	$\mu V/h$	$\mu V/h$
0	924	918	14	927	918	21	18
11	818	814	9	820	814	13	11
22	793	790	6	796	790	14	10
44	766	762	9	770	762	17	13
66	748	744	9	753	744	19	14
89	733	729	11	739	729	23	17
111	721	715	14	728	717	24	19
133	710	703	16	717	704	28	22
155	699	691	18	707	694	30	24
177	689	680	21	697	683	32	27
199	680	668	26	689	673	36	31
221	670	657	28	680	664	36	32
243	660	646	32	672	654	40	36
265	651	635	38	663	645	43	41
287	641	623	43	654	635	43	43
310	632	610	49	646	625	47	48
354	611	582	65	628	606	50	57
376	599	566	76	619	595	53	65
398	587	547	91	608	585	53	72
420	574	524	114	597	574	53	83
442	559	496	143	586	562	55	99

Table 8 Polarization curves and degradation rates of MEA 272 and MEA 273

These performance degradation results are quite in accordance with the results obtained for similar non-commercial HT-PEM PBI membranes by [42,72] and [142], but actually differs with data reported by the manufacturer of Celtec P-1000 MEAs [21,144] that indicates that lower degradation rates are obtainable for this kind of MEAs.

Figure 37 shows the EIS evolution during the degradation test of the MEA 272 and MEA 273 respectively at 22 mA/cm², 220 mA/cm² and 330 mA/cm². Results in terms of the EIS spectrum and its evolution with ageing are in accordance with similar studies [22,145] on similar HT-PEM MEAs. EIS plots are related to the polarization processes occurring at the cathode and their shape is affected by the current regime selected for the test. In general, the polarization decreases as the current increases. Two main components at high and low frequency are present and are attributable to charge transfer and mass transfer processes respectively as already explained in §2.6.1.2. At low current the mass transfer phenomena are negligible and it is possible to distinguish only one arc related to activation losses. The dependence of this component on the current implies that charge transfer resistance represents the largest contribution to the MEA internal losses. However, with the increase of

current, diffusion processes become also significant. The effect of aging is similar for the two membranes: at low current no changes are observed, meaning, presumably, that the nature and morphology of the electrode/electrolyte interface remain the same; at higher currents the high frequency and low frequency components increase, which implies a decrease of catalytic active area within the electrode. The cause of this degradation is probably related to the agglomeration of platinum particles. Several studies [22,146] have confirmed that the acidic conditions encountered in this type of MEA favour the dissolution of platinum and its agglomeration over time, recognizing this as one of the main causes of cell deactivation. Another possible mechanism of MEA degradation, which was observed when a cell operates at high potential, is carbon corrosion [80,146]. Oxidation of the support leads to the possible loss, isolation and agglomeration of the catalyst. Moreover, carbon corrosion can be responsible of a higher hydrophilicity of the cathode, causing a depletion of acid. A reduction of the acid may be responsible of lower conductivity of the electrode along with a reduction of three phase boundary zone [38].

MEA 272	MEA 273
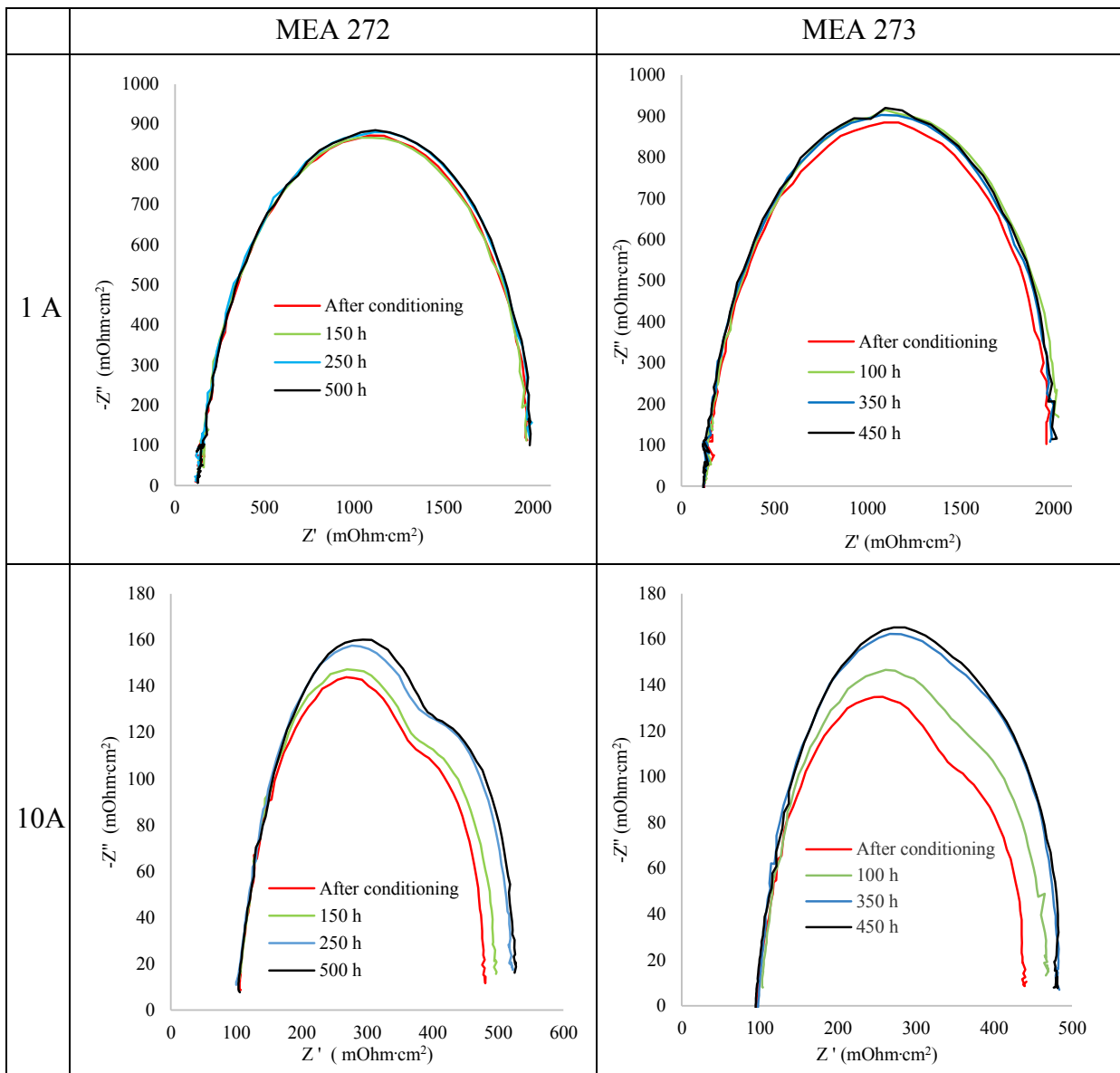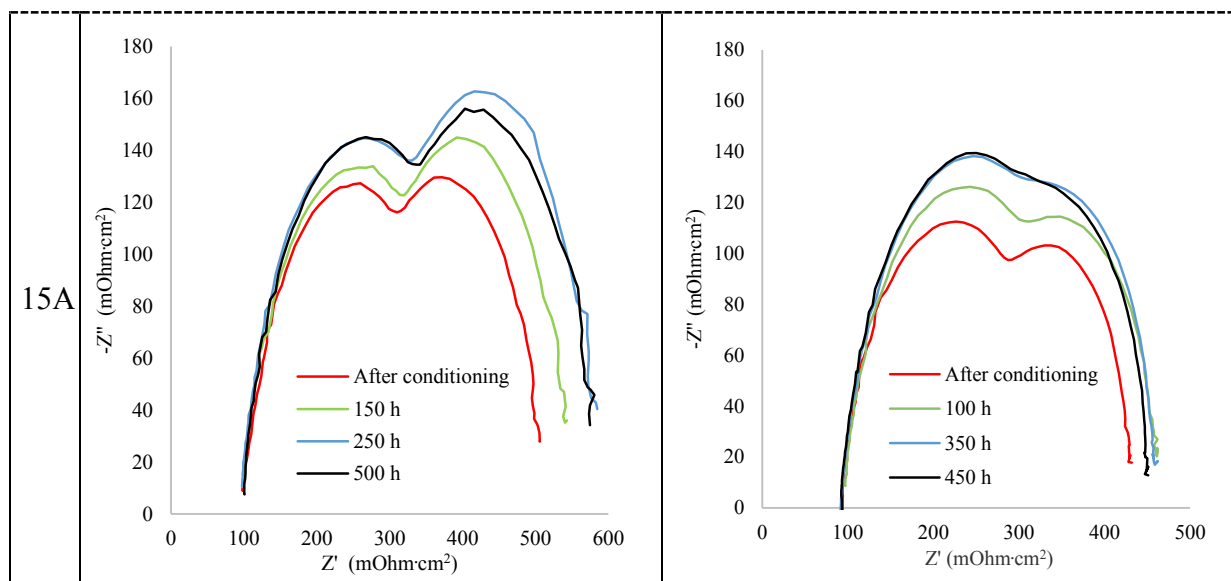
Figure 37 EIS results during constant load degradation test for MEAs 272 and 273

After the ageing test a CV measurement has been carried out. The aim of the CV measurements was to evaluate the order of magnitude of ECSA changes with the aging treatment since, as reported in literature, for this kind of membrane the interaction with the adsorbed acid may hamper a precise quantification of ECSA [22].The ECSA has been calculated from the H_2 adsorption peak applying the methodology described in §2.6.1.3.

As reported in Figure 38 the ECSA underwent to a degradation of about 30% for both MEA 272 and MEA 273.

Values of degradation of ECSA are comparable with degradation found by other authors in similar works [22].
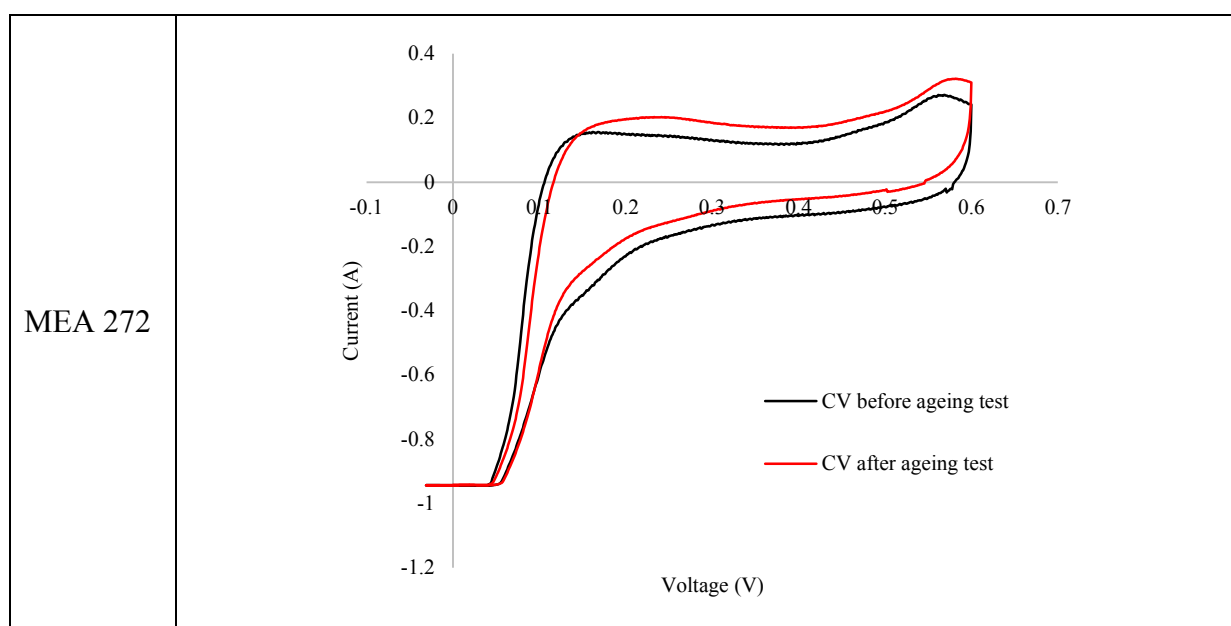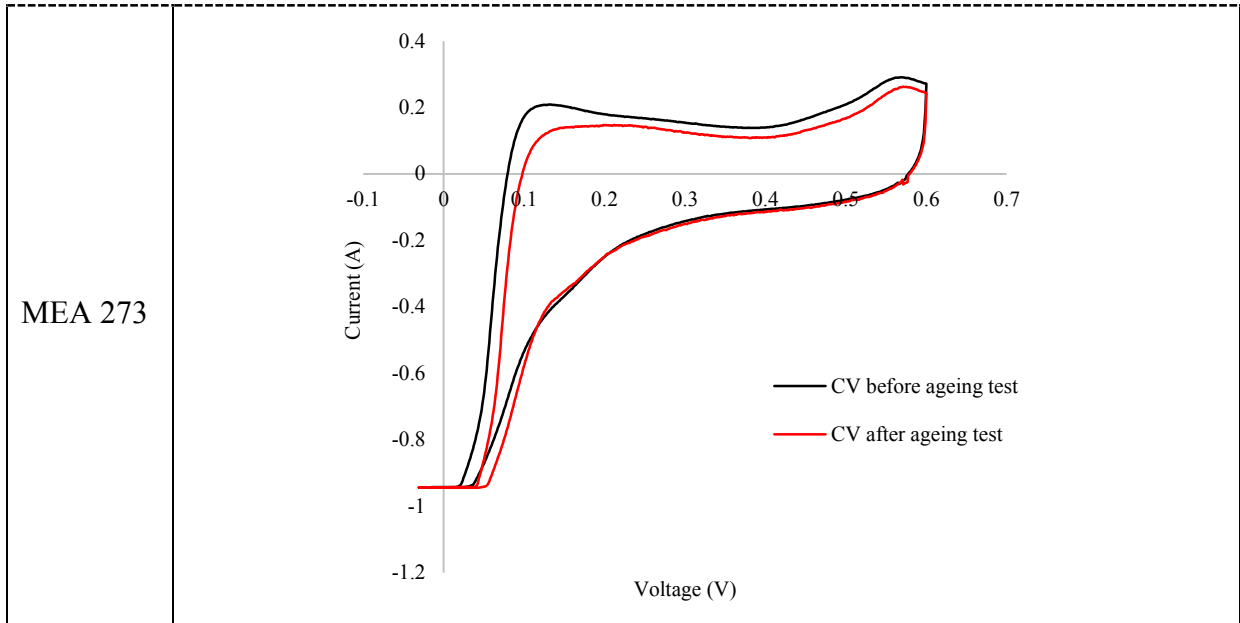
Figure 38 CV measurements before and after the ageing test for MEA 272 and MEA 273

MEA 272 and MEA 273, at the end of the ageing test have been then analysed with the SAXS technique following the methodology described in §3.3.2. The purpose of the SAXS analysis was to bring supplementary information concerning the state of aggregation of the platinum catalyst. This information can allow to infer if performance degradation, recorded with electrochemical tools, could be attributed to platinum catalyst aggregation or if other degradation processes are involved as described in §2.4. Results have been compared with the one obtained for the new MEA 275.

Figure 39 shows log-normal volume distributions obtained by the SAXS data analysis.
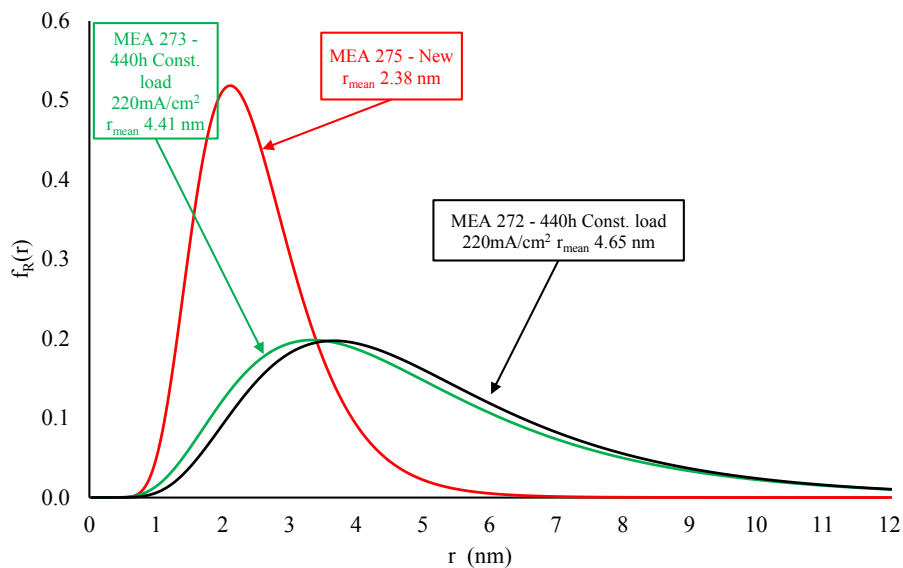
Figure 39 SAXS analysis. Volume size distributions of MEA 272 (black line), 273 (green line) and 275 (red line)

As reported in Figure 39, it is visible that the constant load ageing test caused an increasing of the medium radius and a spreading of the log-normal distribution over a much larger radius range. This means that the probability of finding platinum nano-particles with higher radius has strongly increased. The mean radius of MEA 272 after the ageing test has been measured to be 4.65 nm (st. deviation 0.70), while, for MEA 273 the mean radius after the ageing test has been measured to be 4.41 nm (st. deviation 0.72). With reference to the untouched MEA 275 (2.38 nm with st. deviation 0.59) the increasing of the mean radius is 95% for MEA 272 and 85% for MEA 273.

It can hence be inferred that catalyst layer structure has changed in such a way that could justify a performance degradation of the cell. However, even if platinum agglomeration has definitely played a role in this performance loss, it is hard to establish its partial weight with respect to other degradation processes.

For MEA 273 TEM analysis showed an average Pt particles radius after the ageing test of 3.32 nm (st. deviation 0.81) at the anode as shown in Figure 40 and an average particle radius of 2.77 nm (st. deviation 1.02) at the cathode as shown in Figure 41. The weighted average of anode and cathode Pt particles radius is 2.95 (st. deviation 0.98).
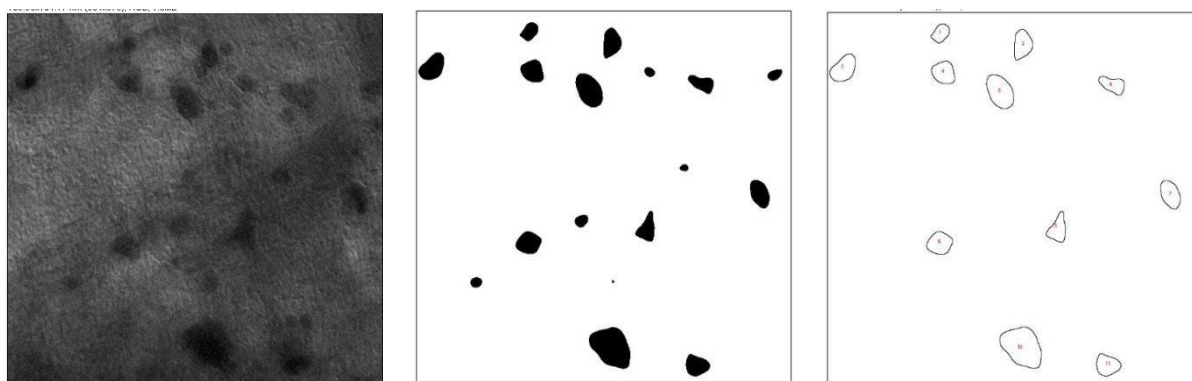
Figure 40 TEM analysis of MEA 273 anode - a) TEM image before treatment b) ImageJ treated image c) ImageJ particles selection
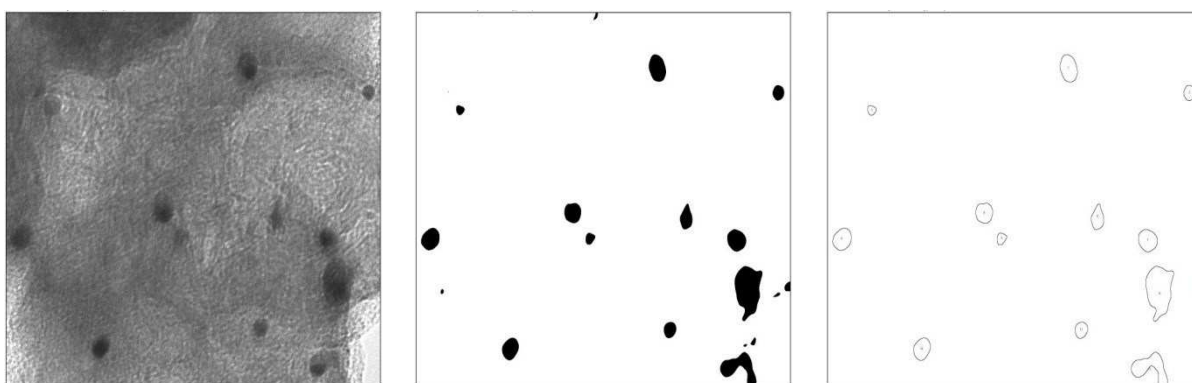
Figure 41 TEM analysis of MEA 273 cathode - a) TEM image before treatment b) ImageJ treated image c) ImageJ particles selection

4.2.2.   Load cycles

As already seen in §2.4 operating conditions strongly affect cell durability.

Since, at present, the main potential application for HT-PEM FC is distributed micro co-generation, literature on HT-PEM durability and performance degradation is mainly focused on steady-state operation. Specific tests to characterize the electrocatalyst degradation based on load cycling operation are common in low temperature PEMFCs research [48] as dynamic load operation is widely investigated because of its importance for automotive applications. Load cycling has been proved to be a significant stressor for catalyst degradation in HT-PEM as well [47,147] and it is possible to perform this operation keeping constant other parameters such as temperature and reactants flow.

In Table 9 are reported literature degradation values for HT-PEM fuel cells in a single cell configuration operated with load cycles.

Type of membrane	PA doping level	Type of load cycle	Operating temperature	Operating stochiometry	Duration of the test	Current density for degradation measure	Degradation rate	Reference
type	PA/repeat unit		°C		h	A/cm2	μV/h	
para-PBI	27.7	2 min at OCV, 30 min at 0.2 A/cm^2 and 30 min at 0.6 A/cm^2	160	$\lambda H_2=1.2$ $\lambda_{air}=2$	100h of conditioning (160°C 0.2A/cm2) + 500 load cycles	OCV	34.1	[47]
						0.2	27.9	
						0.6	41.3	
2OH-PBI	25.4	2 min at OCV, 30 min at 0.2 A/cm^2 and 30 min at 0.6 A/cm^2	160	$\lambda H_2=1.2$ $\lambda air=2$	100h of conditioning (160°C 0.2A/cm2) + 500 load cycles	OCV	45.5	
						0.2	46.9	
						0.6	77.7	
m-Polybenzimidazole (m-PBI)	8 -9	4 min OCV 16 min 0.3 A/cm^2	160	$\lambda(78.1\% H_2$ $21.9\% CO_2)$ $=1.5$ $\lambda air(30\%$ $O_2)=2.85$	840	OCV	33	[148]
						0.3	81	
Unfilled PBI	-	2 min at OCV, 30 min at 0.2 A/cm^2, and 30 min at 0.6 A/cm^2	-	-	-	OCV	33	[149]
						0.2	27	
						0.6	40	
Filled PBI	-	2 min OCV, 30 min at 0.2 A/cm^2 , and 30 min at 0.6 A/cm^2	-	-	-	OCV	20	
						0.2	12	
						0.6	19	
Celtec - P1100W	70	16 min at 1.0A/cm^2, 4 min at 0.6A/cm^2 and every 6 h 10 min at 0.0A/cm^2,	160	$\lambda H_2=1.5$ $\lambda air=2$	48 h conditioning (0.3A)+70h	OCV	19	[147]
						0.6	189	
						1	218	
		16 min at 0.3A/cm^2 and 4 min at 0.0A/cm^2				OCV	48	
						0.6	363	
		16 min at 1.0A/cm^2, 4 min at 0.6A/cm^2 and every 6 h 10 min at 0.0A/cm^2,			48 h conditioning (0.3A)+230h	OCV	27	
						0.6	116	
						1	126	

Table 9 Degradation rates in literature of HT-PEM single cells operated with different load cycles

Experimental testing of MEA 271

For load cycling test protocols there are many studies and propositions [12,28,65,87,88] and, in this work, it has been chosen to implement, for the HT-PEM FC, a load cycle derived from the accelerated stress test protocol developed in 2009 for electrocatalysts analysis in low temperature PEM fuel cells by U. S. DOE [150,151] The modified protocol, had already been used a first time in an experimental test [13] carried out in the laboratory of the University of Trieste; one of the aims of the experimental analysis carried out during this PhD work, was to asses if the protocol, applied a second time on the same type of MEAs, gives the same data in terms of performance degradation, results of this analysis have been published in [38].

In the previous experimental test [13] two load cycles profiles had been compared: a triangular load cycle applied on MEA 264 was a triangular sweep cycle between 0.01 A/cm^2 and 0.5 A/cm^2 as shown in Figure 42.
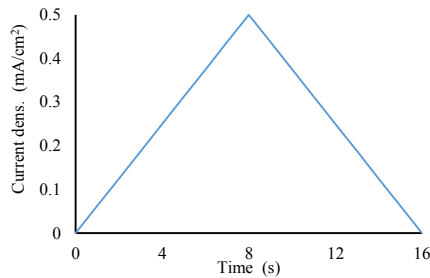
Figure 42 Load profile A – MEA 264

While the triangular load cycle applied on MEA 265 was a triangular sweep cycle between OCV and 0.5 A/cm^2 with 2 seconds of permanence at OCV at each cycle as shown in Figure 43.
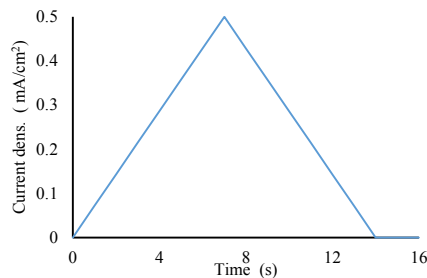
Figure 43 Load profile B (2sec. at OCV) – MEA 265 and MEA 271

In the experimental analysis carried out during this PhD work [38] it has been chosen to reproduce this last load cycle profile. Hence MEA 271 has been subjected to 125 000 triangular load cycles corresponding to 550 hours of operation. Results have been compared with the ones obtained for MEA 265 to verify the reproducibility of the test and hence with the results obtained for MEA 264 to evaluate the effect of the variation in the load profile (2 sec permanence at OCV) on the total performance degradation.

As for MEA 272 and 273, MEA 271 has been subjected to a 100 h conditioning period at 0.22 A/cm^2. After the first set of measurement presented in § 4.1 the aging test has been carried out for 550 h following the methodology described in §3. Polarization curves and EIS measurements have been performed periodically during the test in order to check the evolution of the degradation of the MEA performance over time. Polarization curves measured during the ageing test are reported in Figure 44.
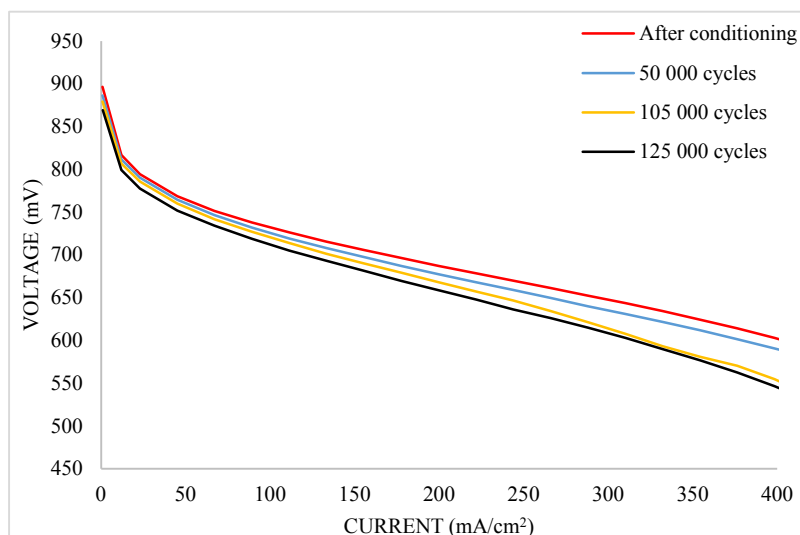
Figure 44 Polarization curves recorded during load cycling degradation test of MEA 271

As for MEA 272 and MEA 273, the degradation rate caused by the load cycling test has been calculated considering two polarization curves: one at the beginning of the test and the other one after 100 000 cycles. For each current density, the voltage degradation value has been calculated and divided by the operational time as shown in Table 10.

	MEA 271		
Current density	Voltage after conditioning	Voltage after 100 000 cycles	Degradation rate
A/cm^2	mV	mV	µV/h
1	897	879	37
12	817	807	21
23	794	786	18
45	768	760	18
67	751	742	21
89	738	727	23
111	726	714	26
133	716	701	30
156	706	690	32
178	696	679	36
200	687	668	40
222	678	657	44

244	670	647	49
266	661	634	56
288	652	621	65
310	643	608	74
332	634	593	86
354	624	581	90
376	614	570	91
399	603	554	101
421	590	534	116

Table 10 Polarization curves and degradation rates of MEA 271

As reported in [38] the performance loss, in terms of potential reduction, between the beginning and the end of the 100 000 load cycling procedure, is less than 6% for all current densities. These results are comparable with the data obtained in previous work for MEA 265 [13] with the same membrane and load cycle profile. Degradation after 100 000 cycles at 200 mA/cm^2 has been found to be 19 mV (2.8%) while on MEA 265, for the same current level, it has been found a degradation of 20 mV which is in good accordance and confirms the reproducibility of the test. Table 11 shows the degradation rates values for the MEAs subjected to triangular cycle and constant load operation. It can be inferred, as expected, that load cycles stress more the MEAs and that OCV operation is detrimental [43].

MEA label	Load profile	Degradation Rate
MEA 264 - [13]	Triangular [0-0.5]V	34 µV/h
MEA 265 - [13]	Triangular [0-0.5]V – 2sec OCV	45 µV/h
MEA 271 - [38]	Triangular [0-0.5]V – 2sec OCV	44 µV/h
MEA 272 - [38]	Constant load	30 µV/h
MEA 273 - [38]	Constant load	29 µV/h

Table 11 MEAs degradation rates at 220 mA/cm^2

The increased degradation observed in MEA 265 and MEA 271 with respect to the other MEAs is complex to analyse as it could be attributed to an higher degree of Pt particles agglomeration, favoured by permanence at OCV or, as it can be inferred by the voltage shift at OCV conditions in the polarization curves of MEA 271, other mechanisms, such as reactants crossover and internal short circuit, could play a role [152]. However, as it will be presented in later below, SAXS analysis confirmed that Pt agglomeration played an important role in the increased degradation of MEA 271.

Another variable that could affect the degradation during the stress tests is the total energy produced by the cell during the entire test. Since one typical application of HT-PEM is cogeneration, it can be interesting to compare the degradation at constant total energy

production, in order to analyse which operating conditions are more favourable. Hence, to allow comparison between cycles, energy yields have been calculated:

MEA 264 - Triangular [0.01e0.5]V : 11.8 MJ

MEA 265 and MEA 271 - Triangular [0e0.5]V e 2s OCV: 10.0 MJ

MEA 272 and MEA 273 - Constant load 0.22 A/cm^2: 10.0 MJ

One of the information that can be inferred from these values is that the total energy produced with MEA 264 (11.8 MJ) is higher than that produced with MEA 265, and MEA 271 (10.0 MJ) therefore, as expected, this is an additional confirmation that the operating cycle (in this case the permanence at OCV conditions) is affecting the degradation (higher in MEA 265 and 271 compared to MEA 264).

EIS measurements are reported in Figure 45. It can be observed that the EIS spectra evolution follow the same behaviour as the one of MEA 272 and MEA 273 described in §4.2.1. However, it is interesting to notice that while in spectrum of MEA 272 and MEA 273 (see Figure 37) there is almost no variation of ohmic resistance, in the spectrum of the ageing test of MEA 271 the ohmic resistance has increased from the beginning to the end of the test.

The higher potential degradation of MEA 271 found with the polarization curves analysis, could be related to the conditions selected for the aging. At OCV, high voltage strongly favours oxidation processes which can accelerate the decay rate [153].
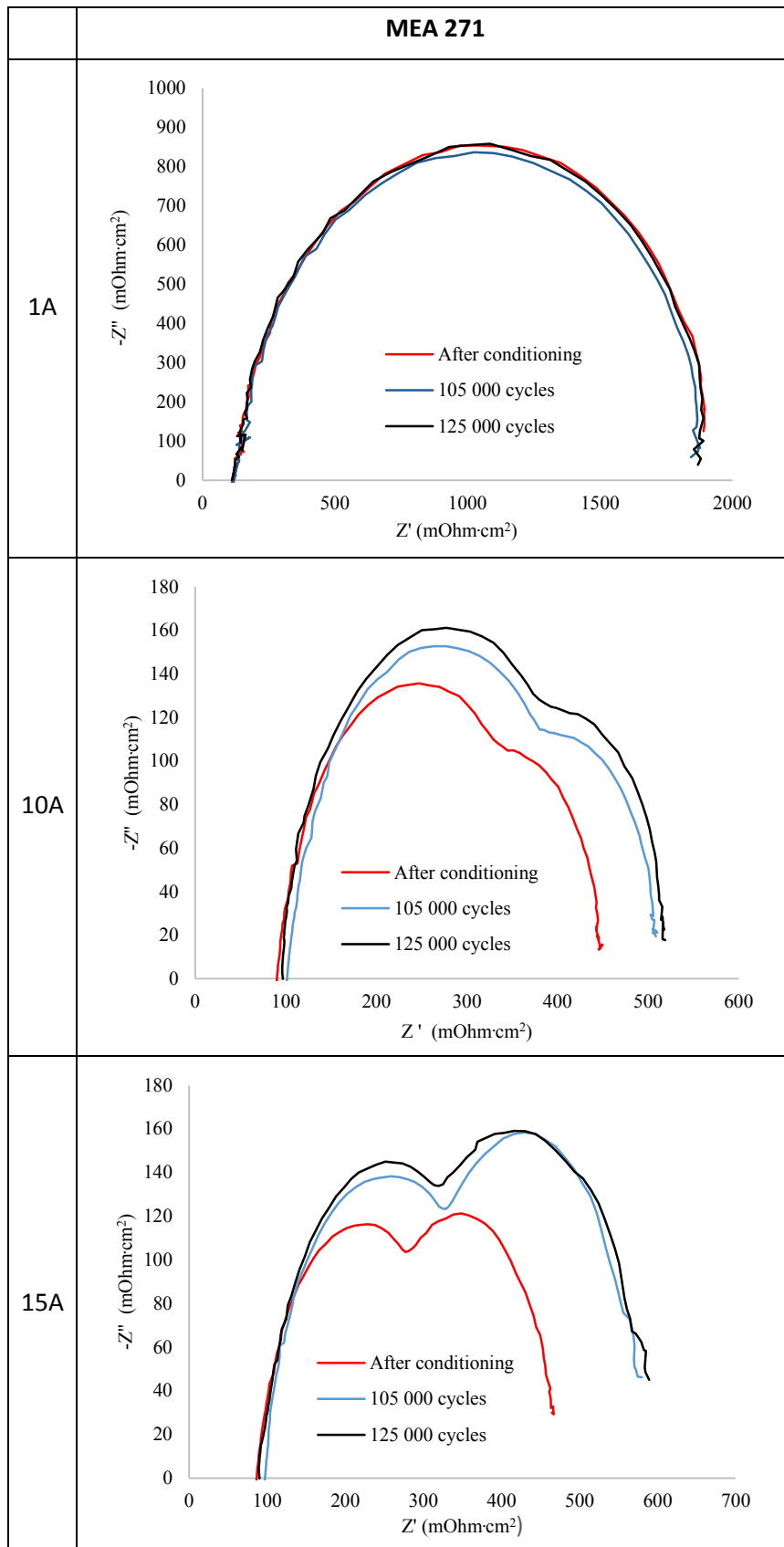
Figure 45 EIS results during load cycling degradation test for MEA 271

CV measurement effectuated after the ageing test and reported in Figure 46, shows a reduction of 50% of the ECSA.
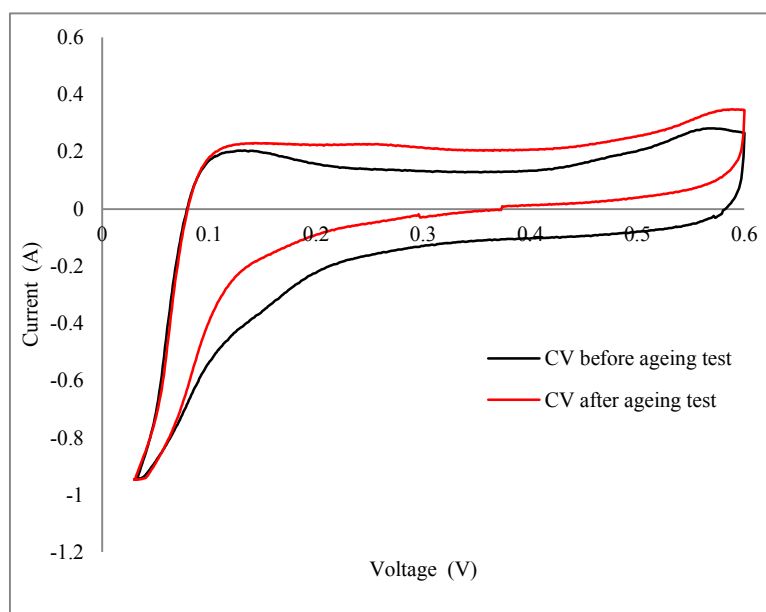
Figure 46 CV measurement before and after the ageing test for MEA 271

SAXS analysis reported in Figure 47, allows to highlight that the ageing test based on the triangular load cycle with 2 seconds of permanence of OCV caused a larger increase of the medium radius and a spreading of the log-normal distribution with respect to constant load operation. The mean radius variation of MEA 271 has been hence estimated to be about 132%, from the initial value of 2.38 nm to the final value of 5.51 nm (st. deviation 0.76), while for MEAs operated at constant load was 85-95 %. It is interesting to notice that the increased variation of the catalyst structure registered by SAXS measurements can also be found through the ECSA calculation effectuated with the cyclic voltammetry. However, the quantitative link between the two techniques is not straightforward.
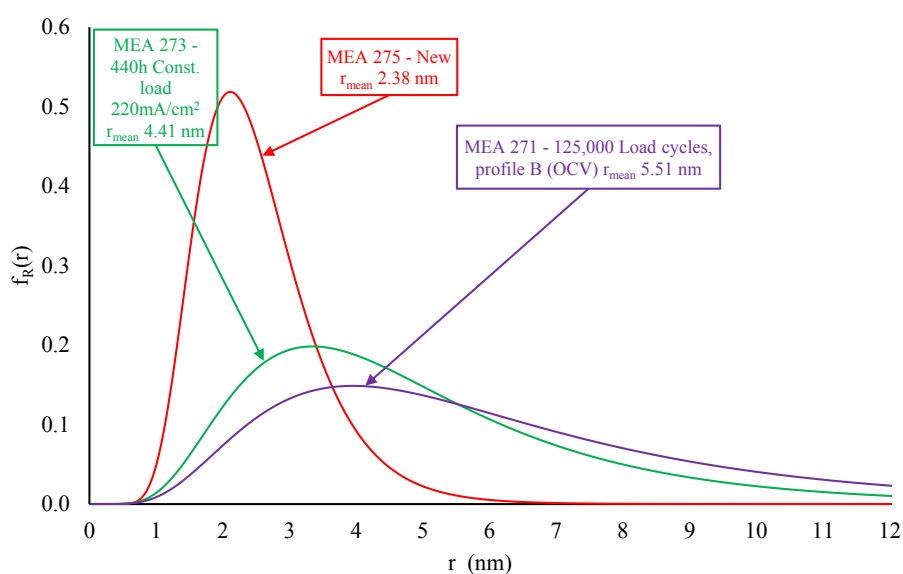
Figure 47 SAXS analysis. Volume size distributions of MEA 271 (purple line), 273 (green line) and 275 (red line)

Figure 48 compares SAXS results of MEA 271, with the results obtained in a previous work [13] on MEA 265 subjected to the same load cycle profile and with MEA 263 (untouched).

MEA 263 - New r_{mean} 2.78 nm

MEA 271 - 125,000 Load cycles, profile B (OCV) r_{mean} 5.51 nm

MEA 265 - 100,000 Load cycles, profile B (OCV) r_{mean} 5.60 nm
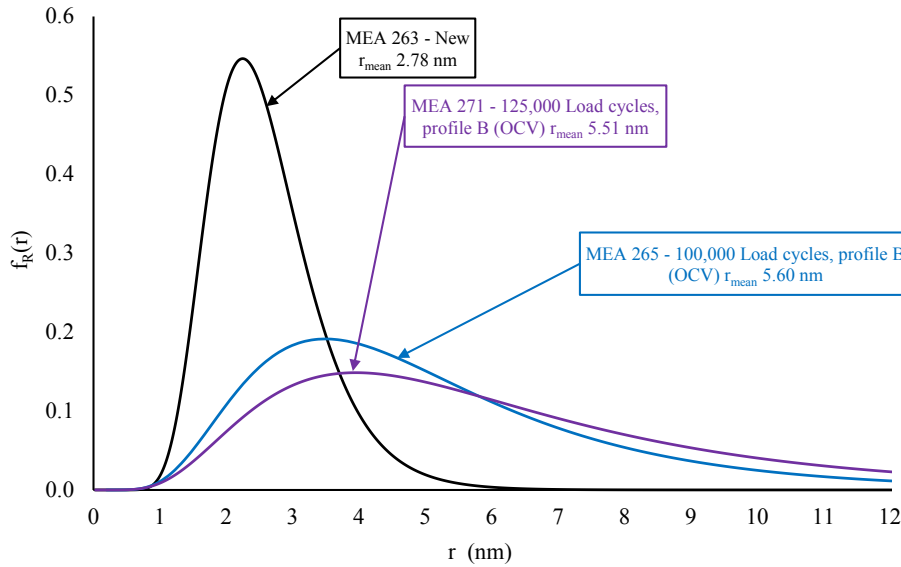
Figure 48 SAXS analysis. Volume size distributions of MEA 271 (purple line), 263 (black line) and 265 (blue line)

In [13] mean radius of the untouched MEA 263 was found to be 2.78 nm (st. deviation 0.64) and mean radius of MEA 265 was found to be 5.60 nm (st. deviation 0.66). It can be noticed that the log-normal evolution caused by the ageing test is similar, even if a higher values of deviation and mean radius values have been found in the analysis of MEA 271 with respect to the one of MEA 265. However, it must be highlighted that MEA 271, actually performed 125 000 load cycles, while MEA 265 performed only 100 000 load cycles. Figure 49 compares the log-normal volume distribution obtained for the two load profiles: Profile A (Triangular [0-0.5]V) and Profile B (Triangular [0-0.5]V – 2sec OCV). Profile A was applied on MEA 264 while profile B was applied on MEA 265.

MEA 263 - New r_{mean} 2.78 nm

MEA 264 - 100,000 Load cycles, profile A r_{mean} 4.88 nm

MEA 265 - 100,000 Load cycles, profile B (OCV) r_{mean} 5.60 nm
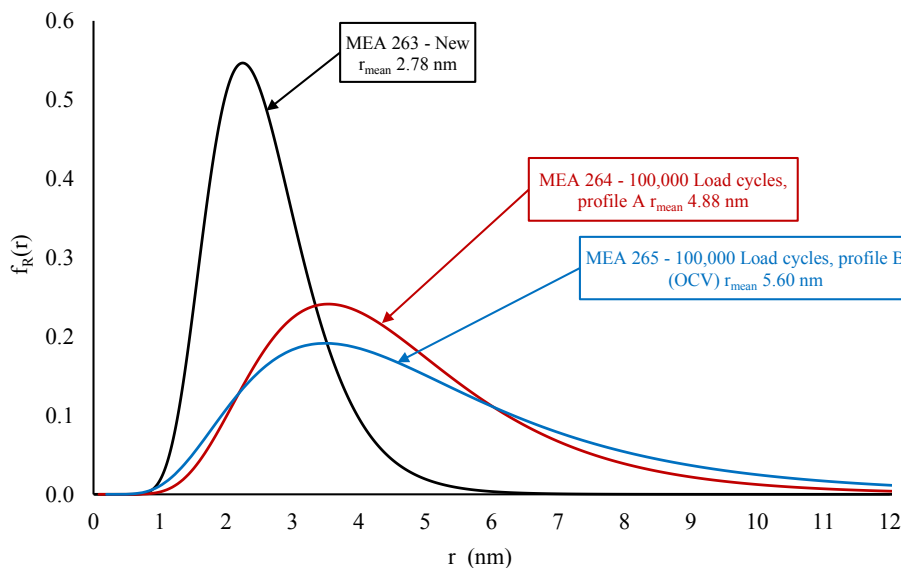
Figure 49 SAXS analysis. Volume size distributions of MEA 263 (black line), 264 (brown line) and 265 (blue line)

In [13] the mean radius of MEA 264 was found to be 4.88 nm (st. deviation 0.66). It is hence possible to infer that, as already mentioned above, the increased degradation observed in MEA 265 and MEA 271 with respect to MEA 264 could be attributed to an higher degree of Pt particles agglomeration, favoured by permanence at OCV.

For MEA 271 TEM analysis showed an average Pt particles radius after the ageing test of 3.54 nm (st. deviation 1.35) at the anode as shown in Figure 50 and an average particle radius of 3.15 nm (st. deviation 0.67) at the cathode as shown in Figure 51. The weighted average of anode and cathode Pt particles radius is 3.46 (st. deviation 1.24).
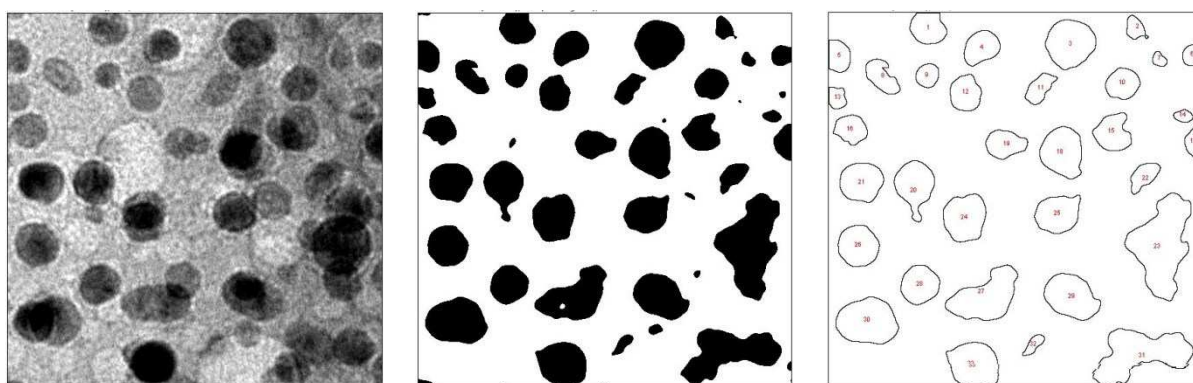
Figure 50 TEM analysis of MEA 271 anode - a) TEM image before treatment b) ImageJ treated image c) ImageJ particles selection
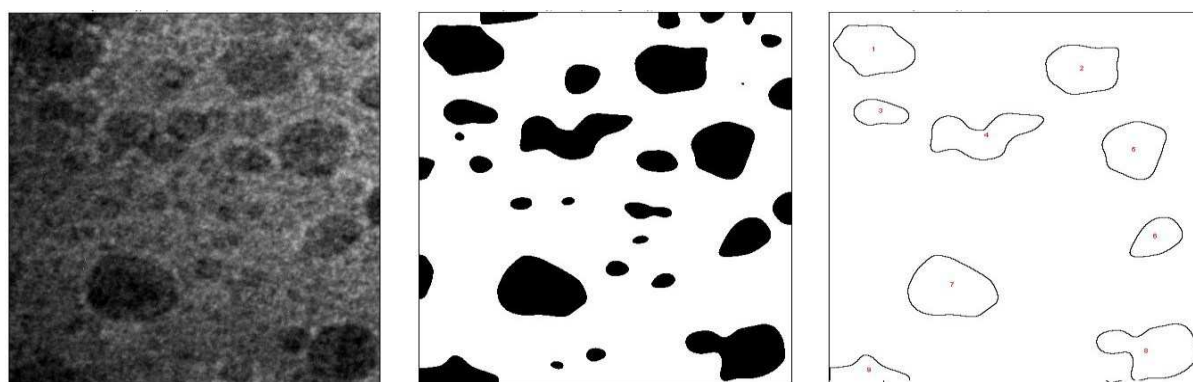
Figure 51 TEM analysis of MEA 271 cathode - a) TEM image before treatment b) ImageJ treated image c) ImageJ particles selection

4.2.3. OCV permanence

OCV permanence is the operational condition that affects the most the MEA performance over time. However, in this operating condition no power is produced and hence it is not a common operating condition for micro-CHP generation. For this reason literature is poor of data concerning OCV operation of HT-PEM systems. However, it is important to analyse this operation condition since it represents an extreme condition that exacerbates some

degradation processes that are actually visible also in other operating conditions. High potentials are an important cause of the degradation of the catalyst and its support [80]. Open Circuit Voltage (OCV) increases the Pt particle agglomeration because both Pt oxidation and carbon corrosion are favoured at high electrode potential. The Pt oxidation starts the dissolution and the Ostwald ripening process, while the carbon corrosion triggers the agglomeration by coalescence [49,141]. Wu et al. [154] carried out a 1,200 h test with a six-cell LT-PEMFC stack operating close to OCV. The cell degradation increased after 800 h: in the first period, the degradation of fuel cell performance was mainly attributed to catalyst degradation, while the subsequent dramatic decay has been supposed to be caused by membrane failure.

Qi and Buelte [86] investigated the impact of OCV on the performance of HT-PEMFCs and measured a fast OCV increase in the first few minutes followed by a slower increase and a peak after 35 min. Electrochemical Impedance Spectroscopy (EIS) indicated loss of catalyst activity and XRD showed an increase of the cathode Pt crystallites size of 430% after 244.5 h of OCV exposure. A similar result has been reported by Zhang et al. [152] during a 250 h ageing test under OCV condition.

It is interesting to notice that for this operational condition the duration of the test seems to strongly influence the results. Indeed, in [86] a 350h test has been carried out on similar PBI membranes operated at OCV at 180°. Estimation from polarization curves reported in the paper seems to indicate an initial degradation of 2285 µV/h at 0.2 mA/cm^2 during the first 17h of test, while the overall degradation during the 350h has been estimated to be 408 µV/h at 0.2 mA/cm^2. Table 12 reports literature data of degradation.

Type of membrane	Operating temperature	Operating stoichiometry	Duration of the test	Current density for degradation	Degradation rate	Ref.
type	*°C*		*h*	*A/cm^2*	***µV/h***	
H3PO4/PBI HT-PEMFC	180	H$_2$ flow: 0.5 SLM λair = 1.35 at 0.2 A/cm^2	350 (244 OCV)	OCV	**368** *(estimeted PC)*	[86]
				0.2	**408** *(estimated from PC)*	
				0.4	**737** *(estimated from PC)*	
		H$_2$ flow: 0.5 SLM λair = 1.35 at 0.2 A/cm^2	17 hours of OCV First part of the test 350 (244 OCV)	OCV	**1714** *(estimated from PC)*	
				0.2	**2285** *(estimated from PC)*	
				0.4	**4571** *(estimated from PC)*	

Table 12 Degradation rates in literature of HT-PEM single cells operated at OCV

Experimental testing of MEA 274 and 277

This operating condition has been tested on two MEAs: MEA 274 and MEA 277. As for the other membranes, the experimental testing of the MEAs has been carried out following the methodology described in chapter 3. The two membranes have been operated for two different durations to evaluate the possible influence of test duration on the degradation rate evaluation. Total operational time of MEA 274 has been of 220 hours, 126 of which at OCV while MEA 277 has been operated for 500 h, 400 of which at OCV.

Polarization curves of the two MEAs recorded periodically during ageing test are reported here below in Figure 52 and Figure 53.

The PC analysis of MEA 274 shows high total performance degradation at high current level, a less important degradation at low current densities and, actually, a slight increase of the OCV value. This could be explained attributing the performance degradation to mass transport losses likely due to H_3PO_4 flooding caused by the enhanced hydrophilicity of the carbon support due to initial corrosion.

The degradation rate at 0.22 mA/cm^2 for MEA 274 has been found to be 444 μV/h over the 126h of the test.
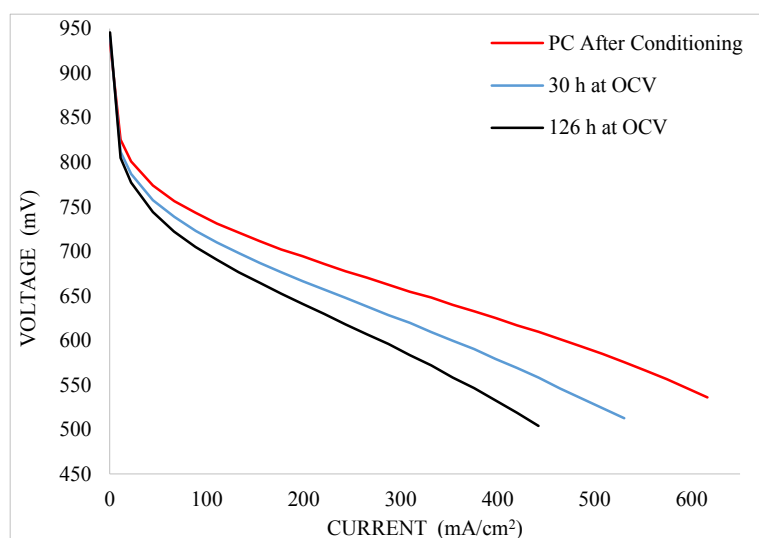
Figure 52 Polarization curves recorded during OCV degradation test of MEA 274

MEA 277 has been operated for 400h at OCV and, as visible in Figure 53, total degradation rate over the 400h of test at 0.22 mA/cm^2 has been found to be 124 μV/h, while when considering just the first 140h of operation a degradation rate of 237 μV/h has been recorded. It can be notice that in both tests the first hours of operation at OCV seem to have a very important impact on the total degradation of the membrane. Going on with the degradation test the OCV permanence seems to have a smaller impact on performance degradation rate even if values are still definitely above the ones obtained for the other operational conditions.
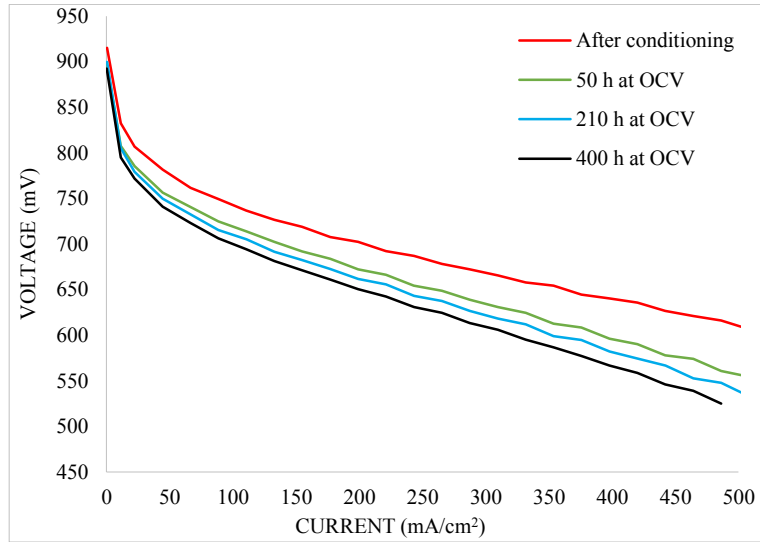
Figure 53 Polarization curves recorded during OCV degradation test of MEA 277

Table 13 reports the degradation rates of MEA 274 and MEA 277 calculated over the entire test. To allow comparison with the degradation rate values of MEA 274, the degradation rate of MEA 277 has been as well calculated for the first 140 h of operation.

	MEA 274			MEA 277				
Current density	Voltage after conditioning	Voltage after 126 h OCV	Deg. Rate 126 h	Voltage after conditioning	Voltage after 400 h of OCV	Deg. Rate 400 h	Voltage after 140 h of OCV	Deg. Rate 140 h
A/cm^2	mV	mV	μV/h	mV	mV	μV/h	mV	μV/h
0	935	946	-86	915	892	57	901	103
11	826	805	164	833	795	94	804	203
22	801	777	189	807	772	88	782	182
44	774	744	238	781	741	101	752	208
66	756	722	269	762	723	96	735	191
88	743	705	306	749	706	108	719	215
111	731	691	320	737	694	106	707	212
133	721	676	355	727	681	113	696	216
155	712	665	371	719	671	119	685	245
177	702	653	394	708	661	117	677	220
199	694	641	425	702	651	129	665	269
221	686	630	442	692	642	124	659	237
243	678	618	473	687	631	139	647	283
265	671	607	504	678	625	134	640	270
287	662	596	528	672	613	148	632	288
309	655	583	567	665	606	149	621	314
331	648	572	604	658	595	157	616	296
354	640	558	647	654	587	169	603	364
376	633	546	684	645	577	168	599	329
420	617	519	780	636	559	192	580	399
442	610	504	840	627	546	202	572	392

Table 13 Polarization curves and degradation rates of MEA 274 and MEA 277

It can be noticed that differently from other MEAs operated with different load profiles, degradation rates of MEAs operated at constant OCV encounter a wide variability. This is possibly due to the acid flooding and leaching phenomena that can strongly vary during the test.

Figure 54 shows the EIS results of MEA 274 and MEA 277 at 22 mA/cm^2, 220 mA/cm^2 and 330 mA/cm^2 before and during the ageing tests

It is interesting to notice that, differently from the EIS results for the other MEAs, where the cathode activation arc and the mass transport arc were clearly distinguishable at high current densities during all the test, for MEA 274 and MEA 277, the increasing of losses during ageing test caused a merging of the two arcs, not allowing the distinction between the degradation due to activation losses and the one due to mass transport losses also at high current densities. The reduction of the polarization with the increasing of the current indicates that charge transfer resistance represents the largest contribution to the MEA internal losses. The evolution of the spectra of MEA 274 is in accordance with data obtained by [86] with similar membranes subjected to 244 h of OCV permanence. MEA 277, despite its longer permanence at OCV showed a reduced increasing of the polarization of the EIS spectra. Since, for MEA 274, the dependence of the EIS spectra with the increasing of the current seems to be lower than for MEA 277, it can be inferred that mass transport contribution to the polarization of the EIS spectrum is more important in MEA 274 than in MEA 277. Another important observation is that while for the other MEAs, at low currents the effect of ageing did not caused any change in the EIS spectra, for MEA 274 and MEA 277 it varies significantly. This could be interpreted as a variation of the morphology of the electrode/electrolyte interface.

The increasing of the charge transfer resistance can be attributed to three different degradation mechanisms: catalyst agglomeration, carbon corrosion and acid loss from the electrodes. As reported by [84] a lower acid content in the cathode catalyst layer increases the proton transport resistance of the electrodes. This effect becomes evident in the EIS spectra with the increase of the 45° linear branch at high frequency [22] which is quite evident in the EIS spectra of MEA 277 at high current densities. This could indicate that, in MEA 274, the polarization of the EIS spectra increase is due to a combined effect of the increasing of charge transfer resistance due to carbon corrosion and the mass transport resistance due to phosphoric acid flooding of the carbon pores. For MEA 277 it can be conjectured that the depletion of acid caused a reduction of the ECSA, but mass transport resistance is less important since there is less or no flooding effect. This could explain the reduced total EIS spectra of MEA 277 with respect to MEA274 in spite of the higher ECSA loss for MEA 277 with respect to MEA 274.
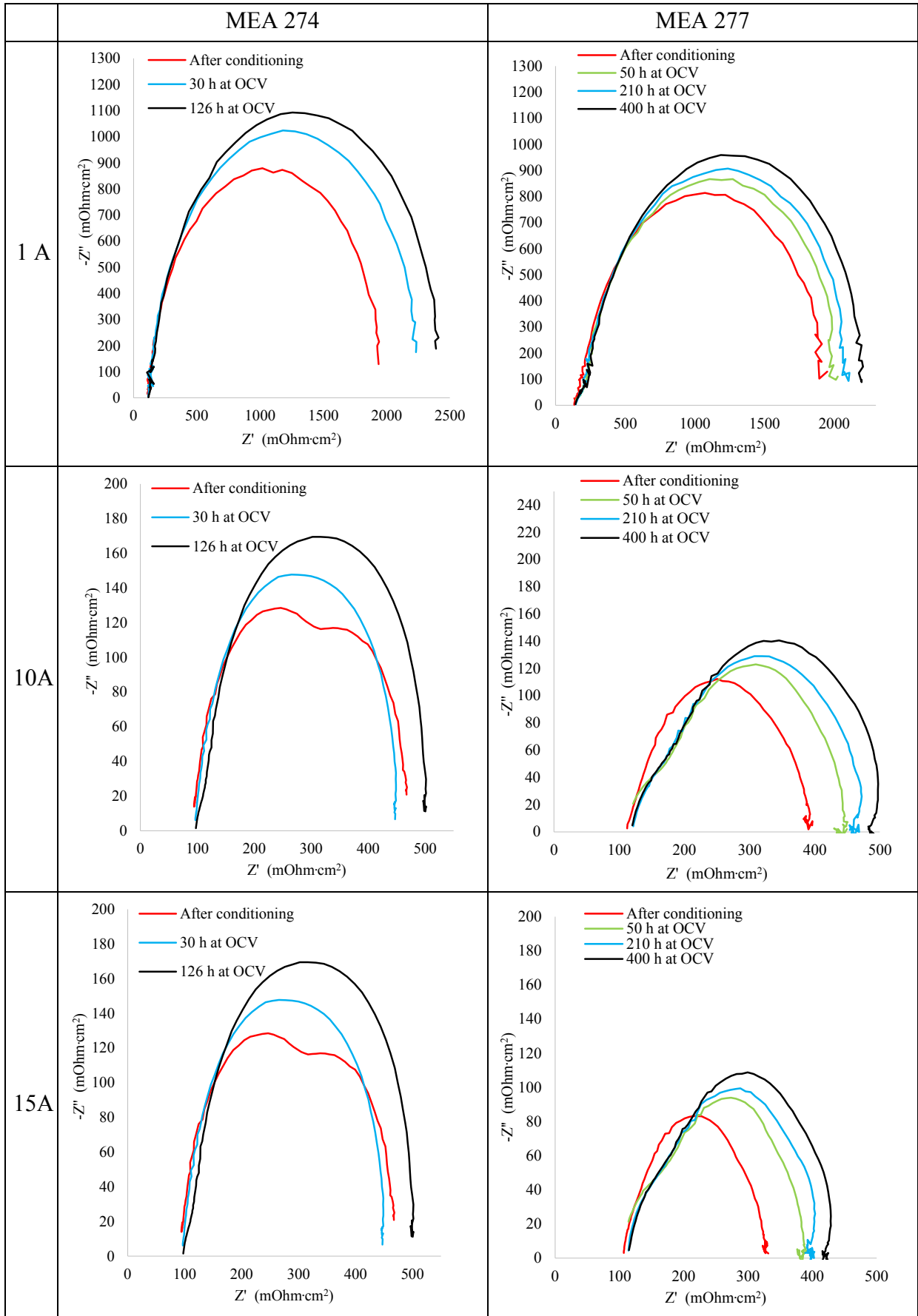
Figure 54 EIS results during OCV degradation test for MEAs 274 and 277

Indeed, for MEA 274 cyclic voltammetry results seems to indicate that activation losses should be of minor impact on the found degradation rate, letting infer that the major degradation comes from mass transport effects. As shown in Figure 55, even if the degradation rate of MEA 274 is much higher than the one calculated, for example, for the MEAs subjected to constant load operation, the ECSA of MEA 274 underwent to a reduction of about 10% which is much lower than the one calculated in the constant load test (30%). Concerning MEA 277 ECSA reduction is about 25%; however, it is likely that the reduction of the ECSA is due to the reduction of the three-phase boundary zone as a combined effect of carbon corrosion, acid depletion and platinum agglomeration.
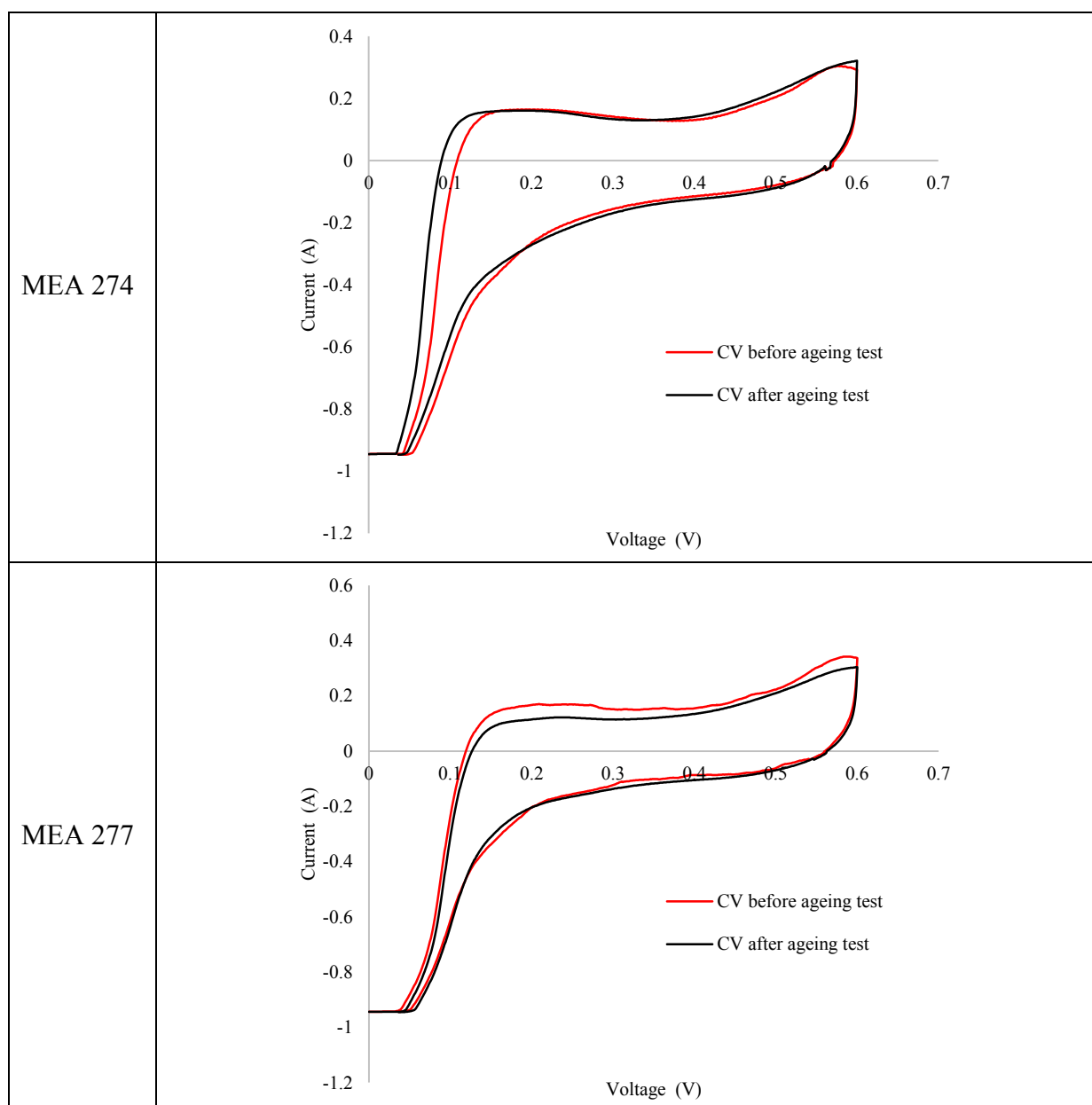
Figure 55 CV measurements before and after the ageing test for MEA 274 and MEA 277

MEAs 274 and MEA 277 has then been analysed with the SAXS technique. Results are reported in Figure 56 and compared with the results obtained for the other analysed MEAs in Figure 57.
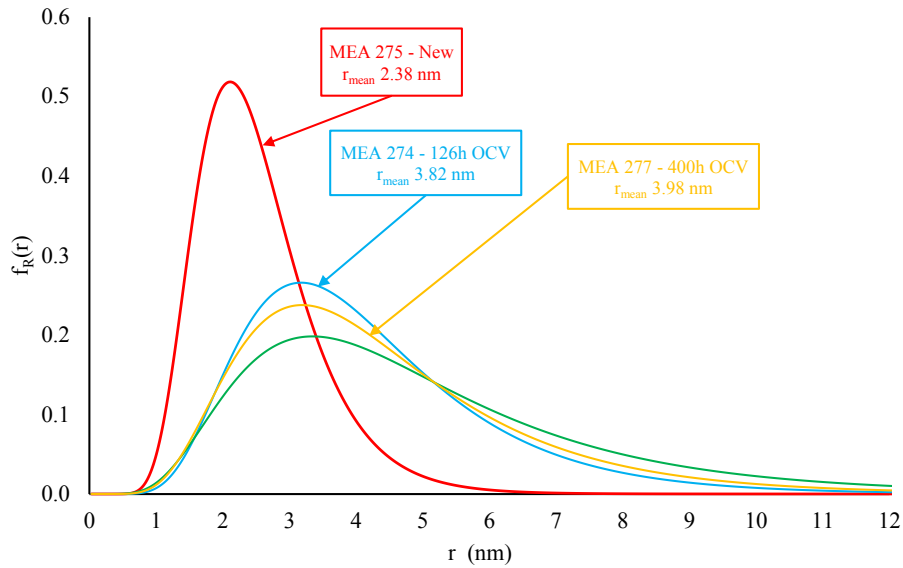
Figure 56 SAXS analysis. Volume size distributions of MEA 274 (blue line), 277 (yellow line) and 275 (red line)
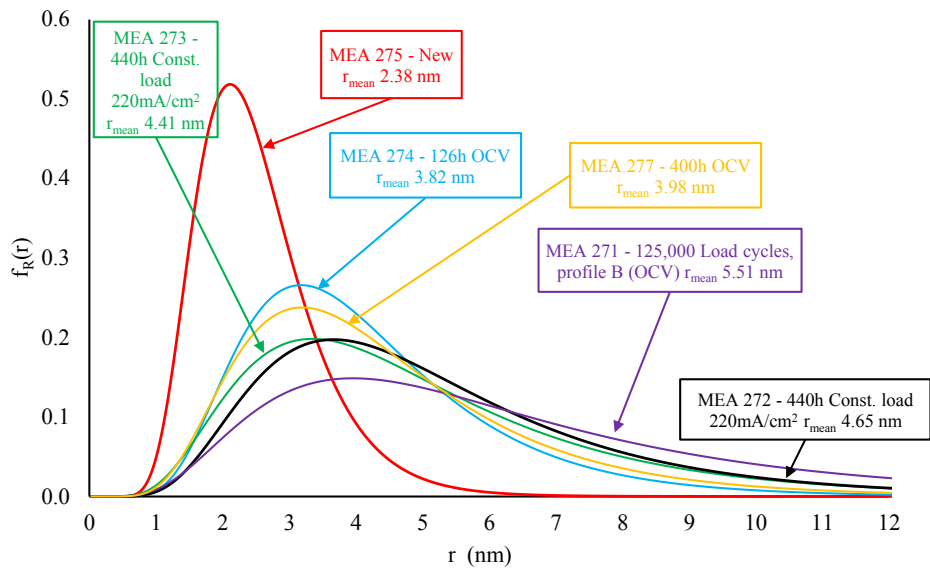
Figure 57 SAXS analysis. Comparison of volume size distributions of MEA 271 (purple line), 272 (black line), 273 (green line), 274 (blue line), 277 (yellow line) and 275 (red line)

It can be noticed that the Pt mean radius at the end of the test has increased by 60% from the initial reference value of 2.38 nm (MEA 275) to the final value of 3.82 nm (st. deviation 0.66) for MEA 274 and by 67 % for MEA 277 with the mean radius of 3.98 nm (st. deviation

0.69) after the ageing test. These values are low if compared to the ones of the other MEAs that range from 85% to 132%, while the degradation rates of MEA 274 and 277 are almost 10 times higher than the degradation rate of the other MEAs.

As mentioned before the polarization curves and EIS analysis suggest that degradation of MEA 274 could mainly be attributed to mass transport phenomena linked to carbon corrosion, and consequent flooding of the cathode catalyst layer structure with phosphoric acid [35]. Indeed, SAXS showed a limited platinum particle agglomeration; this seems to supports this conjecture. Concerning MEA 277 polarization curves and EIS let infer a higher contribution to degradation due to charge transfer phenomena. This means that flooding phenomena are reduced but degradation can still be caused by acid leaching, platinum agglomeration and carbon corrosion.

In literature the OCV operation is often cited as one of the main causes of platinum agglomeration [86], however, the process of platinum agglomeration is a complex phenomenon that occurs through others intermediate steps: firstly carbon corrosion happens favoured by high potentials, this causes the augmentation of hydrophilicity of the carbon support which causes phosphoric acid flooding which can be at the origin of platinum depletion and agglomeration.

For MEA 274 and MEA 277 the platinum agglomeration does not seem to be the major cause of degradation. For MEA 274, since it has been operated for a relatively short time, it could be possible that, in spite, of the high total performance degradation, platinum did not have the time yet to agglomerate and deplete. Analysing data of degradation of MEA 277, in the polarization curves is visible a slight reduction of OCV voltage after 400 h of test and an higher reduction of the ECSA recorded with the cyclic voltammetry; this could indicate that in this case Pt agglomeration actually played a role. However, EIS data showed that phosphoric acid depletion could also have an important role on the ECSA reduction. Finally SAXS results strongly suggests that even if an higher agglomeration of platinum actually occurred for MEA 277, the mayor role in the degradation due to OCV operation should be attributed to acid leaching effects.

4.2.4.   Start & Stop cycles

It is widely recognised that start-up and shut-down processes negatively affect performance of the fuel cell. This is an important issue for cogeneration systems. Indeed, when energetic demand is low or there is not demand, it is not obvious to identify which is the best option between switching off the fuel cell system or maintain the plant at a minimum operation load. This choice depends mainly on two factors: duration of the low demand / no demand and the value of the degradation caused by a Start and Stop cycle. Understanding, how detrimental is for the system a single Start and Stop cycle is, hence, very useful in order to choose the operational strategy to be implemented in a micro-CHP system.

As already mentioned in § 2.4, Start and Stop cycles have been recognised as strong stressors for the catalyst layer. During start-up and shut-down processes the high potential at the cathode, introduced by the hydrogen/air interface at the anode, is the major cause of performance degradation [74]. Start-Stop cycling can also cause the electrolyte redistribution due to volume expansions/contractions.

The raising of temperature during the start-up process causes phosphoric acid evaporation, while the water condensation due to the cool-down during the shut-down process causes phosphoric acid dilution and loss [73].

Start/stop cycling are also considered to strongly affect carbon corrosion, indeed, as reported by [21] this type of cycling can causes high stress to the cathode due to local excursions to high potentials, where significant corrosion of the cathode carbon materials occurs.

Start and stop cycles induce also thermal and mechanical stress that can affect membrane structure, causing membrane thinning, cracking and formation of pin-holes, with consequent cross-over [28,47].

Table 14 reports literature degradation values for HT-PEM fuel cells in a single cell configuration operated at constant load. In grey are highlighted the data referred to Celtec P1000 membranes which correspond to the ones used for the experimental test carried out in this PhD activity.

Type of membrane	PA doping level	Type of SS cycle	Operating temperature	Operating stoichiometry	Duration of the test	Current density for degradation measure	Degradation rate	Reference
type	PA/repeat unit		°C		h	A/cm^2	μV/h	
para-PBI	27.7	3h 0.2A/cm^2 180°C 1min OCV min. flow	55-120-180	λH$_2$=1.2 λair=2	100 SS cycles (6h each)	0.2	48.4	[47]
2OH-PBI	25.4	Cooling to 55°C no gas flow Reheating to 120°C min. flow Temperature raise to 180°C at constant current 0.01A/cm^2					30	
Celtec-P 1000	70	12h at 0.2 A/cm^2 160°C Cooling to 20-25°C 12h stop period no Purge no gas flow	160	λH$_2$=1.2 λair=2	6000	0.2	11	[21]
Celtec-P 1000	-	1h at 0.2 A/cm^2 150°C Cooling to 60° Nitrogen purge Heating to 150°	150	λH$_2$=1.2 λair=2 .2	3200	0.5	17.2	[23]
Celtec-P 1000	70	12 h at 0.2 A/cm^2 at 150°C 12h Stop	150	λH$_2$=1.6 λair=2 .5	-	0.2	170	[155]
				λ(80%H$_2$+17.5%CO$_2$+0.5%CO+2%CH$_4$)=1.6 λair=2 .5			160	
				λ(80%H$_2$+16%CO$_2$+2%CO+2%CH4)=1.6 λair=2 .5			270	

Table 14 Degradation rates in literature of HT-PEM single cells operated in start and stop cycling mode

Experimental testing of MEA 276

This operating condition had been tested in a previous work effectuated in the laboratory of the University of Trieste a first time on MEA 266, afterward, during this PhD work, the same Start & Stop (SS) cycle has been applied as well on MEA 276.

The cycle consists in the following steps schematically presented in Figure 58:

1. Start heating
2. Output valves opening
3. Reactants introduction
4. Switching on load
5. Regime operation with constant temperature
6. Load to minimum and fan on
7. N_2 purge
8. Stop N_2 purge
9. Output valves closing
10. Fan off and standby mode
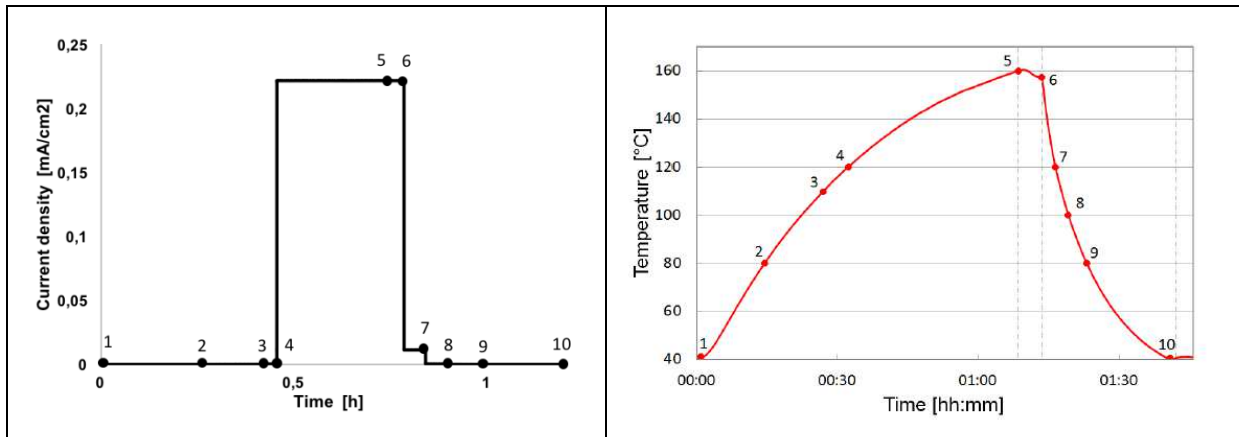
Figure 58 Start and Stop cycle diagram

As for the other MEAs, MEA 276 has been subjected to a 100 h conditioning period at 0.22 A/cm^2. After the first set of measurement the aging test has been carried out for 450 h, corresponding to 300 Start-Stop cycles. Polarization curves and EIS measurements have been performed periodically during the test in order to check the evolution of the degradation of the MEA performance over time. Polarization curves measured during the ageing test are reported in Figure 59.
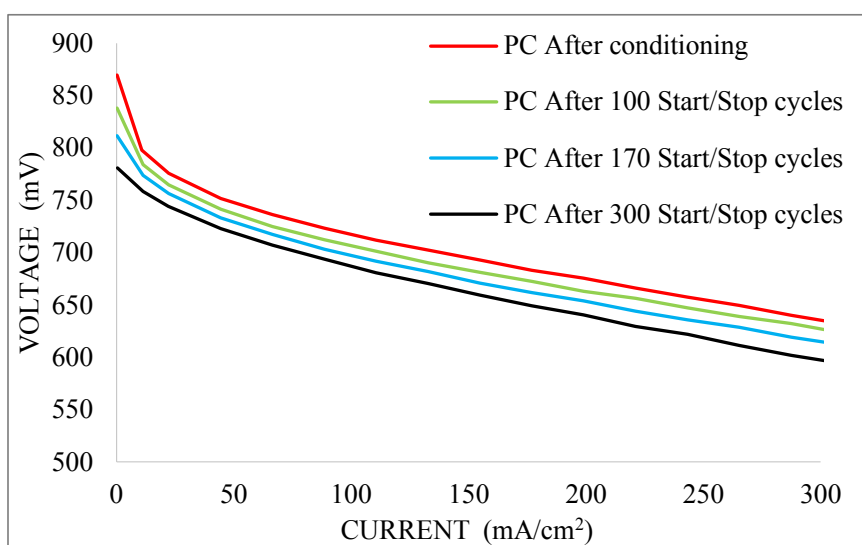
Figure 59 Polarization curves of MEA 276

Differently from the other operational conditions, Start and stop cycles seem to sensibly affect OCV value. This could be attributed to fuel cross-over due to membrane thinning and creation of pin-holes and/or reduction of ECSA, caused by platinum agglomeration. The loss in OCV value during start and stop cycles has been reported be many authors and membrane degradation is usually considered the main degradation factor [12], together with a loss in ECSA [43].

As for the other MEAs, the degradation rate caused by the load cycling test has been calculated considering two polarization curves: one at the beginning of the test and the other one after 300 Start and Stop cycles. For each current density, the voltage degradation value has been given in terms of voltage degradation per hour and per cycle as shown in Table 15.

Degradation rate at 0.22 mA/cm^2 of MEA 276 is 81 µV/h. The research group, in a previous work [13] performed a 1000 cycles test and found a degradation rate of 55 µV/h.

Also in this case it could be inferred that duration of test could influence degradation rate value. Schmidt and Baurmeister [21] performed a 6000 h test (240 Start-Stop cycles) on Celtec-P1000 MEAs operated at 160°C and reported a degradation rate of 11 µV/h at 0.2 mA/cm^2, while [155] reported a degradation rate of 170 µV/h for the same membranes operated in Start-Stop mode at 150°C for about 480h (20 Start-Stop cycles).

Current density	MEA 276			
	Voltage after conditioning	Voltage after 300 S&S cycles	Degradation rate	
A/cm^2	mV	mV	$\mu V/cycle$	$\mu V/h$
0	870	781	295	195
11	798	759	131	86
22	776	744	106	70
44	752	723	97	64
66	736	707	97	64
89	723	694	99	65
111	712	681	104	69
133	702	671	106	70
155	693	659	112	74
177	683	649	113	74
199	676	641	116	77
221	666	629	123	81
243	657	622	119	78
265	650	611	128	84
287	640	602	127	84
310	632	594	126	83
332	622	583	130	86
354	612	573	127	84
376	602	565	121	80
420	574	543	105	69
442	556	533	77	51

Table 15 Polarization curves and degradation rates of MEA 276

EIS measurements are reported in Figure 60. It can be notice that, in a similar manner than for MEA 274 and MEA 277 also in this case the increasing of polarization in the EIS spectrum during ageing test causes a merging of the two arcs not allowing the distinction between the component of degradation due to cathode activation losses and the one due to mass transport losses. Also in this case, the ageing test influenced the EIS spectra also at low currents indicating that probably the nature and morphology of the electrode/electrolyte interface has changed, but in this case it is remarkable that, while for high current densities the evolution of the spectra brings to an increasing of the polarization, at low current the polarization actually decreased during the ageing test. This was visible also on the EIS spectra of MEA 271, but for MEA 276 is very pronounced. This phenomena has already be encountered by [156] and has been explained as a result of water-back diffusion which increases the conductivity in the ionomer. In [157] for humidity of less 10% has been shown as well a reduction of the EIS spectra for LT-PEM fuel cells subjected to on-off cycles, while at high humidity the polarization increased with time during the ageing test. Even if the effect is lower than in LT-PEM the impact of humidification on charge transfer of HT-PEM is well known and in this case could justify the EIS spectra evolution of MEA 276 at low current densities.
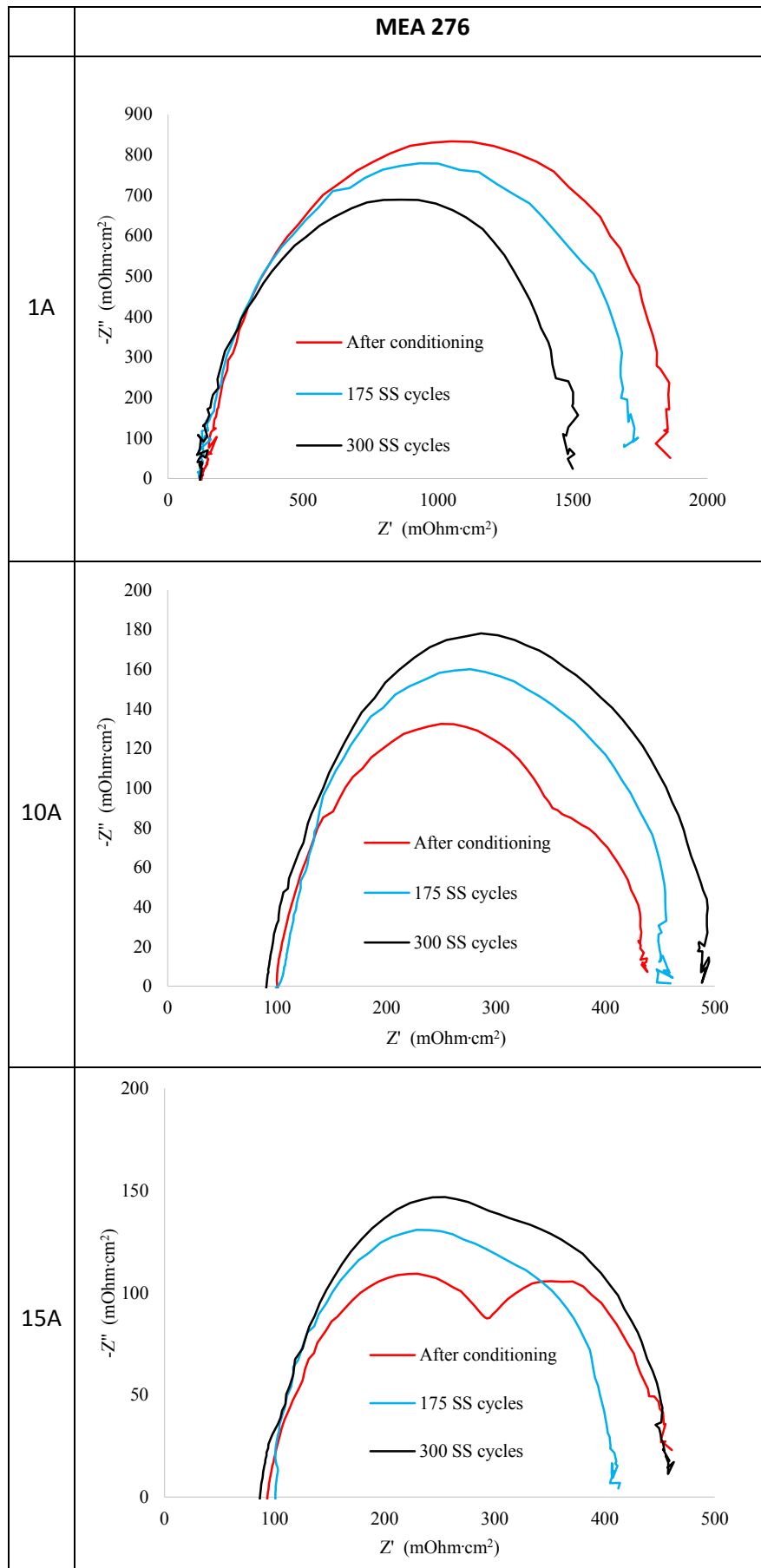
Figure 60 EIS results before and after Start and Stop degradation test for MEA 276

The cyclic voltammetry analysis shows a strong increase of the current in the surface oxidation region compatible with an increased presence of water at the anode due to water back diffusion caused by the membrane failure, as already observed in the EIS spectra. It is interesting to notice that membrane failure had also be encountered on MEA 266 subjected to the same Start and Stop cycle during a previous test performed by the research group of the University of Trieste. This let infer that Start and Stop cycle is an important stressor for membrane structure degradation as already mentioned in 4.2.4.
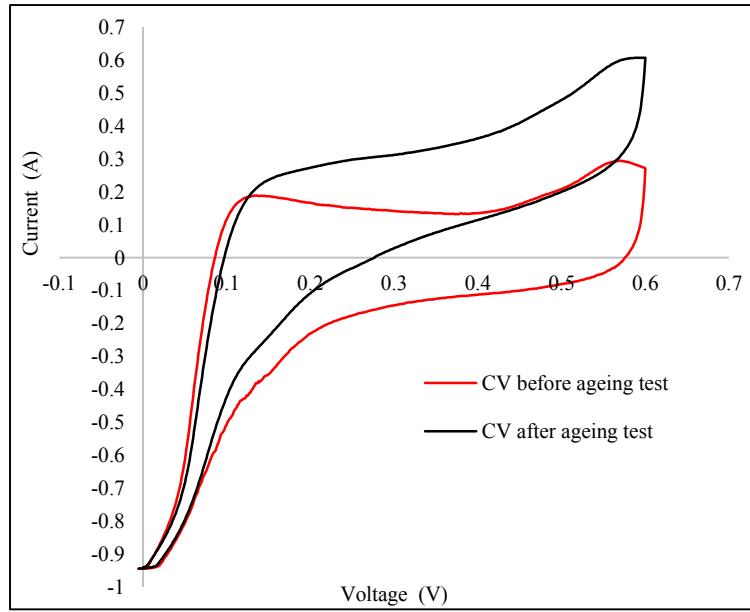
Figure 61 CV measurement before and after the ageing test for MEA 276

The ECSA after the ageing test of this MEA has not been calculated since the procedure chosen for the calculation of the ECSA is not applicable for this cyclic voltammogram; indeed the hydrogen adsorption and desorption peaks are not delimited.

The analysis of the hydrogen flow and potential trend during the start-stop ageing test is reported in Figure 62.
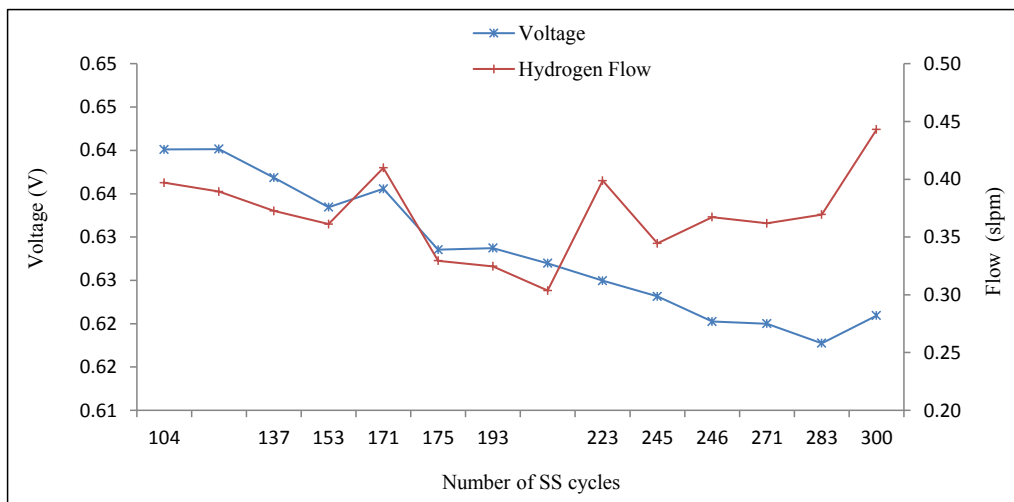
Figure 62 Hydrogen flux and cell potential during SS ageing test

The increase of hydrogen flow at the end of the test seems to confirm that membrane failure occurred at the end of the ageing test. This behaviour was reported, as well, in [100] performing the same ageing test.

SAXS analysis results for MEA 276 are reported in Figure 63 compared with data obtained in a previous work by the research group on MEA 266. For MEA 276 the Pt mean radius at the end of the test has increased by 98% from the initial reference value of 2.38 nm (MEA 275) to the final value of 4.71 nm (st. deviation 0.53), while for MEA 266 the Pt mean radius at the end of the test has increased by 110% from the initial reference value of 2.38 nm (MEA 275) to the final value of 5.02 nm (st. deviation 0.65). It can be noticed that the lower number of Start and Stop cycles performed on MEA 276 with respect to MEA 266 had the double effect of slightly lowering the mean radius of the Pt particles, as expected, but also lowering the spreading of the distribution due to degradation. However, it is noticeable that the two distributions follows the same behaviour during the Start and Stop ageing test that seems to cause a displacement toward right in the direction of higher radii values in a most noticeable manner with respect to other operating conditions, as shown in Figure 64. This means that Start and Stop cycles causes increase of the mode radius value stronger that the mean radius increase, which could suggest that degradation due to Start Stop cycles causes a more generalized and uniform particle size growing over the entire MEA surface compared to other operational conditions.
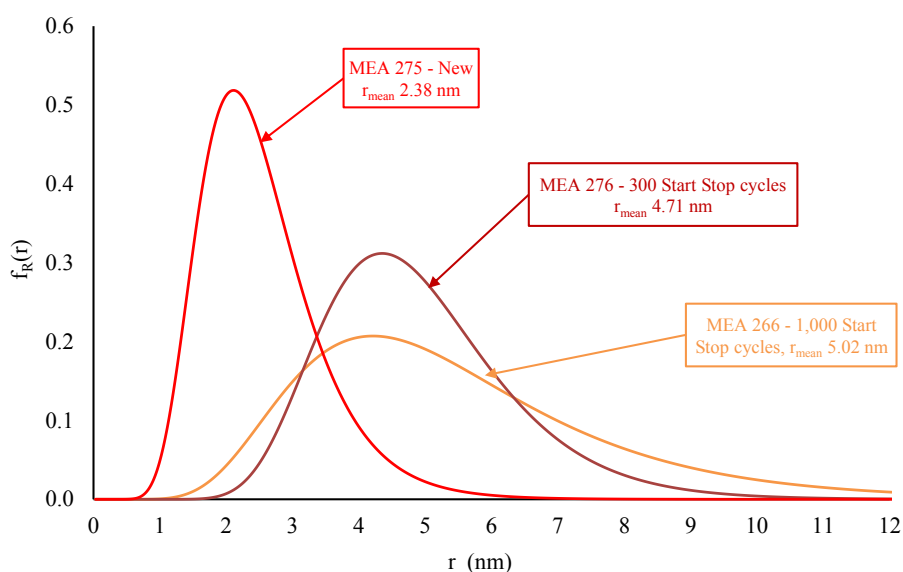
Figure 63 SAXS analysis. Volume size distributions of MEA 276 (brown line), 266 (yellow line) and 275 (red line)
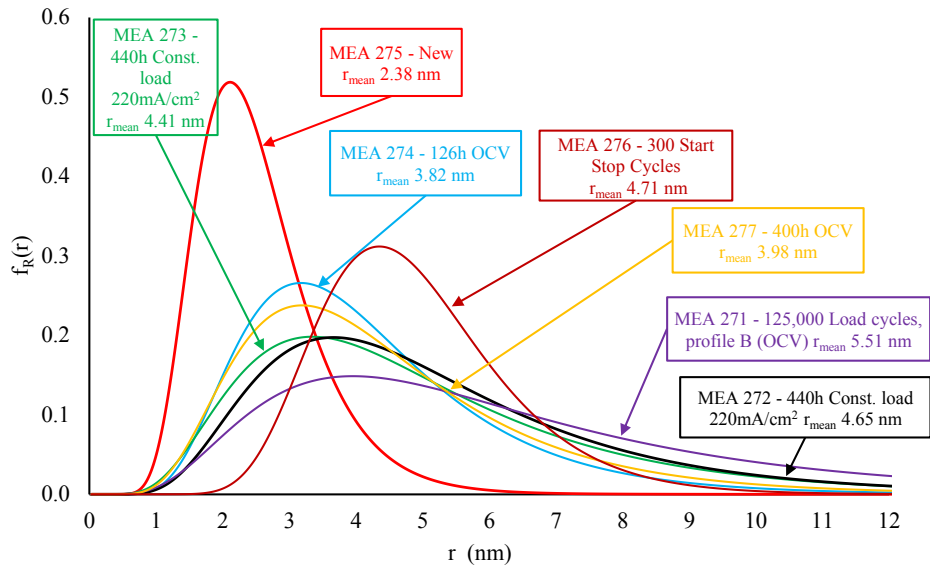
Figure 64 SAXS analysis. Comparison of volume size distributions of MEA 271 (purpule line), 272 (black line), 237 (green line), 274 (blue line), 275 (red line), 276 (brown line) and 277 (yellow line)

MEA 276 has then been analysed as well with TEM technique. The mean radius of the Pt particles at the anode (see Figure 65) has been found to be 4.07 nm (st. deviation 0.88), while the mean radius of the cathode (see Figure 66) has been found to be 3.39 nm (st. deviation 1.33). The weighted average of anode and cathode Pt particles radius is 3.58 (st. deviation 1.22).
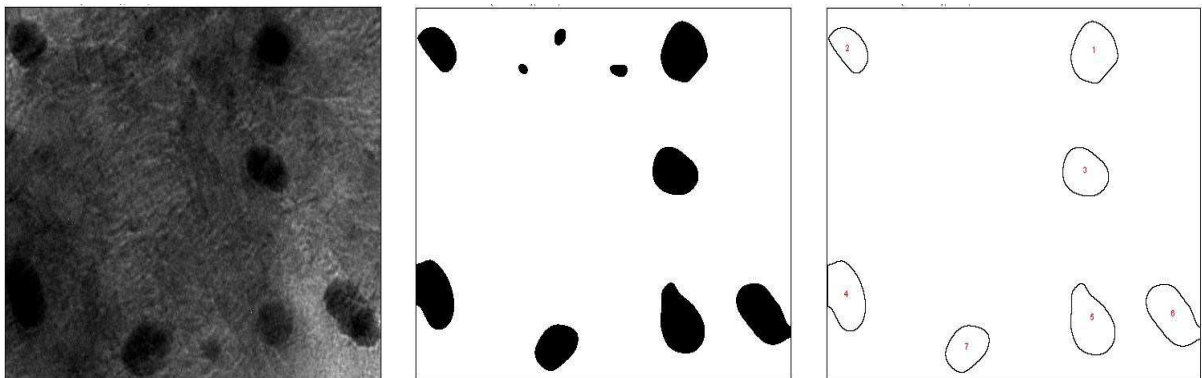
Figure 65 TEM analysis of MEA 276 anode - a) TEM image before treatment b) ImageJ treated image c) ImageJ particles selection
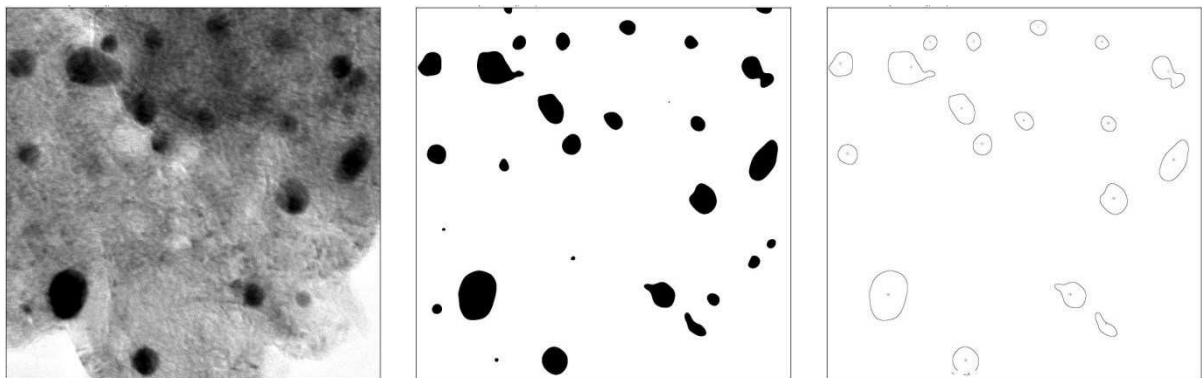
Figure 66 TEM analysis of MEA 276 cathode - a) TEM image before treatment b) ImageJ treated image c) ImageJ particles selection

Table 16 compares platinum particles sizes after ageing tests obtained with SAXS and with TEM techniques. TEM results shown in table are obtained by the average between anode and cathode side. For MEA 263, are reported both the values obtained in the previous TEM analysis performed by the research group and the results obtained during this PhD TEM analysis.

MEA label	Load profile	SAXS Pt particles size (nm)		TEM Pt particles size (nm)	
		r_{mean}	st. dev.	r_{mean}	st. dev.
MEA 263 [13]	Untouched	2.78	0.64	2.55	0.86
MEA 263	Untouched	-	-	2.30	1.13
MEA 264 [13]	Triangular [0.001 - 0.5]V	4.88	0.66	3.26	1.29
MEA 265 [13]	Triangular [0 - 0.5]V – 2sec OCV	5.60	0.66	3.75	1.68
MEA 266 [13]	Start & Stop cycles	5.02	0.65	-	-
MEA 271	Triangular [0 - 0.5]V – 2sec OCV	5.51	0.76	3.46	1.24
MEA 272	Constant load 0.22A/cm^2	4.65	0.70	-	-
MEA 273	Constant load 0.22A/cm^2	4.41	0.72	2.95	0.98
MEA 274	Constant OCV	3.82	0.66	-	-
MEA 275	Untouched	2.38	0.59	-	-
MEA 276	Start & Stop cycles	4.71	0.53	3.58	1.22
MEA 277	Constant OCV	3.98	0.69	-	-
MEA 278	3 month stop period	-	-	-	-

Table 16 Pt particles mean radii obtained with SAXS and with TEM

4.2.5. Degradation in micro-CHP systems

When the analysis of the degradation of MEAs is performed on fuel cell stacks installed in micro-CHP system; two main differences must be considered with respect to experimental tests performed of single cells test bench fed with pure hydrogen.

Firstly, the influence of fuel composition on the degradation of the stack must be considered. As already discussed in the previous chapters, the important advantage of HT-PEM fuel cells consists in the fact that at high temperatures the CO adsorption on the anode catalyst is less favoured and the tolerance to CO is increased allowing the use of fuels different from pure hydrogen. If, on one hand, a high concentration of CO can anyway negatively [145,158] affect the fuel cell performance, on the other hand can actually have a beneficial effect on the duration of the fuel cell MEA. Indeed, for example, as highlighted by [159] the presence of CO in the fuel gas can reduce carbon corrosion during start/stop cycles. In [141] an investigations of degradation of HT-PEM installed in micro-CHP system has been conducted with different oxidants and fuels. As already reported in Table 7 the test performed with synthetic reformate demonstrated a degradation rate of 63 µV/h at 0.3 A/cm^2 and showed an increase of anode charge and mass transfer resistances. This behaviour suggested that CO may be generated from the CO_2 included in the synthetic reformate via reverse water gas shift reaction. The fuel cell test performed with pure O_2 developed the highest degradation rates (70 µV/h) due to fast oxidative degradation of membrane electrode assembly materials such

as cathode catalyst and membrane. Fuel cell operation with H_2/air exhibited the lowest degradation rates (57 µV/h).

The second issue to take into account is the different degradation of the fuel cell in a stack configuration with respect to a single cell configuration. The main difference consists in the inhomogeneous distribution of oxidant and reactant gas with a consequent variation of the operating conditions of the cells depending on their position on the stack. In this sense, [14] carried out an analysis of the ageing behaviour of the fuel cell in a micro-CHP system in single cell and stack configuration. At single cell level, evolutions with ageing showed a strong dependence on cell position. Indeed, it was shown that, depending on cell position and CO content in the fuel, ageing decreased the anodic actual active area by 70–90%. It was also evidenced that cell voltage distribution was less and less uniform as ageing proceeded and that CO doubled the cell voltage distribution heterogeneities. Conversely, CO_2 had little effect on stack performances or on cell voltage distribution. The same author in [160] compared degradation rates of a HT-PEM micro-CHP system in single cell mode and 24 cells stack configuration based on Celtec P1000 MEAs and showed a 2.3% performance degradation of the stack at 0.4 A/cm^2 after 674 hours. However, the ageing effect was not uniform within the stack. On one hand, the best cell exhibits a negligible voltage loss, while the worst cell had lost a significant part (i.e. 35%) of its output power. In addition, although no clear trend was identified, the extent of degradation strongly varied with position in the stack, with some cells exhibiting an average degradation ranging between 10 and 20 µV/h while some others exhibited degradation rates above 100 µV/h. In single cell testing, the cell performance was extremely stable and in accordance with average single cell degradation of the stack. In [161] performances of a micro-CHP system fed with natural gas and biogas have been compared and demonstrates that MEA degradation rate obtained with biogas resulted higher to the values found in literature for hydrogen operation, but similar to the ones obtained with simulated reformates. With biogas, the stack average cell degradation rate was found to be 10% greater than the single cell values (66 µV/h against 60 µV/h), probably because of non-homogeneous temperature distributions. The stack operated with an electrical efficiency of 23.2% and the fuel processor, with the anode-off recirculation, reached an efficiency of 60.0%. In [36] it is highlighted that some anomalies of performance of a single cell inside the stack can have a significant impact on the stack life and to the performance of the neighbouring cells which also tend to fail due to increased degradation rates affected by the higher local temperatures. It is thus imperative with an efficient quality control considering the cell production and it is very important to avoid operational situations where there is a risk of failure of the cells. Also making sure that the temperature gradient along the stack is low, is a very important.

Table 17 reports literature data on degradation of HT-PEM fuel cell stacks operated in micro-CHP systems. In grey are highlighted the data referred to Celtec P1000 membranes which correspond to the ones used for the experimental test carried out in this PhD activity.

Type of membrane	PA doping level	Load profile	Operating current density	Operating temperature	Operating stochiometry	Duration of the test	Current density for degradation	Single cell averaged degradation rate	Reference
type	*PA/repeat unit*		*A/cm²*	*°C*		*h*	*A/cm²*	*µV/h*	
5 cells stack BASF P1100W	70	Start and Stop cycles 30s at OCV 115°C 900s 0.25A/cm² 165°C 600s cooling at 0.03A/cm² Purge and cooling to 80°C	-	165	λref.(74.8%H_2 + 25%CO_2 + 0.2% CO) =1.25 λair=2.5 or 80%H_2 + 20%N_2	120h + 4160h (430h H_2/N_2 and 3612 h with reformate)	OCV	**51.4**	[43]
							0.03	**10.2**	
							0.25	**4.3**	
12 cells stack BASF P1100W		Constant load	0.25			1600	0.25	**13.25**	
Single Cell Celtec P1000	70	Constant load 170h 0.11 A/cm² 651 h 0.22A/cm²	0.11 0.22	160	-	821	-	**60**	[161]
22 cells stack Celtec P1000	70	Constant load 200h 0.11 A/cm² 200h 0.22 A/cm²	0.11 0.22	160	-	417	-	**66**	
24 cells stack Celtec P1000	70	250h at 0.4A/cm² 120h daily cycling at 0.4A/cm² and 0.2A/cm² 120h at 0.2Acm² 240h SS cycles 120h daily cycling at 0.2A/cm² and 0.4A/cm² 120h at 0.2A/cm²	-	160	λref.(70%H_2 + 29%CO_2 + 1% CO) = 1.4 λair=2	970	0.4	**30**	[160]

Table 17 Degradation rates in literature of HT-PEM stack operated in micro-CHP systems with reformat

4.2.6.   HT-PEM degradation rate comparison with LT-PEM

As previously detailed in §2.4, catalyst layer degradation of PEM fuel cells during long-term operation is a complex process that includes many mechanisms that occur in parallel. The analysis of HT-PEM fuel cells degradation during long term operation is not as mature as for LT-PEM fuel cells. The experimental campaign carried out during this PhD activity represents, hence, a step forward to provide structural understanding of the significant factors affecting catalyst layer degradation. This approach had already successfully been applied to LT-PEM allowing to obtain information on the degradation mechanisms to allow the choice of some mitigation strategies that successfully induce an improvement of LT-PEM lifetime [152].

As already cited in §1.1, lifetime of LT-PEM FC is much longer than the one of HT-PEM fuel cells. This is partially due to the HT-PEM higher degrading operating conditions, but also by the fact that, in the last decades, research mainly focused on LT-PEM strongly increasing their durability. Table 18 reports data presented in a literature review [28] concerning degradation rates of LT-PEM fuel cells operated at constant load.

However, data reported in Table 18 refers to different type of LT-PEM MEAs produced by different manufacturers and operated at different test conditions; hence variability of results is important, however these data can furnish a rough approximation of the mean degradation rate value for LT-PEM to allow comparison with HT-PEM data collected during this research activity.

Time Test	Degradation Rate
h	*μV/h*
5000	4
5000	1
4700	6
8000	2.2
4000	2
8000	2-3
11000	2
1350	11
1800	>4
4000	3.1
2500	20
26300	4-6

Table 18 Summary of steady state lifetime tests in the literature – *elaborated from[28]*

Table 19 reports data presented in a literature review carried out by [162] concerning degradation rates of LT-PEM fuel cells operated with load cycling, start and stop cycles and OCV. As for Table 18, data refer to different types of LT-PEM MEAs, operated with different test conditions.

Hence, the reported data, aims to give an order of magnitude of degradation in variable load conditions for LT-PEM, but cannot be used as reference values for direct comparison for each specific operating condition.

Type of Test	Degradation Rate
H	*µV/h*
Start and Stop	1
Start and Stop	1.4
Start and Stop	1.3
Load Cycling	1.5
Start and Stop	2.5
Start and Stop	6
Start and Stop	6.4
Start and Stop + OCV	20
Start and Stop	25
Start and Stop	28
Start and Stop	29
Start and Stop	33
Load Cycling	2.5-50
Start and Stop + OCV	45
Load Cycling	75
Start and Stop + OCV	75-114
Start and Stop	95
Start and Stop + OCV	180
Load Cycling	210

Table 19 Summary of dynamic lifetime tests in the literature – *elaborated from [162]*

However, except for some particular experimental tests that reports very high degradation rates, literature data of degradation for LT-PEM FC operated at constant load, range from 1 to 10 µV/h, while, for HT-PEM FC, as reported in §4.2.1, data of degradation at constant load found in literature and measured during this research activity range from 5 to 80 µV/h.

Variability of degradation rates is higher when analysing load cycles, Start and Stop cycles and OCV permanence. Literature data for LT-PEM FC reports degradation rates ranging from about 1 to 100 µV/h, while for HT-PEM FC, as reported in § 4.2.2, 4.2.3 and 4.2.4, degradation rates range from 10 to 300 µV/h, and reaching even higher degradation rates for OCV permanence.

4.3.   Modelling Results

As already mentioned in § 3.4, the aim of this modelling activity consisted in the implementation of a fuel cell degradation model based on the experimental results collected during this PhD into a previously existing model of a micro-CHP system.
The purpose was to study the effect that the degradation of the fuel cell had on the global micro-CHP system and the mitigation strategies that could be adopted to reduce the degradation effect, answering in this way to the research question:

*"**How does the degradation issue for HT-PEM fuel cells, installed in micro-CHP systems, can be handled to make the system become suitable for long term operation in terms of performance?**"*

Considering exclusively the electricity production, degradation of the fuel cell strongly affect the performance; however, since, the reducing of the electrical performance causes an increasing in the heat power produced by the fuel cell, its integration in a micro-CHP system can reduce the total degradation effects on CHP system performance.

The micro-CHP system model, upgraded with the implementation of the fuel cell degradation model, has been used to perform the analysis of the operation of the micro-CHP system over a long period of time (1 year). The purpose was to evaluate the effect of degradation in terms of system energy balance and primary energy saving index for different micro-CHP system configurations. The analysed period of one year has been chosen to simplify the energy balance analysis, but, in the future, it can easily be extended to more years of operation in order to take into account the entire micro-CHP system lifetime.

The fuel processor, HT-PEM fuel cell, BOP efficiency coefficient and ξ_{REC} evaluation have been calculated by means of a previously developed simulation model and experimental data [60,163].

In order to carry out the performance analysis, a typical Italian 100 m^2 single family dwelling energy demand profile has been taken into account. Annual electric demand has been estimated to be 4,415 kWh/year while annual thermal energy demand has been estimated to be 12,412 kWh/year. The annual energy profile has been obtained by considering 12 typical days corresponding to the twelve month of the year as reported in Figure 67 and Figure 68.
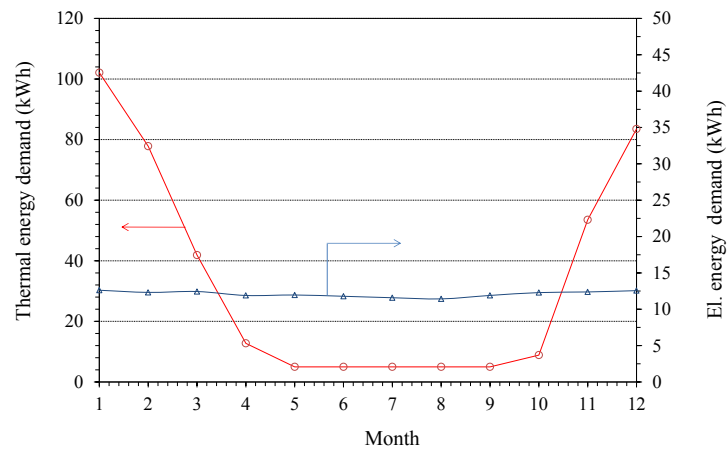
Figure 67 Thermal and electrical power demand of a typical 100 m² single family dwelling
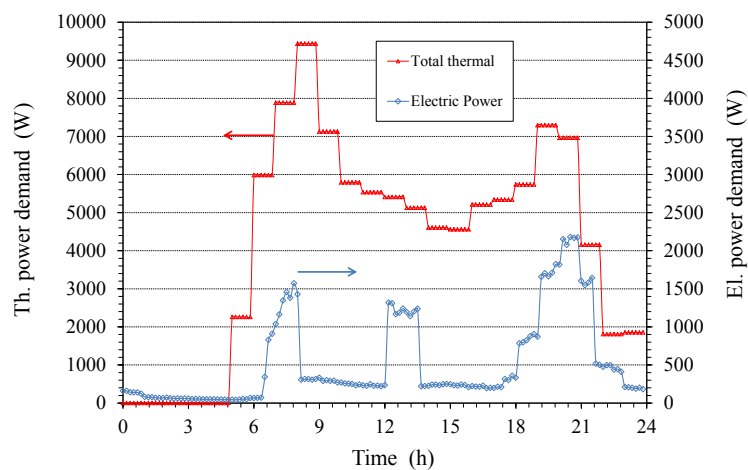
Figure 68 Thermal and electrical power demand - January typical day

The operational profile of the system has been implemented in the model taking care to avoid the operational conditions that affect too much the fuel cell performance with the purpose to maximize the operational time.

The first important issue to be analysed consists in the choice between keeping the system always operating or switching it on and off when there is no energy demand or when the demand is very low. This choice obviously depends on the duration of the no-demand (or very low) period. Indeed if the no demand period is long enough, the degradation caused by the start and stop cycle (see § 4.2.4) will be lower than the one caused by the constant load operation, while if the no-demand period is short, it is more convenient to keep the system in operation at low load. For a household application, this last option demonstrated to be the best choice, considering as well the opportunity to sell the excess production to the grid. The choice of the minimum power has been done based on the experimental data collected until now that showed a slower degradation rate and a maximum of the performance for 35% of

140

the nominal power of the fuel cell system. In the same manner, also OCV operation has been avoided through an adapted operational strategy to avoid the strong degradation issues highlighted in § 4.2.3. Other operational strategies have been implemented in order to preserve as well the performance and lifetime of the battery. For example, in the developed model, the lithium battery was not allowed to discharge more than 20%.

The system operational strategies have then been implemented in the model following an electrical led strategy; in particular the following operating conditions have been considered:

- If the electrical demand is higher than the maximum fuel cell system electrical output and the battery State Of Charge (SOC) is higher than 20%, then the fuel cell system works at the maximum capacity and battery is discharged. While, if SOC is lower than 20%, electricity is imported from the grid;
- If the electrical demand is lower than the minimum fuel cell system electrical output and battery is fully charged, then the fuel cell system works at its minimum capacity and excess electricity is sold to the grid;
- If electrical demand is between the lower and the maximum fuel cell system electrical output and the battery is fully charged, then the fuel cell system follows the electrical demand;
- If electrical demand is lower than 30% of fuel cell system capacity, then the fuel cell system operates at 35% capacity (highest efficiency); Part of the electricity output is used to meet demand and part is used to charge the battery.

Figure 69 shows the contributions to the electrical power demand of the fuel cell system and the battery during a typical January day. It can be noticed that the fuel cell system and the battery system manage to follow the demand of electrical energy from 6h to 21h while, before 6h, when the power demand is low, the fuel cell operates at its lower capacity, but excess electrical production must be sold to the grid. The opposite situation is noticeable from 21h to 22h where it is visible a pick of electric demand that cannot be satisfy nor by the fuel cells that operates at maximum capacity, neither by the battery that is discharged since it strongly contributed to the pick of demand from 19h to 21h.
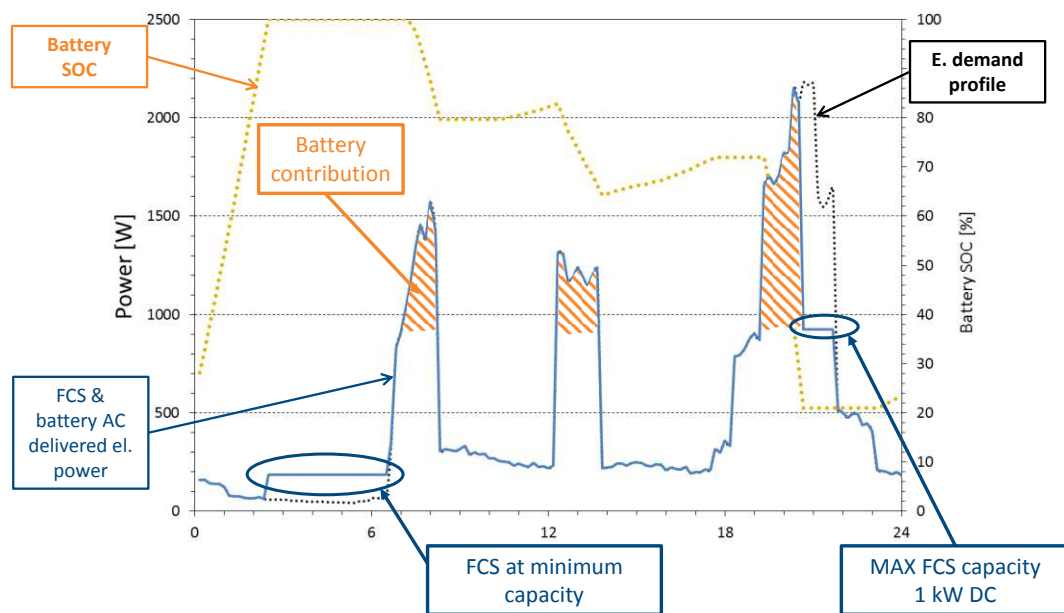
Figure 69 Electrical power contributions over a typical january day operation

Figure 70 shows the electrical power demand profile and the Fuel Cell System (FCS) electrical power profile before and after one year of operation highlighting the effect of the degradation on the electrical production with the consequent increasing of the electricity imported from the grid.
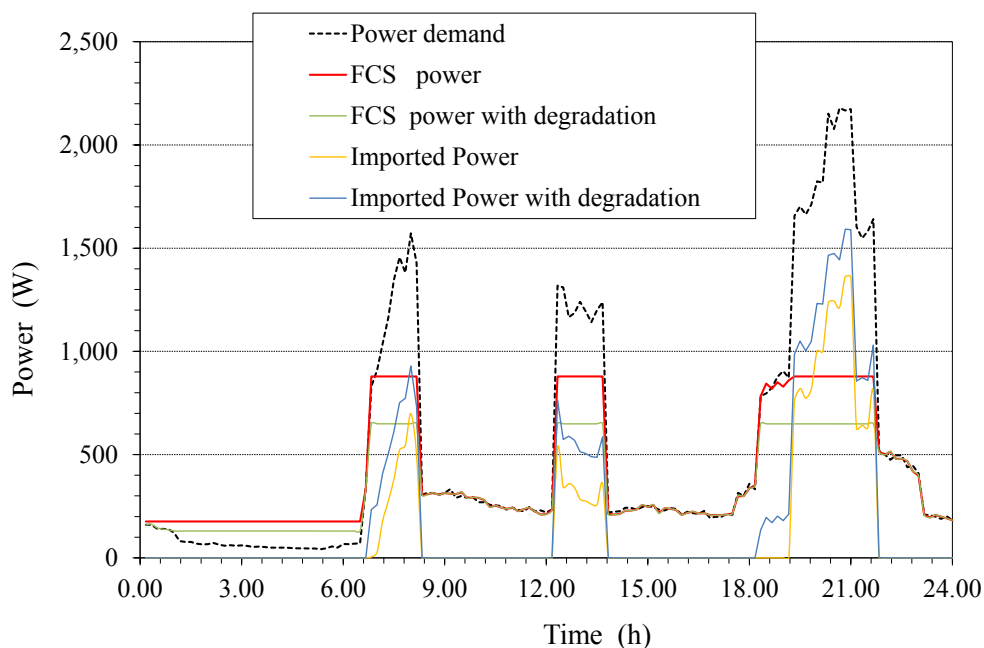
Figure 70 Electric power demand profile and Fuel Cell System (FCS) profile and imported power profile with and without FCS degradation

The impact of fuel cell stack performance degradation on the system performance has been analysed. The purpose of this analysis is to suggest a methodology of modelling of the degradation in a HT-PEM based micro-CHP system in order to analyse the performance of the system using fuel cells with any other degradation rate. The degradation rate values has been chosen on the basis of literature and from experimental data collected by the authors. In order to take into account for possible variations of degradation values due to real operational conditions of the fuel cell stack in a micro-CHP system configuration, two different hypothesis of degradation rates, named in the following DR1 and DR2, have been used to perform the energy balance of the micro-CHP considered system. The DR2 values of degradation has been chosen, considering the average of literature degradation rates at 220 mA/cm^2 [19,21,22,35,42,47,142,149]. The trend of evolution as function of the current density has been then extrapolated from the average variation of the polarization curves obtained by our experimental data. DR1, corresponds to half of DR2 and is close to LT-PEM degradation in micro-CHP systems.

The values of the degradation used by the authors in this model are presented in Table 20.

Current density mA/cm^2	Degradation rate (DR1) [µV/h]	Degradation rate (DR2) [µV/h]
0.0001	5.8	11.6
10	3.69	7.38
20	3.97	7.94
40	4.68	9.36
80	5.40	10.8
100	5.85	11.7
150	6.95	13.9
200	7.77	15.54
220	8.30	16.6
250	9.55	19.1
300	10.22	20.44
350	11.27	22.54
400	12.29	24.58
450	13.18	26.36
500	14.79	29.58

Table 20 Degradation rates considered in the model

The system has been analysed for four different configurations:

- 1 kWel micro-CHP only;
- 1 kWel micro-CHP and battery storage;
- 1.2 kWel micro-CHP only;
- 1.2 kWel micro-CHP and battery storage;

For each configuration 2 different degradation rates DR1 and DR2 have been tested.

The 1 kWel fuel cell stack size configuration with no degradation is the reference case while the other cases are named "test cases" as described in Table 21 . The configuration with a 1.2 kWel fuel cell stack has been taken into account in order to compensate the loss in electric energy production that is expected after one year of operation considering the DR1 degradation rate previously defined.

	Ref. case [164] (Ref)	Test case 1 TC1	Test case 2 TC2	Test case 3 TC3	Test case 4 TC4	Test case 5 TC5
Degradation rate	-	DR1	-	DR1	DR2	DR2
Stack size (kW)	1	1	1.2	1.2	1	1.2

Table 21 Test cases

For each configuration, system annual performances have been calculated and compared. Figure 71, Figure 72 and Figure 73 show annual electrical and thermal energy production, annual exported and imported electrical energy and annual auxiliary boiler thermal energy production for the micro-CHP system configurations previously defined.

Micro-CHP produced thermal. Energy – Et [kWh/year]

Micro-CHP produced AC electricity – Ee [kWh/year]

Exported electricity [kWh/year]

Imported electricity [kWh/year]

Auxiliary boiler energy production [kWh/year]

| a) | Reference Case – 1kW not degraded | b) | Test Case 1 – 1kW degraded DR1 |

Figure 71 Electrical and thermal energy annual production; annual exported or imported electrical energy; annual auxiliary boiler thermal energy production; (a) Reference case (Ref) [150]; (b) deg. rate DR1 (TC1) [137].

Figure 71 a) shows the system annual energy production obtained for the reference case (Ref) which does not take into account the degradation of the fuel cell, while Figure 71 b) shows the test case 1 (TC1) where a degradation rate DR1 is considered. It can be noticed that in both systems with and without battery, fuel cell degradation causes a 10% annual electrical production reduction, and an increase of the thermal energy production of 4% and 6% respectively. Moreover it can be noticed a strong increase in the imported electricity caused by the degradation of the fuel cell together with a reduction of the exported electricity. On the other hand the increased production of heat power allowed, as expected, a reduction of the boiler energy production.

Neglecting cost issues, in order to recover the annual electrical energy loss due to the fuel cell performance degradation over time, a larger fuel cell stack has been considered.

| a) | Test Case 2 – 1.2 kW not degraded | b) | Test Case 3 – 1.2 kW degraded DR1 |

Figure 72 Electrical and thermal energy annual production; annual exported or imported electrical energy; annual auxiliary boiler thermal energy production; (a) 1.2 kW not degraded (TC2); (b) 1.2 kW deg. rate DR1 (TC3) [137]**.**

Figure 72 a) shows the results of (TC2) where the stack power is 1.2 kWel and no degradation effect is considered, while Figure 72 b) shows the results for (TC3) where the same fuel cell stack power is considered and the degradation rate DR1 is taken into account.

Comparing (TC2) and (TC3), the reduction of the electrical production due to degradation is about 8% while the increasing of thermal production is about 6% which is quite comparable with the situation encountered for the 1kW fuel cell system (see (Ref) and (TC1)) even if a slight reduction of the electrical loss can be noticed. However, when comparing (TC3) with (Ref) case the electrical production loss due to degradation is of just about 3%, while thermal energy production, has increased of 17% with respect to (Ref) case for both configurations with and without battery. This is an interesting issue; indeed the benefit of the increased thermal production can in such a way compensate the loss of electrical production.

In Figure 73 the case with a higher degradation (DR2) is analysed.

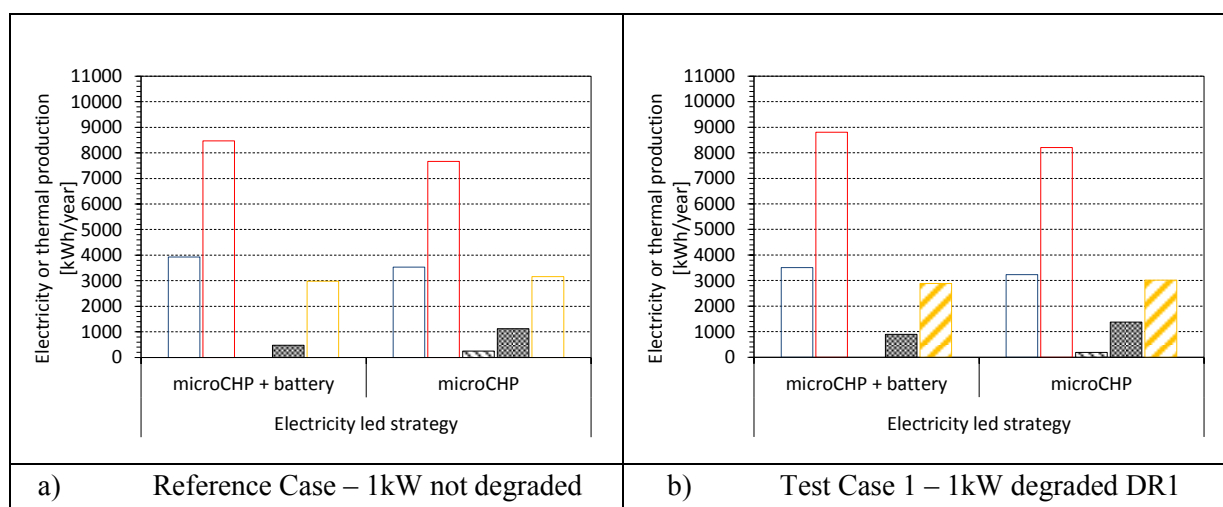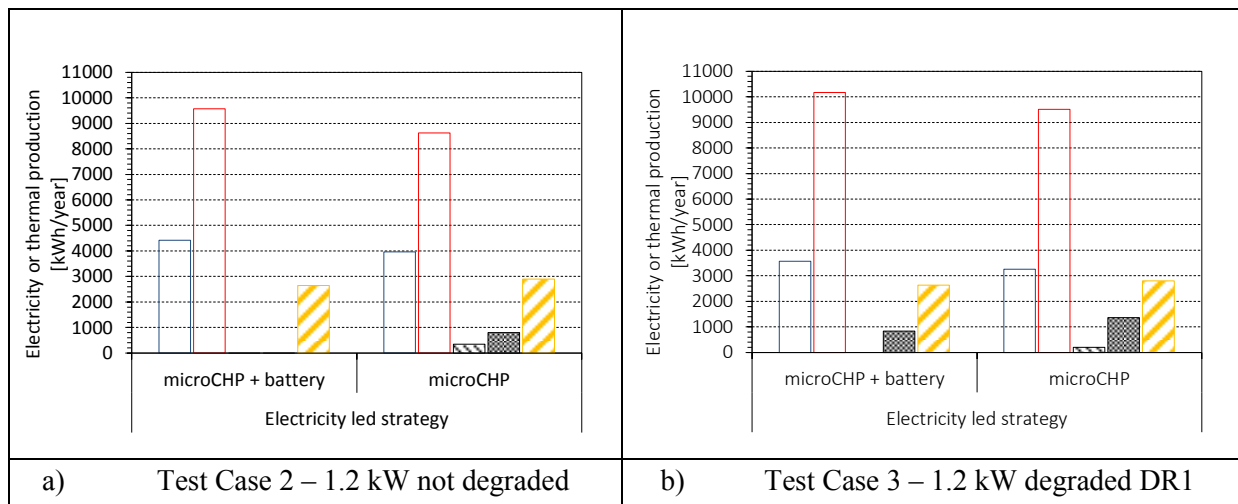| a) | Test Case 4 – 1kW degraded DR2 | b) | Test Case 5 – 1.2 kW degraded DR2 |
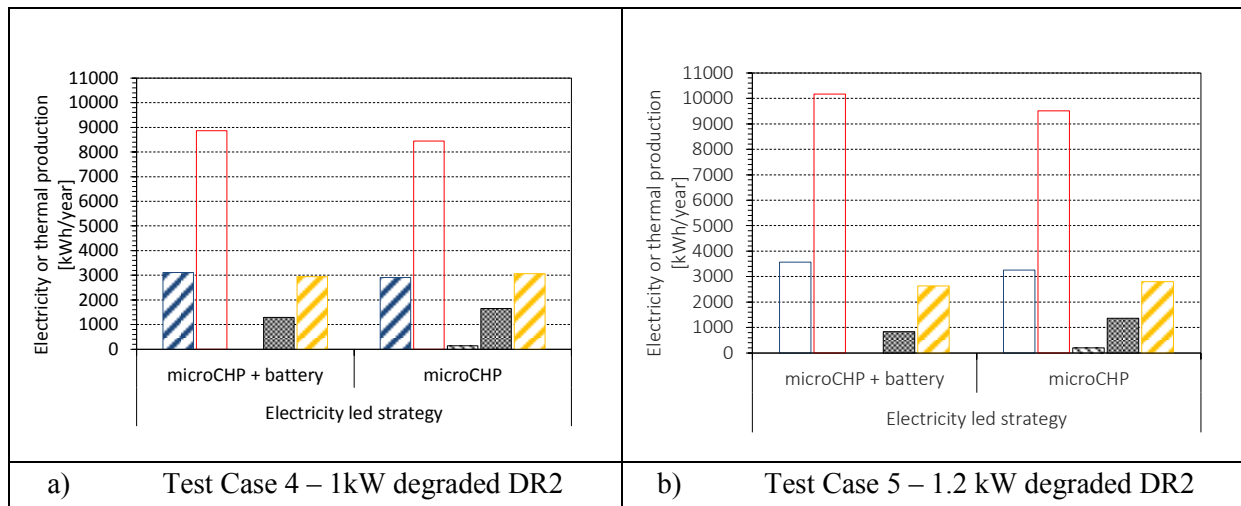
Figure 73 Electrical and thermal energy annual production; annual exported or imported electrical energy; annual auxiliary boiler thermal energy production; (a) 1kW deg. rate DR1 (TC4); (b) 1.2 kW deg. rate DR2 (TC5) [137]**.**

Comparing Figure 73 a) (TC4) with the (Ref) case it can be noticed that the electrical power is reduced of about 18% and 20% due to degradation, while thermal power is increased of 4.5% and 9% in the cases with and without battery respectively. In Figure 73 b) (TC5), the case with 1.2 kW stack power output and (DR2) is shown. In this case, it can be noticed that, with respect to (Ref) case the electricity loss due to degradation is 9% and 7%, while the heat production is increased by 17% and 19% again in the cases with and without battery, respectively.

These results show that, if the degradation is higher, then increasing the size of the fuel cell system has a stronger effect in the mitigation of the degradation issues. This analysis does not take into account the cost issues. However, it indicates that when sizing a micro-CHP system, to take into account the energy demand profile and cost of the fuel cell stack is not sufficient, indeed the optimum sizing of the fuel cell stack should be done in function of the degradation rate of the chosen fuel cell, which can also be influenced by the operational conditions, moreover the choice depends on the expected lifetime of the plant.

The optimum size for each energy demand profile will be then a three parameters optimization process based on: the energy demand profile, the degradation rate and the cost of the system.

The test cases have than been analysed in terms of a simplified Primary Energy Saving index (PES) defined as follows:

$$PES = 1 - \frac{E_f}{\dfrac{E_e}{\eta_{es}} + \dfrac{E_t}{\eta_{ts}}}$$

Where E_e and E_t are the produced electrical and thermal energy and E_f is the energy of the fuel feeding the fuel cell system in micro-CHP configuration, while η_{es} and η_{ts} are efficiency reference values for the separate production of electricity (0.39) and heat (0.9), respectively. Value of reference electrical efficiency has been chosen as the mean efficiency value of the Italian electrical production [165], while the heat production reference efficiency corresponds to a typical non-condensing natural gas boiler. As the installed power is small, all the heat generated can be used and, therefore, the PES is always positive, reaching 0.22 in the (Ref) case with battery. In all the cases, the configuration with battery shows a higher PES. Values of PES for the different test cases are reported in Table 22.

Test case	PES	
	Micro-CHP + battery	Micro-CHP only
(Ref)	0.22	0.20
TC1	0.20	0.18
TC2	0.22	0.19
TC3	0.20	0.18
TC4	0.18	0.17
TC5	0.18	0.16

Table 22 PES values for different system configurations

5. Conclusions

This PhD activity has been carried out with the purpose to answer to the research question:

"*How does the degradation issue for HT-PEM fuel cells, installed in micro-CHP systems, can be handled to make the system become suitable for long term operation in terms of performance?*"

Firstly, a literature review has been carried out on the test procedures and degradation results for HT-PEMFC, as well as on the existing fuel cell and micro-CHP numerical models.

Afterwards, a methodology to assess the performance analysis for long term use of HT-PEM fuel cells based micro-CHP systems has been developed.

A long term experimental analysis based on the accelerated stress test methodology has been carried out using three *in-situ* electrochemical diagnostics tools: polarization curves; electro-impedance spectroscopies and cyclic voltammetries.

Eight Membrane Electrode Assemblies (MEAs) subjected to different operational conditions have been tested. In particular, carbon corrosion, acid leaching and flooding as well as catalyst layer Electro Chemical Surface Area (ECSA) variation has been studied. Experimental data, summarized in Table 23, showed a strong influence of OCV permanence to the fuel cell performance degradation which has been attributed to acid flooding/leaching due to carbon corrosion. For this load profile an important variability on the determination of the degradation rate values has been registered. Start and Stop cycles showed a strong influence on performance degradation mainly due to fuel cross-over due to membrane thinning, creation of pin-holes and reduction of ECSA. Load cycling stress test demonstrates an influence on the variation of the ECSA higher than the one recorded for constant load operation; this increment has been attributed mainly to catalyst particles agglomeration.

Afterwards, an *ex-situ* nano-morphological technique (SAXS) has been validated through additional experimental data obtained during this PhD activity and its comparison with data previously obtained by the research group. An additional comparison has been done with TEM analysis that showed reproducibility with previous data collected by the research group. The comparison between SAXS and TEM data showed that there is a difference in terms of mean radius detected by the two techniques. This difference could be attributed to differences in the analysed portion of the MEA, higher sensitivity to bigger particles of the SAXS technique and the fact that probably not all the catalyst layer thickness can be analysed by TEM. Nano-morphological analysis helped to better interpret the electrochemical diagnostic tools results allowing separating the contribution of each degradation process and linking it with the operational conditions. Table 23 summarize the main experimental data obtained during this PhD (highlighted in grey) and compares them to the ones previously obtained by the research group of the University of Trieste.

Degradation rate of MEA 278 has been calculated on the base of stop period hours instead of operational hours.

MEA label	Load profile	SAXS Pt particles size (nm)		TEM Pt particles size (nm)		Degradation Rate (µV/h)
		r$_{mean}$	st. dev.	r$_{mean}$	st. dev.	
MEA 263	Untouched	2.78	0.64	2.55	0.86	-
MEA 263	Untouched	-	-	2.30	1.13	-
MEA 264	Triangular [0.001 - 0.5]V	4.88	0.66	3.26	1.29	34
MEA 265	Triangular [0 - 0.5]V – 2sec OCV	5.60	0.66	3.75	1.68	45
MEA 266	Start & Stop cycles	5.02	0.65	-	-	55
MEA 271	Triangular [0 - 0.5]V – 2sec OCV	5.51	0.76	3.46	1.24	44
MEA 272	Constant load 0.22A/cm^2	4.65	0.70	-	-	30
MEA 273	Constant load 0.22A/cm^2	4.41	0.72	2.95	0.98	29
MEA 274	Constant OCV	3.82	0.66	-	-	444
MEA 275	Untouched	2.38	0.59	-	-	-
MEA 276	Start & Stop cycles	4.71	0.53	3.58	1.22	81
MEA 277	Constant OCV	3.98	0.69	-	-	124
MEA 278	3 month stop period	-	-	-	-	26*

Table 23 Degradation rate values and mean catalyst Pt particles radii of tested MEAs obtained with SAXS and TEM analysis.

An important objective obtained through the experimental campaign performed during this PhD activity has been the development of a reproducible test methodology to evaluate the degradation rate for each load condition. In addition to the degradation rate evaluation, different diagnostic tools have been used in the purpose to separate contribution of each degradation process. In particular:

- experimental data on degradation values for HT-PEM fuel cells for different load condition have been collected;
- main degradation mechanisms has been identified and correlated to operating conditions thanks to electrochemical and nano-morphological diagnostic tools;
- understanding degradation affecting factors is the first step in identifying mitigation strategies. This approach had already successfully been applied to LT-PEM allowing to obtain enough information to determine some mitigation strategies that successfully induce an improvement of LT-PEM lifetime.
- degradation data showed that lifetime of HT-PEM fuel cells is still far from LT-PEM but specific operating strategies and specific fields of application, such as micro-CHP systems, could make HT-PEM competitive with LT-PEM.

The main objective of this PhD work was to understand how the degradation of the fuel cell stack influenced the total performance of a micro-CHP system and how to handle it in order to allow long term operation. The degradation rate values implemented in the model has then been chosen on the basis of literature and from experimental data collected by the authors, in order to take into account for variations of degradation values due to real operational conditions of the fuel cell stack in a micro-CHP system configuration.

The modelled system has been analysed in terms of operational performance over a long period of time (1 year). The analysed period of one year has been chosen to simplify the energy balance analysis, but, in the future, it can easily be extended to longer periods of operation in order to take into account the entire micro-CHP system lifetime.

The applied load profile consisted on the electrical and heat demands for a single-family dwelling. The model allowed assessing the impact of degradation of the fuel cell on the system energy production, primary energy saving and on the import and export of energy from the electrical grid.

Results indicate that stack degradation is still a hampering issue also in a micro-CHP system configuration; however, the detrimental effect can be mitigated choosing to increase the size of the stack, even if this choice affects system cost. Moreover, in a micro-CHP system, heat production can partially compensate electrical energy loss.

Finally, it has been possible to conclude that, when sizing a micro-CHP system, it is not sufficient to take into account the energy demand profile and cost of the fuel cell stack. The optimum sizing of the fuel cell stack should be done as a function of the degradation rate of the chosen fuel cell which is influenced by the operational conditions. The choice of the size of the system depends, as well, on the expected lifetime of the plant.

The simulation model can be a valuable tool for conducting sensitivity analysis and to provide insights in battery storage operations, to find the optimal size of system components taking into account different values of system performance degradation over time.

In the future, this model could be upgraded introducing different degradation behaviour for each operational condition encountered during the lifetime of the micro-CHP system and taking into account the performance degradation of the battery. In this way, each degradation process could be modelled and linked with the real operational condition of the micro-CHP system allowing to quantitatively link degradation and operational condition.

Bibliography

[1]   Ellamla HR, Staffell I, Bujlo P, Pollet BG, Pasupathi S. Current status of fuel cell based combined heat and power systems for residential sector. J Power Sources 2015;293:312–28. doi:10.1016/j.jpowsour.2015.05.050.

[2]   IEA. Electricity Information: Overview. 2017.

[3]   Bertoldi P. Electricity Consumption and Efficiency Trends in the Enlarged European Union - Status report 2006-. 2007.

[4]   The International Energy Agency (IEA) n.d. http://www.iea.org. (accessed April 27, 2017).

[5]   Maghanki MM, Ghobadian B, Najafi G, Galogah RJ. Micro combined heat and power (MCHP) technologies and applications. Renew Sustain Energy Rev 2013;28:510–24. doi:10.1016/j.rser.2013.07.053.

[6]   Carter D, Ryan M, Wing J, Ryan M, Wing J. The Fuel Cell Industry Review 2011, 2012, 2013. Fuel Cell Today 2013;56:1–56. doi:10.1595/147106712X657535.

[7]   Hashimoto DM. Japan ' s Hydrogen Policy and Fuel Cells Development in NEDO. ExCo 50th Meet 2015.

[8]   Napoli R, Gandiglio M, Lanzini A, Santarelli M. Techno-economic analysis of PEMFC and SOFC micro-CHP fuel cell systems for the residential sector. Energy Build 2015;103:131–46. doi:10.1016/j.enbuild.2015.06.052.

[9]   Zhang J, Xie Z, Zhang J, Tang Y, Song C, Navessin T, et al. High temperature PEM fuel cells. J Power Sources 2006;160:872–91.

[10]   Jannelli E, Minutillo M, Perna A. Analyzing microcogeneration systems based on LT-PEMFC and HT-PEMFC by energy balances. Appl Energy 2013;108:82–91. doi:10.1016/j.apenergy.2013.02.067.

[11]   Romero-Pascual E, Soler J. Modelling of an HTPEM-based micro-combined heat and power fuel cell system with methanol. Int J Hydrogen Energy 2014;39:4053–9. doi:10.1016/j.ijhydene.2013.07.015.

[12]   Jeon Y, Na H, Hwang H, Park J, Hwang H, Shul Y. Accelerated life-time test protocols for polymer electrolyte membrane fuel cells operated at high temperature. Int J Hydrogen Energy 2015;40:3057–67. doi:10.1016/j.ijhydene.2015.01.010.

[13]   Valle F, Zuliani N, Marmiroli B, Amenitsch H, Taccani R. SAXS Analysis of Catalyst Degradation in High Temperature PEM Fuel Cells Subjected to Accelerated Ageing Tests. Fuel Cells 2014;14:938–44. doi:10.1002/fuce.201300221.

[14]   Moçotéguy P, Ludwig B, Scholta J, Barrera R, Ginocchio S. Long term testing in continuous mode of HT-PEMFC based H3PO4/PBI Celtec-P MEAs for μ-CHP applications. Fuel Cells 2009;9:325–48. doi:10.1002/fuce.200800134.

[15]   Oono Y, Sounai A, Hori M. Long-term cell degradation mechanism in high-temperature proton exchange membrane fuel cells. J Power Sources 2012;210:366–73. doi:10.1016/j.jpowsour.2012.02.098.

[16]   Oono Y, Sounai A, Hori M. Prolongation of lifetime of high temperature proton exchange membrane fuel cells. J Power Sources 2013;241:87–93. doi:10.1016/j.jpowsour.2013.03.122.

[17]   Voorhees PW. Ostwald Ripening of Two-Phase Mixtures. Annu Rev Mater Sci 1992;22:197–215. doi:10.1146/annurev.ms.22.080192.001213.

[18]   Takajo S. Analysis of particle growth by coalescence during liquid phase sintering. Acta Met 1984;32:107.

[19]   Kerr R, García HR, Rastedt M, Wagner P, Alfaro SM, Romero MT, et al. Lifetime and

degradation of high temperature PEM membrane electrode assemblies. Int. J. Hydrogen Energy, vol. 40, 2015, p. 16860–6. doi:10.1016/j.ijhydene.2015.07.152.

[20] Smith MC, Gilbert JA, Mawdsley JR, Seifert S, Myers DJ. In situ small-angle X-ray scattering observation of Pt catalyst particle growth during potential cycling. J Am Chem Soc 2008;130:8112–3. doi:10.1021/ja801138t.

[21] Schmidt TJ, Baurmeister J. Properties of high-temperature PEFC Celtec-P 1000 MEAs in start/stop operation mode. J Power Sources 2008;176:428–34. doi:10.1016/j.jpowsour.2007.08.055.

[22] Galbiati S, Baricci A, Casalegno A, Marchesi R. Degradation in phosphoric acid doped polymer fuel cells: A 6000 h parametric investigation. Int J Hydrogen Energy 2013;38:6469–80. doi:10.1016/j.ijhydene.2013.03.012.

[23] Lang S, Kazdal TJ, Ku F, Hampe MJ. Experimental investigation and numerical simulation of the electrolyte loss in a HT-PEM fuel cell 2014;0:0–9. doi:10.1016/j.ijhydene.2014.11.041.

[24] Li Q, Oluf J, Savinell RF, Bjerrum NJ. Progress in Polymer Science High temperature proton exchange membranes based on polybenzimidazoles for fuel cells 2009;34:449–77. doi:10.1016/j.progpolymsci.2008.12.003.

[25] Mench MM. Fuel Cell Engines. 2008.

[26] Shao Y, Yin G, Gao Y. Understanding and approaches for the durability issues of Pt-based catalysts for PEM fuel cell 2007;171:558–66. doi:10.1016/j.jpowsour.2007.07.004.

[27] Hinds G. Performance and durability of PEM fuel cells: a review. 2004.

[28] Wu J, Yuan XZ, Martin JJ, Wang H, Zhang J, Shen J, et al. A review of PEM fuel cell durability: Degradation mechanisms and mitigation strategies. J Power Sources 2008;184:104–19. doi:10.1016/j.jpowsour.2008.06.006.

[29] Fowler M., Mann R.F., Amphlett J.C., Peppley A. RPR. Handbook of Fuel Cells - Reliability issues and voltage degradation. 2010.

[30] Cleghorn SJC, Mayfield DK, Moore DA, Moore JC, Rusch G, Sherman TW, et al. A polymer electrolyte fuel cell life test: 3 years of continuous operation. J Power Sources 2006;158:446–54. doi:10.1016/j.jpowsour.2005.09.062.

[31] Anghel V. Prediction Failure for Pem Fuel Cells. Int J Adv Eng Technol 2012;4:1–14.

[32] Ozden E, Tari I. Proton exchange membrane fuel cell degradation : A parametric analysis using Computational Fluid Dynamics 2016;304:64–73.

[33] Zhang S, Yuan X, Wang H, Mérida W, Zhu H, Shen J, et al. A review of accelerated stress tests of MEA durability in PEM fuel cells. Int J Hydrogen Energy 2009;34:388–404. doi:10.1016/j.ijhydene.2008.10.012.

[34] Yuan XZ, Li H, Zhang S, Martin J, Wang H. A review of polymer electrolyte membrane fuel cell durability test protocols. J Power Sources 2011;196:9107–16. doi:10.1016/j.jpowsour.2011.07.082.

[35] Schmidt TJ. Durability and degradation in high-temperature polymer electrolyte fuel cells. ECS Trans 2006;1:19–31.

[36] Nielsen PM, Andreasen JS, Rasmussen LP, Kær KS. Experimental study and modeling of degradation phenomena in HTPEM fuel cell stacks for use in CHP systems Experimental study and modeling of degradation phenomena in HTPEM fuel cell stacks for use in CHP systems 2009.

[37] Kim J, Kim M, Kang T, Sohn YJ, Song T, Choi KH. Degradation modeling and operational optimization for improving thelifetime of high-temperature PEM (proton exchange membrane) fuel cells. Energy 2014;66:41–9. doi:10.1016/j.energy.2013.08.053.

[38] Taccani R, Chinese T, Boaro M. Effect of accelerated ageing tests on PBI HTPEM

fuel cells performance degradation. Int J Hydrogen Energy 2017;42:1875–83. doi:10.1016/j.ijhydene.2016.09.164.

[39] Rosli RE, Sulong AB, Daud WRW, Zulkifley MA, Husaini T, Rosli MI, et al. A review of high-temperature proton exchange membrane fuel cell (HT-PEMFC) system. Int J Hydrogen Energy 2016:1–22. doi:10.1016/j.ijhydene.2016.06.211.

[40] Hu J, Zhang H, Zhai Y, Liu G, Yi B. 500 h Continuous aging life test on PBI/H3PO4 high-temperature PEMFC. Int J Hydrogen Energy 2006;31:1855–62. doi:10.1016/j.ijhydene.2006.05.001.

[41] Zuliani N, Taccni R. Micro Combined heat and power systems based based on HTPEM fuel cell ans Li-batteries: analysis of performance under different operating strategies n.d.

[42] Modestov AD, Tarasevich MR, Filimonov VY, Zagudaeva NM. Degradation of high temperature MEA with PBI-H3 PO4 membrane in a life test. Electrochim Acta 2009;c:7121–7. doi:10.1016/j.electacta.2009.07.031.

[43] Kannan A, Kabza A, Scholta J. Long term testing of start e stop cycles on high temperature PEM fuel cell stack. J Power Sources 2015;277:312–6. doi:10.1016/j.jpowsour.2014.11.115.

[44] Wannek C, Kohnen B, Oetjen HF, Lippert H, Mergel J. Durability of ABPBI-based MEAs for high temperature PEMFCs at different operating conditions. Fuel Cells 2008;8:87–95. doi:10.1002/fuce.200700059.

[45] Oono Y, Fukuda T, Sounai A, Hori M. Influence of operating temperature on cell performance and endurance of high temperature proton exchange membrane fuel cells. J Power Sources 2010;195:1007–14. doi:10.1016/j.jpowsour.2009.08.097.

[46] Kamat A, Herrmann M, Ternes D, Klein O, Krewer U, Scholl S. Experimental investigations into phosphoric acid adsorption on platinum catalysts in a high temperature PEM Fuel cell. Fuel Cells 2011;11:511–7. doi:10.1002/fuce.201000102.

[47] Yu S, Xiao L, Benicewicz BC. Durability studies of PBI-based high temperature PEMFCs. Fuel Cells 2008;8:165–74. doi:10.1002/fuce.200800024.

[48] Matsutani K, Hayakawa K, Tada T. Effect of particle size of platinum and platinum-cobalt catalysts on stability against load cycling: Towards the development of high performance, stable fuel cell catalysts with low platinum loadings. Platin Met Rev 2010;54:223–32. doi:10.1595/147106710X523698.

[49] Zhang J. PEM Fuel Cell Electrocatalysts and Catalyst Layers. Springer. 2008.

[50] Borup RL, Davey JR, Garzon FH, Wood DL, Inbody MA. PEM fuel cell electrocatalyst durability measurements. J Power Sources 2006;163:76–81. doi:10.1016/j.jpowsour.2006.03.009.

[51] Reimer U, Schumacher B, Lehnert W. Accelerated Degradation of High-Temperature Polymer Electrolyte Fuel Cells : Discussion and Empirical Modeling 2015;162. doi:10.1149/2.0961501jes.

[52] Jiao K, Alaefour IE, Li X. Three-dimensional non-isothermal modeling of carbon monoxide poisoning in high temperature proton exchange membrane fuel cells with phosphoric acid doped polybenzimidazole membranes. Fuel 2011;90:568–82. doi:10.1016/j.fuel.2010.10.018.

[53] Kim M, Kang T, Kim J, Sohn Y-J. One-dimensional modeling and analysis for performance degradation of high temperature proton exchange membrane fuel cell using PA doped PBI membrane. Solid State Ionics 2014;262:319–23. doi:10.1016/j.ssi.2013.08.036.

[54] Korsgaard AR, Refshauge R, Nielsen MP, Bang M, KÆ SK. Experimental characterization and modeling of commercial polybenzimidazole-based MEA performance. J Power Sources 2006;162:239–45. doi:10.1016/j.jpowsour.2006.06.099.

[55] Suzuki A, Oono Y, Williams MC, Miura R, Inaba K, Hatakeyama N, et al. Evaluation for sintering of electrocatalysts and its effect on voltage drops in high-temperature proton exchange membrane fuel cells (HT-PEMFC). Int J Hydrogen Energy 2012;37:18272–89. doi:10.1016/j.ijhydene.2012.09.016.

[56] Korsgaard AR, Nielsen MP, Kær SK. Part one: A novel model of HTPEM-based micro-combined heat and power fuel cell system. Int J Hydrogen Energy 2008;33:1909–20. doi:10.1016/j.ijhydene.2008.01.009.

[57] Arsalis A, Nielsen MP, Kær SK. Modeling and parametric study of a 1 kWe HT-PEMFC-based residential micro-CHP system. Int J Hydrogen Energy 2011;36:5010–20. doi:10.1016/j.ijhydene.2011.01.121.

[58] Najafi B, Haghighat Mamaghani A, Baricci A, Rinaldi F, Casalegno A. Mathematical modelling and parametric study on a 30 kWel high temperature PEM fuel cell based residential micro cogeneration plant. Int J Hydrogen Energy 2015;40:1569–83. doi:10.1016/j.ijhydene.2014.11.093.

[59] Arsalis A, Nielsen MP, Kær SK. Modeling and optimization of a 1 kWe HT-PEMFC-based micro-CHP residential system. Int J Hydrogen Energy 2012;37:2470–81. doi:10.1016/j.ijhydene.2011.10.081.

[60] Zuliani N, Taccani R. Microcogeneration system based on HTPEM fuel cell fueled with natural gas: Performance analysis. Appl Energy 2012;97:802–8. doi:10.1016/j.apenergy.2011.12.089.

[61] Zuliani N. Energy simulation model and parametric analysis of a micro cogeneration system based on a HTPEM fuel cell and battery storage. Spec Issue ICAE 2013 2013:1–10.

[62] Haghighat Mamaghani A, Najafi B, Casalegno A, Rinaldi F. Predictive modelling and adaptive long-term performance optimization of an HT-PEM fuel cell based micro combined heat and power (CHP) plant. Appl Therm Eng 2017;192:519–29.

[63] O'Hayre R, Cha SW, Colella W PF. Fuel Cell Fundamentals. John Wiley. 2006.

[64] Engl T. Electrode Degradation in High-Temperature Polymer Electrolyte Fuel Cells: Characterization, Mechanisms and Mitigation. Ethz 2015. doi:10.1017/CBO9781107415324.004.

[65] Borup R, Meyers J, Pivovar B, Kim YS, Mukundan R, Garland N, et al. Scientific Aspects of Polymer Electrolyte Fuel Cell Durability and Degradation 2007:3904–51.

[66] Li Q, He R, Jensen JO, Bjerrum NJ. PBI-based polymer membranes for high temperature fuel cells - Preparation, characterization and fuel cell demonstration. Fuel Cells 2004;4:147–59. doi:10.1002/fuce.200400020.

[67] Kim JH, Kim HJ, Lim TH, Lee HI. Dependence of the performance of a high-temperature polymer electrolyte fuel cell on phosphoric acid-doped polybenzimidazole ionomer content in cathode catalyst layer. J Power Sources 2007;170:275–80. doi:10.1016/j.jpowsour.2007.03.082.

[68] Zhang J, Tang Y, Song C, Zhang J. Polybenzimidazole-membrane-based PEM fuel cell in the temperature range of 120-200 °C. J Power Sources 2007;172:163–71. doi:10.1016/j.jpowsour.2007.07.047.

[69] Pan C, Li Q, Jensen JO, He R, Cleemann LN, Nilsson MS, et al. Preparation and operation of gas diffusion electrodes for high-temperature proton exchange membrane fuel cells. J Power Sources 2007;172:278–86. doi:10.1016/j.jpowsour.2007.07.019.

[70] Kabza A. Fuel Cell Formulary. Http://WwwPemfcDe 2015:1–84.

[71] Korsgaard AR, Nielsen PM, Bang M, Kær KS. Modeling of CO Influence in PBI Electrolyte PEM Fuel Cells. ASME 2006 4th Int. Conf. Fuel Cell Sci. Eng. Technol., 2006, p. 911–5.

[72] Hu J, Zhang H, Zhai Y, Liu G, Yi B. 500 h Continuous aging life test on PBI / H 3 PO

4 high-temperature PEMFC 2006;31:1855–62. doi:10.1016/j.ijhydene.2006.05.001.

[73] Lim KH, Oh H-S, Jang S-E, Ko Y-J, Kim H-J, Kim H. Effect of operating conditions on carbon corrosion in polymer electrolyte membrane fuel cells. J Power Sources 2009;193:575–9. doi:10.1016/j.jpowsour.2009.04.006.

[74] Yu Y, Li H, Wang H, Yuan X-Z, Wang G, Pan M. A review on performance degradation of proton exchange membrane fuel cells during startup and shutdown processes: Causes, consequences, and mitigation strategies. J Power Sources 2012;205:10–23. doi:10.1016/j.jpowsour.2012.01.059.

[75] Chandesris M, Vincent R, Guetaz L, Roch J-S, Thoby D, Quinaud M. Membrane degradation in PEM fuel cells: From experimental results to semi-empirical degradation laws. Int J Hydrogen Energy 2017:1–11. doi:10.1016/j.ijhydene.2017.02.116.

[76] Won S, Oh K, Ju H. Numerical degradation studies of high-temperature proton exchange membrane fuel cells with phosphoric acid-doped PBI membranes. Int J Hydrogen Energy 2016;41:8296–306. doi:10.1016/j.ijhydene.2015.10.153.

[77] Schmidt TJ, Baurmeister J. Durability and Reliability in High-Temperature Reformed Hydrogen PEFCs. ECS Trans 2006;3:861–9.

[78] Zhai Y, Zhang H, Xing D, Shao ZG. The stability of Pt/C catalyst in H3PO4/PBI PEMFC during high temperature life test. J Power Sources 2007;164:126–33. doi:10.1016/j.jpowsour.2006.09.069.

[79] Torija S, Prieto-sanchez L, Ashton SJ. In-situ electrochemically active surface area evaluation of an open-cathode polymer electrolyte membrane fuel cell stack. J Power Sources 2016;327:543–7. doi:10.1016/j.jpowsour.2016.07.072.

[80] Büchi FN, Inaba M, Schmidt JT. Polymer Electrolyte Fuel Cell Durability. Springer. 2009.

[81] Paik CH, Saloka GS, Graham GW. Influence of Cyclic Operation on PEM Fuel Cell Catalyst Stability. Electrochem Solid-State Lett 2007;10:B39–42.

[82] Uribe FA, Zawodzinski TA. A study of polymer electrolyte fuel cell performance at high v oltages . Dependence on cathode catalyst layer composition and on v oltage conditioning 2002;47.

[83] Salomov UR, Chiavazzo E, Asinari P. ScienceDirect Gas-dynamic and electro-chemical optimization of catalyst layers in high temperature polymeric electrolyte membrane fuel cells. Int J Hydrogen Energy 2015;40:5425–31. doi:10.1016/j.ijhydene.2015.01.059.

[84] Kim J, Yi JS, Song T. Investigation of degradation mechanisms of a high-temperature polymer-electrolyte-membrane fuel cell stack by electrochemical impedance spectroscopy. J Power Sources 2012;220:54–64. doi:10.1016/j.jpowsour.2012.07.129.

[85] Fairweather JD, Spernjak D, Weber a Z, Harvey D, Wessel S, Hussey DS, et al. Effects of Cathode Corrosion on Through-Plane Water Transport in Proton Exchange Membrane Fuel Cells. J Electrochem Soc 2013;160:F980–93. doi:Doi 10.1149/2.024309jes.

[86] Qi Z, Buelte S. Effect of open circuit voltage on performance and degradation of high temperature PBI-H3PO4 fuel cells. J Power Sources 2006;161:1126–32. doi:10.1016/j.jpowsour.2006.06.020.

[87] International Electrotechnical Commission. IEC/TS 62282-7-1 2010:1–8.

[88] Bloom I, Walker LK, Basco JK, Malkow T, Saturnio A, De Marco G, et al. A comparison of Fuel Cell Testing protocols - A case study: Protocols used by the U.S. Department of Energy, European Union, International Electrotechnical Commission/Fuel Cell Testing and Standardization Network, and Fuel Cell Technical Team. J Power Sources 2013;243:451–7. doi:10.1016/j.jpowsour.2013.06.026.

[89]   Roadmap T. Fuel Cell Technical Team Roadmap Hydrogen Storage Technologies Roadmap 2013.

[90]   Tsotridis G, Pilenga A, Marco G De, Malkow T. EU Harmonised Test Protocols for PEMFC MEA Testing in Single Cell Configuration for Automotive Applications; JRC Science for Policy report. 2015. doi:10.2790/54653.

[91]   Wang H, Yuan XZ, Li H. PEM fuel cell diagnostic tools. Taylor & F. 2012.

[92]   Mason TJ, Millichamp J, Neville TP, El-Kharouf A, Pollet BG, Brett DJL. Effect of clamping pressure on ohmic resistance and compression of gas diffusion layers for polymer electrolyte fuel cells. J Power Sources 2012;219:52–9. doi:10.1016/j.jpowsour.2012.07.021.

[93]   Chang J-Y, Kuan Y-D, Lee S-M. Experimental Investigation of a Direct Methanol Fuel Cell with Hilbert Fractal Current Collectors. J Chem 2014:7.

[94]   Yuan X, Wang H, Colin Sun J, Zhang J. AC impedance technique in PEM fuel cell diagnosis-A review. Int J Hydrogen Energy 2007;32:4365–80. doi:10.1016/j.ijhydene.2007.05.036.

[95]   Wagner N, Gülzow E. Change of electrochemical impedance spectra (EIS) with time during CO-poisoning of the Pt-anode in a membrane fuel cell. J Power Sources 2004;127:341–7. doi:10.1016/j.jpowsour.2003.09.031.

[96]   Gode P, Jaouen F, Lindbergh G, Lundblad A, Sundholm G. Influence of the composition on the structure and electrochemical characteristics of the PEFC cathode. Electrochim Acta 2003;48:4175–87. doi:10.1016/S0013-4686(03)00603-0.

[97]   Dale N V., Mann MD, Salehfar H, Dhirde AM, Han T. ac Impedance Study of a Proton Exchange Membrane Fuel Cell Stack Under Various Loading Conditions. J Fuel Cell Sci Technol 2010;7:031010. doi:10.1115/1.3207871.

[98]   Zakrisson E. The Effect of Start / Stop Strategy on PEM Fuel Cell Degradation Characteristics 2011.

[99]   Łukaszewski M, Soszko M, Czerwiński A. Electrochemical Methods of Real Surface Area Determination of Noble Metal Electrodes – an Overview 2016;11:4442–69. doi:10.20964/2016.06.71.

[100] Valle F. Electrocatalyst degradation in high temperature PEM fuel cells. Tesi Di Dottorato Di Ric Sci Dell'ingegneria 2014.

[101] Lambert L, MulveyT. Ernst Ruska (1906–1988), Designer Extraordinaire of the Electron Microscope: A Memoir. Adv Imaging Electron Phys 1996;95:2–62.

[102] Liu G, Zhang H, Hu J, Zhai Y, Xu D, Shao Z gang. Studies of performance degradation of a high temperature PEMFC based on H3PO4-doped PBI. J Power Sources 2006;162:547–52. doi:10.1016/j.jpowsour.2006.07.008.

[103] Singh H, Schnablegger Y. The SAXS guide. Anton Paar. 2013.

[104] Glatter O, Kratky O. Small angle X-ray scattering. 1982.

[105] Haubold HG, Wang XH, Jungbluth H, Goerigk G, Schilling W. Molecular structure 1996;383:283–9.

[106] Stevens DA, Zhang S, Chen Z, Dahn JR. On the determinatio On the determination of plat supported platinum e on of platinum particle size in supported platinum electrocata On the determination electrocatalysts for Stevens fuel cell ap On supported the determination of platinum par platinum 2003;41:2769–77.

[107] Yu C, Holby EF, Yang R, Toney MF, Morgan D, Strasser P. Growth Trajectories and Coarsening Mechanisms of Metal Nanoparticle Electrocatalysts. ChemCatChem 2012;4:766–70. doi:10.1002/cctc.201200090.

[108] Gilbert JA, Kropf AJ, Kariuki NN, DeCrane S, Wang X, Rasouli S, et al. In-Operando Anomalous Small-Angle X-Ray Scattering Investigation of Pt 3 Co Catalyst Degradation in Aqueous and Fuel Cell Environments. J Electrochem Soc

2015;162:F1487–97. doi:10.1149/2.0531514jes.

[109]   Srinivasan S, Ticcianelli AE, Derouin RC, Redondo A. Advances in solid polymer electrolyte fuel cell technology with low platinum loading electrodes. J Power Sources 1988;22:359–75.

[110]   Kim J, Lee S-ML, Srinivasan S, Chamberlin CE. Modeling of Proton Exchange Membrane Fuel Cell Performance with an Empirical Equation. J Electrochem Soc 1995;142:2670–4.

[111]   Squadrito G, Maggio G, Passalacqua E, Lufrano F, Patti A. Empirical equation for polymer electrolyte fuel cell (PEFC) behaviour. J Appl Electrochem 1999;29:1449–55. doi:10.1023/A:1003890219394.

[112]   Sena DR, Ticianelli EA, Paganin VA, Gonzalez ER. Effect of water transport in a PEFC at low temperatures operating with dry hydrogen. J Electroanal Chem 1999;477:164–70. doi:10.1016/S0022-0728(99)00401-5.

[113]   Pisani L, D'Aguanno B. A new semi-empirical approach to performance curces of polymer electrolyte fuel cells. J Power Sources 2002;108:192–203.

[114]   Cheddie D, Munroe N. Mathematical model of a PEMFC using a PBI membrane. Energy Convers Manag 2006;47:1490–504. doi:10.1016/j.enconman.2005.08.002.

[115]   Cheddie D, Munroe N. Parametric model of an intermediate temperature PEMFC. J Power Sources 2006;156:414–23. doi:10.1016/j.jpowsour.2005.06.010.

[116]   Sousa T, Mamlouk M, Scott K. An isothermal model of a laboratory intermediate temperature fuel cell using PBI doped phosphoric acid membranes. Fuel Cells 2010;65:2513–30. doi:10.1002/fuce.200900178.

[117]   Sousa T, Mamlouk M, Scott K. A non-isothermal model of a laboratory intermediate temperature fuel cell using PBI doped phosphoric acid membranes. Fuel Cells 2010;10:993–1012. doi:10.1002/fuce.200900178.

[118]   Cheddie DF, Munroe NDH. Three dimensional modeling of high temperature PEM fuel cells. J Power Sources 2006;160:215–23. doi:10.1016/j.jpowsour.2006.01.035.

[119]   Peng J, Shin JY, Song TW. Transient response of high temperature PEM fuel cell. J Power Sources 2008;179:220–31. doi:10.1016/j.jpowsour.2007.12.042.

[120]   Peng J, Lee SJ. Numerical simulation of proton exchange membrane fuel cells at high operating temperature. J Power Sources 2006;162:1182–91. doi:10.1016/j.jpowsour.2006.08.001.

[121]   Jiao K, Li X. A Three-Dimensional Non-isothermal Model of High Temperature Proton Exchange Membrane Fuel Cells with Phosphoric Acid Doped Polybenzimidazole Membranes. Fuel Cells 2010;10:351–62. doi:10.1002/fuce.200900059.

[122]   Hu J, Zhang H, Zhai Y, Liu G, Hu J, Yi B. Performance degradation studies on PBI/H3PO4 high temperature PEMFC and one-dimensional numerical analysis. Electrochim Acta 2006;52:394–401. doi:10.1016/j.electacta.2006.05.020.

[123]   Liu D, Case S. Durability study of proton exchange membrane fuel cells under dynamic testing conditions with cyclic current profile. J Power Sources 2006;162:521–31. doi:10.1016/j.jpowsour.2006.07.007.

[124]   Reimer U, Schumacher B, Lehnert W. Accelerated Degradation of High-Temperature Polymer Electrolyte Fuel Cells: Discussion and Empirical Modeling. J Electrochem Soc 2015;162:F153–64. doi:10.1149/2.0961501jes.

[125]   Xu J, Froment GF. Methane steam reforming, methanation and water-gas shift: I. Intrinsic kinetics. AIChe 1989;35:88–96. doi:10.1002/aic.690350109.

[126]   Hawkes AD, Brett DJL, Brandon NP. Fuel cell micro-CHP techno-economics: Part 2 - Model application to consider the economic and environmental impact of stack degradation. Int J Hydrogen Energy 2009;34:9558–69.

doi:10.1016/j.ijhydene.2009.09.095.

[127] Antoni L. FCTESTNET / FCTESQA PEFC power stack performance testing procedure I . Polarisation curve test method. 2009. doi:10.2790/18880.

[128] Song J. BASF Stack Handbook. n.d.

[129] Commission E. Testing the voltage and power as function of current density: Polarisation curve for a SOFC single cell. JRC Sci Tech Reports 2010.

[130] Thalau O, Antoni L, Rosini S, Kabza a, Bogaert G Van. PEFC power stack performance testing procedure Measuring voltage , power and efficiency as function of pressure for a water-cooled PEFC stack 2010.

[131] Cooper KR. in Situ Pem Fuel Cell Electrochemical Surface Area and Catalyst Utilization Measurement. Fuel Cell Mag 2009:1–3. doi:10.1016/S1464-2859(00)80060-7.

[132] Amenitsch H, Bernstorff S, Kriechbaum M, Lombardo D, Mio H, Rappolt M, et al. Performance and First Results of the ELETTRA High-Flux Beamline for Small-Angle X-ray Scattering. J Appl Crystallogr 1997;30:872–6. doi:10.1107/S0021889897001593.

[133] Hammersley AP. FIT2 V10.3 Reference Manual V4.0 - ESRF98HA01T. Eur Synchrotron Radiat Facil 1998.

[134] Pontoni D, Finet S, Narayanan T, Rennie AR. Interactions and kinetic arrest in an adhesive hard-sphere colloidal system. J Chem Phys 2003;119:6157–65. doi:10.1063/1.1601605.

[135] Huang TC, Toraya H, Blanton TN, Wu Y. X-ray powder diffraction analysis of silver behenate, a possible low-angle diffraction standard. J Appl Crystallogr 1993;26:180–4. doi:10.1107/S0021889892009762.

[136] Zuliani N, Taccani R. Simulation model and energy analysis of a micro cogeneration system based on a HTPEM fuel cell and battery storage, 2013, p. 1–10.

[137] Taccani R, Chinese T, Zuliani N. Performance analysis of a micro CHP system based on high temperature PEM fuel cells subjected to degradation. Energy Procedia 2017;126:421–8. doi:10.1016/j.egypro.2017.08.198.

[138] JCGM. Evaluation of measurement data — Guide to the expression of uncertainty in measurement 2008.

[139] Taccani R, Zuliani N. Effect of flow field design on performances of high temperature PEM fuel cells: Experimental analysis. Int J Hydrogen Energy 2011;36:10282–7. doi:10.1016/j.ijhydene.2010.10.026.

[140] Casalegno A, Marchesi R. DMFC performance and methanol cross-over : Experimental analysis and model validation 2008;185:318–30. doi:10.1016/j.jpowsour.2008.06.071.

[141] Pinar FJ, Pilinski N, Wagner P. Long-Term Testing of a High Temperature Polymer Electrolyte Membrane Fuel Cell : The Effect of Reactant Gases. AIChE 2016;62. doi:10.1002/aic.15044.

[142] G Bandlamudi. Systematic Characterization of HT PEMFCs containing Pbi/H3PO4 systems. Thermodynamic analysis and experimental investigations. 2011.

[143] Yang J, Li Q, Cleemann LN, Xu C, Jensen JO, Pan C, et al. Synthesis and properties of poly(aryl sulfone benzimidazole) and its copolymers for high temperature membrane electrolytes for fuel cells. J Mater Chem 2012;22:11185. doi:10.1039/c2jm30217a.

[144] BASF FC. "Celtec ® -P 1000 Membrane Electrode Assembly" Techincal Specification. 2006.

[145] Andreasen SJ, Vang JR, Kær SK. High temperature PEM fuel cell performance characterisation with CO and CO2 using electrochemical impedance spectroscopy. Int J Hydrogen Energy 2011;36:9815–30. doi:10.1016/j.ijhydene.2011.04.076.

[146] Shao Y, Kou R, Wang J, Viswanathan V V, Kwak JH, Liu J, et al. The influence of the electrochemical stressing (potential step and potential-static holding) on the degradation of polymer electrolyte membrane fuel cell electrocatalysts 2008;185:280–6. doi:10.1016/j.jpowsour.2008.07.008.

[147] Schonvogel D, Rastedt M, Wagner P, Wark M, Dyck A. Impact of Accelerated Stress Tests on High Temperature PEMFC Degradation. Fuel Cells 2016;16:480–9. doi:10.1002/fuce.201500160.

[148] Pinar FJ, Pilinski N, Rastedt M, Wagner P. Performance of a high-temperature PEM fuel cell operated with oxygen enriched cathode air and hydrogen from synthetic reformate. Int J Hydrogen Energy 2015;40:5432–8. doi:10.1016/j.ijhydene.2014.12.015.

[149] Staudt R, Intwala KF. Development of Polybenzimidazole-Based , High-Temperature Membrane and Electrode Assemblies for Stationary Applications 2006:771–6.

[150] The United States Council for Automotive Research. USCAR Fuel cell tech team cell component accelerated stress test protocols - Revised May 26, 2010 2010:2–8.

[151] U.S. Energy Department. DOE Solicitation DE-PS36-06GO96017 2009.

[152] Zhang S, Yuan XZ, Hin JNC, Wang H, Wu J, Friedrich KA, et al. A review of platinum-based catalyst layer degradation in proton exchange membrane fuel cells. J Power Sources 2009;194:588–600. doi:10.1016/j.jpowsour.2009.06.073070.

[153] Zhang S, Yuan XZ, Hin JNC, Wang H, Wu J, Friedrich KA, et al. Effects of open-circuit operation on membrane and catalyst layer degradation in proton exchange membrane fuel cells. J Power Sources 2010;195:1142–8. doi:10.1016/j.jpowsour.2009.08.070.

[154] Wu J, Yuan X, Martin JJ, Wang H, Yang D. Proton exchange membrane fuel cell degradation under close to open-circuit conditions Part I : In situ diagnosis 2010;195:1171–6. doi:10.1016/j.jpowsour.2009.08.095.

[155] Kim J, Kim M, Lee BG, Sohn YJ. Durability of high temperature polymer electrolyte membrane fuel cells in daily based start/stop operation mode using reformed gas. Int J Hydrogen Energy 2015;40:7769–76. doi:10.1016/j.ijhydene.2014.12.122.

[156] Paper C. EAP13-4571 PEMFC Carbon Corrosion due to Start-Stop Cycling 2013.

[157] Seo D, Lee J, Park S, Rhee J, Won S, Shul Y. Investigation of MEA degradation in PEM fuel cell by on / off cyclic operation under different humid conditions. Int J Hydrogen Energy 2011;36:1828–36. doi:10.1016/j.ijhydene.2010.02.053.

[158] Taccani R, Radu R. Analisi Delle Prestazioni Di Celle a Combustibile Pem Ad Alta Temperatura. 64° Congr Naz ATI 2009:2–6.

[159] Engl T, Gubler L, Schmidt TJ. On the Positive Effect of CO during Start / Stop in High-Temperature Polymer Electrolyte Fuel Cells 2014;3:47–9. doi:10.1149/2.0011407eel.

[160] Mocotéguy P, Ludwig B, Scholta J, Nedellec Y, Jones DJ, Rozière J. Long-term testing in dynamic mode of HT-PEMFC H3PO 4/PBI celtec-P based membrane electrode assemblies for micro-CHP applications. Fuel Cells 2010;10:299–311. doi:10.1002/fuce.200900153.

[161] Radu R, Taccani R, Scagliotti M, Valli C. HT PEM fuel cell system fed with biogas : experimental characterizations 2013:1–9.

[162] Bruijn FA De, Dam VAT, Janssen GJM. Review : Durability and Degradation Issues of PEM Fuel Cell Components 2008:3–22. doi:10.1002/fuce.200700053.

[163] Zuliani N, Taccani R, Radu R. Experimental and Theoretical Performance Analysis of a High Temperature PEM Fuel Cell Fed With LPG Using a Compact Steam Reformer. ASME 9th Int. Conf. Fuel Cell Sci. Eng. Technol., 2011, p. 991–8. doi:10.1115/FuelCell2011-54618.

[164] Zuliani N, Taccani R. Simulation Model of a High Temperature PEM Fuel Cell Based Cogeneration System. 23th Int. Conf. Effic. Cost, Optim. Simul. Environ. Impact Energy Syst., 2010.

[165] Bergani F. Rapporto di Sintesi RSE A3-021923 2003. http://www.rse-web.it/documenti.page?RSE_manipulatePath=yes&RSE_originalURI=/documenti/doc umento/119225&country=ita.